DESIGN OF A SMALL VERTICAL AXIS WIND TURBINE BASED ON LOCAL WIND DATA IN THE CITY OF GHARYAN IN LIBYA

2022
PhD THESIS
ENERGY SYSTEMS ENGINEERING

Nagi E. Nassir ABDALLA

Thesis Advisor
Assoc.Prof.Dr. Bahadır ACAR

DESIGN OF A SMALL VERTICAL AXIS WIND TURBINE BASED ON LOCAL WIND DATA IN THE CITY OF GHARYAN IN LIBYA

Nagi E. Nassır ABDALLA

T.C.
Karabuk University
Institute of Graduate Programs
Department of Energy Systems Engineering
Prepared as
PhD Thesis

Thesis Advisor
Assoc. Prof. Dr. Bahadır ACAR

KARABUK
June 2022

I certify that in my opinion the thesis submitted by Nagi E. Nassır ABDALLA titled "DESIGN OF A SMALL VERTICAL AXIS WIND TURBINE BASED ON LOCAL WIND DATA IN THE CITY OF GHARYAN IN LIBYA" is fully adequate in scope and in quality as a thesis for the degree of PhD.

Assoc.Prof.Dr. Bahadır ACAR .....
Thesis Advisor, Department of Energy Systems Engineering

This thesis is accepted by the examining committee with a unanimous vote in the Department of Energy Systems Engineering as a PhD thesis. June 1, 2022

Examining Committee Members (Institutions)	Signature
Chairman : Prof.Dr. Mehmet ÖZKAYMAK (KBU)	.....
Member : Prof.Dr. Kurtuluş BORAN (GU)	.....
Member : Assoc.Prof.Dr. Bahadır ACAR (KBU)	.....
Member : Assoc.Prof.Dr. Engin ÖZBAŞ (OMU)	.....
Member : Assist.Prof.Dr. Murat AYDIN (KBU)	.....

The degree of PhD by the thesis submitted is approved by the Administrative Board of the Institute of Graduate Programs, Karabük University.

Prof. Dr. Hasan SOLMAZ .....
Director of the Institute of Graduate Programs

"I declare that all the information within this thesis has been gathered and presented in accordance with academic regulations and ethical principles and I have according to the requirements of these regulations and principles cited all those which do not originate in this work as well."

Nagi E. Nassır ABDALLA

ABSTRACT

PhD Thesis

DESIGN OF A SMALL VERTICAL AXIS WIND TURBINE BASED ON LOCAL WIND DATA IN THE CITY OF GHARYAN IN LIBYA

Nagi E. Nassır ABDALLA

Karabük University
Institute of Graduate Programs
The Department of Energy Systems Engineering

Thesis Advisor:
Assoc.Prof.Dr. Bahadır ACAR
June 2022, 131 pages

The vertical axis wind turbines had several advantages compared with the other types of wind turbines in terms of dominant design principles in wind energy technology. One of the vertical axis wind turbines, called Darrieus Curved Blades axis wind turbine, has many aerodynamic and structural advantages over a horizontal axis wind turbine. However, these turbines are not self-starting at low wind speeds, which is a disadvantage for a simple small-scale installation. In this study, the design of a Darrieus Curved Blades axis wind turbine was examined for Gharyan city, which has potential wind sources, in terms of evaluating wind energy, aerodynamic design, and annual energy calculation. The wind data were taken from a representative meteorological station, and an aerodynamic design was carried out to achieve satisfactory performance of a vertical axis wind turbine concerning those wind data. As a result, it is observed that the height of 10 m and 50 m have proper power density to generate electric energy using the Darrieus wind turbine. Also, the designed

Darrieus wind turbine generates 530131 kWh energy production in Gharyan at the mean annual wind speed of over 4.88 m/s. At the 50 m height, the expected mean annual wind speed is about 7.32 m/s with a capacity factor exceeding 49.94%, and the turbine generates 2187340 kWh per year. Besides, it was seen that the effect of tip speed ratio on rotor performance is higher than other factors. At the low tip speed ratio, the attack angle and azimuth angle increase, and this increment also causes the stall phase and flow separation. In order to improve the performance of the turbine, rotor starting torque and the solidity can be increased at low tip speed ratios.

Key Words : Darrieus turbine, wind turbine, renewable energy sources, wind energy, energy calculations.

Science Code : 92806

ÖZET

Doktora Tezi

LİBYA'NIN GHARYAN KENTİNDE YEREL RÜZGAR VERİLERİNE GÖRE KÜÇÜK DİKEY EKSENLİ RÜZGAR TÜRBİNİ TASARIMI

Nagi E. Nassır ABDALLA

Karabük Üniversitesi
Lisansüstü Eğitim Enstitüsü
Enerji Sistemleri Mühendisliği Anabilim Dalı

Tez Danışmanı:
Doç. Dr. Bahadır ACAR
Haziran 2022, 131 sayfa

Dikey eksenli rüzgar türbinleri diğer tip rüzgar türbinlerine kıyasla, enerji teknolojisi alanındaki baskın tasarım prensipleri bakımından birçok avantaja sahiptir. Dikey eksenli rüzgar türbinlerinden birisi olan Darrieus tip rüzgar türbinleri, aero dinamik ve yapısal özellikleri bakımından yatay eksenli rüzgar türbinlerine göre daha fazla avantajları bulunmaktadır. Ancak, Darrieus tip rüzgar türbinlerinin düşük rüzgar hızlarından, kendi kendine çalışmaya başlayamaması, küçük ölçekli rüzgar türbinleri için dezavantaj olarak sayılabilir. Bu çalışmada, Gharyan şehrinde kullanılmak üzere Darrieus tip Eğri Kanatlı rüzgar türbinin tasarımı, rüzgar enerjisinin değerlendirilmesi, aero-dinamik tasarım ve yıllık enerji hesaplamaları açısından incelenmiştir. Gerekli olan rüzgar bilgileri, meteoroloji istasyonundan alınmış olup, aero dinamik tasarım hesaplamaları, alınan rüzgar bilgileri kullanılarak, dikey eksenli rüzgar türbin performansı göz önünde bulundurularak gerçekleştirilmiştir. Sonuç olarak, Gharyan şehrinde 10 m ve 50 m yükseklik değerlerinin Darrieus tip rüzgar türbini ile elektrik

üretimi için yeterli rüzgar yoğunluğuna sahip oldukları gözlenmiştir. Aynı zamanda, tasarlanan Darrieus tip rüzgar türbinin, Gharyan şehrinde 530131 kWh elektrik enerjisini, 4.88 m/s rüzgar hızında üretebildiği görülmüştür. Diğer yandan, 50 m yükseklikte beklenen ortalama yıllık rüzgar hızının 7.32 m/s, kapasite faktörünün %49.94'ü aştığı durumda, Darrieus tip türbinin yıllık 2187340 kWh elektrik enerjisi ürettiği hesaplanmıştır. Bunların yanında, kanat uç hızının rotor üzerindeki etkisinin diğer etkenlere kıyasla daha fazla olduğu gözlenmiştir. Düşük kanat uç hızlarında, hücum açısının ve istikamet açısının arttığı ve bu artışın sonucunda sürat kaybının ve akış ayrışmasının meydana geldiği belirlenmiştir. Türbin performansını arttırmak amacıyla, rotor başlangıç torkunun ve güvenirliliğinin, düşük kanat uç hızları için arttırılması gerektiği görülmüştür.

Anahtar Kelimeler : Darrieus türbini, rüzgar türbini, yenilenebilir enerji kaynakları, rüzgar enerjisi, enerji hesaplamaları.

Bilim Kodu **:** 92806

ACKNOWLEDGMENT

First of all, I would like to give thanks to my advisor, Assoc. Prof. Dr. Bahadır ACAR, for his great interest and assistance in preparation of this thesis and suggestions in the progress of this study. I would like to thank the staff teachers and the management from the energy systems engineering department that made this research possible. I would also like to thank all my friends who helped me in continue this research. Finally, I would like to amplify my most profound appreciation to my family, brothers, companions and relatives for their back and support all through my ponders studying.

CONTENTS

Page

Page

Page

Page

LIST OF FIGURES

Page

Page

Page

LIST OF TABLES

Page

Page

SYMBOLS AND ABBREVITIONS INDEX

SYMBOLS

A : actuator disc cross sectional area

A_t : rotor swept area

A_s : stream tube cross section area

A : inflow factor

C : blade chord

C_d : aero foil sectional drag coefficient

C_{do} : aero foil sectional zero-lift drag coefficient

C_{dt} : total rotor drag coefficient

C_l : aero foil sectional lift coefficient

C_N : aero foil sectional normal force coefficient

C_T : aero foil sectional thrust force coefficient

C_p : rotor power coefficient

C_{pm} : the maximum value of the torque coefficient

D : rotor drag force

G : height/diameter ratio

H : rotor height

$\dot{m}$: mass flow rate

N : number of turbine blades

P : rotor power

P_1 : free stream static pressure

P_2 : pressure upstream of the actuator disc

P_∞ : free stream pressure

Δp : pressure drop across the actuator disc

Q : rotor torque

r : local radios

R : rotor radios

Re : reynolds number

V_D : wind velocity through the rotor

V_∞ : free stream velocity

V_{out} : output velocity

V_{in} : input velocity

W : relative resultant velocity

GW : gigawatt

KW : kilowatt

MW : megawatt

α : angle of attack

β : blade azimuth angle

θ : blade pitch angle

λ : tip speed ratio based on free stream velocity

λ_D : tip speed ratio based on velocity through the rotor

μ : air viscosity

ρ : air density

σ : solidity

Ψ : the angle between the resultant velocity vector of rotor and the free stream direction

Ω : angular velocity

ABBREVITIONS

AEP : Annual Energy Production
CDF : Cumulative Distribution Function
CF : Capacity Factor
EM : Empirical Method
GECOL : General Electricity Company of Libya
GM : Graphical Method
HAWT : Horizontal Axis Wind Turbine
kWh : Kilo Watt per Hour
MAE : Mean Absolute Error
MBE : Mean Bias Error
PDF : Probability Density Function
PVC : Present Value Cost
RMSE : Root Means Square Error
REAOL : Renewable Energy Authority of Libya
VAWT : Vertical Axis Wind Turbine
WPD : Wind Power Density

CHAPTER 1

INTRODUCTION

1.1. BACKGROUND

Because of the Earth's uneven surface, there are variations in air temperature and pressure. When the gap between high and low pressures is large enough, air travels from one to the other in an attempt to maintain balance. When there is a large difference in pressure, this air movement is known as wind. The earth's rotation has an effect on wind as well. Since altitude rises, so does wind speed, as friction with the earth's surface diminishes. Factors that influence wind speed in a certain region include the weather and geography of that area. In the beginning, there is a 'background' wind speed, arising from current weather systems and local meteorology, which may include sea breezes, storms, and/or other short-term phenomena. Secondly, local variables such as valley systems, terrain, and differences in surface cover alter this background wind. Local impacts can have a significant impact on wind energy production, even if they only extend a few hundred meters away. Horizontal and vertical axis wind turbines (HAWTs and VAWTs) are the two most common types of contemporary wind turbines, and they are used mostly to generate power and pump water. The primary benefit of VAWT is the elimination of the need for yaw mechanisms due to its single moving component (the rotor). Unlike HAWT blades, which should be tapered and twisted for optimal performance, straight-bladed VAWT blades can be of uniform section and untwisted, making them comparatively straightforward to construct or extrude. In addition, nearly all of the VAWT's components that need to be maintained are situated on the ground level, which greatly simplifies maintenance. Wind turbines may compete with traditional sources in specialized markets, and decreased costs make them more affordable in larger markets, as seen by the results of previous studies. Pumping water, generating electricity, purifying and desalinating water with reverse osmosis using environmentally friendly VAWT systems are just some of the many

uses for these environmentally friendly heat pumps. They can also be used to heat and cool water, mix and aerate bodies of water, or simply heat water through the use of fluid turbulence. If there is enough wind in a given location, VAWT can be utilized either as a stand-alone system to power and heat individual homes or as a means of powering and heating independent technological installations. The energy may be sent into the grid if there is a network link, which helps to reduce the cost of power. A solar system or a diesel generator may be quickly and easily added to a VAWT in order to increase the energy supply's security. Local electrical networks for the energy supply of small communities and isolated regions can be formed by combining numerous VAWTs with other renewable energy sources and a backup system [1].

1.2. HISTORICAL BACKGROUND

For some reason, human beings have always been attracted by the wind's free energy, which they feel can be harnessed for their own ends or so they believe. Wind power has been utilized for milling maize, sailing ships, and pumping water for millennia, as well as for producing electricity in recent years. A Hindu epic named “Kautilya Arthasastra” [1] described the usage of wind mills for water pumping in the 5th century BC. A rudimentary vertical axis (Figure 1.1) for grinding grains was invented in Persia around 200 BC. It was decided to position the millstones on top of the rotor blades.

Figure 1.1. Simple vertical axis for the grinding grains [56].

The millstones were later relocated under the rotor of the machine. Perhaps it was discovered that the wind speed rises with height, and the updated design would be more efficient and comfortable for the miller as well. Windmills were widely used in the Middle East by 1100 AD. Horizontal axis windmills, consisting of up to 10 wooden booms, rigged with jib sails, were developed. One such windmill is shown in Figure 1.2. In Europe, the use of windmills introduced was around 1300 AD. At that time, the windmills were used mainly for cereal grinding. Interestingly, the vertical axis windmills were considered more efficient than their horizontal counterparts, which were in the primitive stages of development at that time [2]. By 1400AD, the Dutch had developed improved design of horizontal machines and beyond this point; the horizontal windmills overtook the vertical design A traditional four blades Dutch mill is shown in Figure 1.2. [12].

Figure 1.2. A traditional four blades Dutch mill [57].

Technology advanced slowly until the late 19th century, when wind turbines were first used to generate power." Denmark's first wind turbine was created by Paul la Cour in 1891 (Figure 1.3). Wind turbines' popularity peaked and waned over the nineteenth and twentieth centuries. There were around 2500 windmills in operation in Denmark by the end of the 19th century, which provided roughly 30 MW of power, or about 25 percent of the total power available to Danish industry at the time [2].

Figure 1.3. First wind turbine for generation of electricity in Denmark [56].

When fossil fuel-based electricity became inexpensive enough to knock wind out of the market in the early 1930s, the number of wind turbines was reduced to around 1000. Wind turbines gained prominence during World War II due to a lack of fuel, and new large-scale wind machines were built to provide power. During World War II, the number of these machines rose from 16 in 1940 to 88 in 1944 in Denmark. This happened again after World War II and their population was reduced to 57 in 1947. In 1973, the Arab oil embargo pushed industrialized countries to take a hard look at their dependence on foreign fuel sources for their energy requirements. Once again, wind turbines were seen as a promising alternative energy source, and there was increased

interest in alternative energy development. Many research organizations in the United Kingdom and Canada began experimenting with Darrieus vertical axis wind turbines with renewed vigor. However, the findings were disappointing, and VAWTs remained mostly confined to the laboratories [2].

VAWTs have been around for a long time and have been re-invented many times, but the re-invention of the Darrieus turbine is a fascinating one. George Jean Marie Darrieus, a French inventor, received a patent for his Darrieus VAWT invention in France in 1925 and in the United States in 1931, respectively. In the late 1960s, two Canadian researchers re-invented Darrieus's notion without knowing about his patent, which garnered little notice at the time. A renewed interest in renewable energy resources has been sparked by the depletion of fossil fuel reserves and the frightening signs of global warming due to the ever-increasing proportion of greenhouse gases released by fossil fuel burning for energy. That wind turbines have grown exponentially in the previous decade is proof enough for this statement [2].

1.3. WHAT ARE THE BENEFITS OF WIND TURBINES?

The benefits of the wind turbines can be listed as [1];

- Potential for year-round electricity generation, regardless of the time of day or night.
- They may be used in a wide range of locations.
- They can either be linked to the grid or be completely self-contained.
- They may make a powerful statement about environmental stewardship.

1.4. WIND ENERGY APPLICATIONS

A photovoltaic (solar cell) system can be used in conjunction with a wind turbine or as a stand-alone application. Large numbers of wind turbines are often clustered near together to form a wind farm for utility-scale wind energy sources. Wind farms are being used by a number of electrical companies to deliver power to their consumers. Water pumping and communications are the most common uses for stand-alone wind

turbines. Wind turbines, on the other hand, can help homeowners, farmers, and ranchers who live in very windy regions save money on their power costs. As distributed energy resources, small wind turbines can also be useful. It is possible to increase the efficiency of the electrical distribution system by using distributed energy resources, which are a collection of small, modular power generation systems [25].

1.5. ELECTRICAL POWER GENERATION

For the first time, a wind turbine that generated electricity was built by Poul LaCour in Denmark in 1891. During World War I and World War II, Danish engineers refined the technique and used it to alleviate energy shortages. The wind turbines created by F. L. Smidth in 1941–42 can be regarded the precursors of today's contemporary wind turbines [3].

Figure 1.4. A modern wind farm [4].

Airfoils for the Smidth turbines were pioneered at the time due to advancements in aerodynamics. A 53-meter-diameter wind turbine was built by the American Palmer Putnam for Morgan Smith Co. at the same time. The design concept of this machine was likewise very different from that of the previous model. Upwind rotors were used

by the Danes, and stall regulation was used to keep them at a low speed. It was Putnam's idea to incorporate variable pitch control into the construction of a downwind rotor. Putnam's turbine, on the other hand, was a failure. There were no plans to re-establish it after 1945 [3]. Juul expanded the Danish design paradigm further after World War II in Denmark. There were around 2.2 million hours of electricity created by his turbine between 1956 and 1967 when it was placed in Gedser, Denmark. Meanwhile, the Germans, known as Huetters, came up with a brand-new strategy. A wobbling hub supported two thin fiberglass blades that faced away from the tower. For its exceptional efficiency, Huetter's turbine gained a household name [4].

1.6. PRESENT STATUS OF WIND ENERGY IN LIBYA

Libya, despite being one of the world's leading oil exporters, has discovered promising renewable energy resources. As a result, 10% of Libya's total energy output is expected to come from renewable sources in the near future. In order to lower the cost of national electricity generation, this is the main reason for this. Natural gas, which is abundant in the nation, is the primary source of energy generation. It began looking for professional engineering experts in 2000 to help GECOL (General Electric Company of Libya) determine Libya's wind energy potential and build its first commercially viable wind farm to both generate electricity from renewable energy on economically reasonable terms and educate local engineers about the requirements and interrelated subjects of wind farm development. For the broad utilization of renewable resources, Libya's geographic position provides various benefits. As a result, in order to fulfill the country's growing energy needs while simultaneously preserving the planet's resources, Libya must turn to sources like wind, solar, and geothermal energy [5].

Figure 1.5. Wind farm in Libya [5].

1.7. POTENTIAL OF WIND ENERGY GENERATION

One of the many energy sources that may be replenished over time is wind power. Nearly everywhere, while there are significant regional variations, it is available. Energy from the sun is constantly renewed by the wind. The amount of solar energy that can be generated is nearly limitless [6]. With the exception of turbine construction, shipping, erection, and maintenance, the conversion of solar energy to wind energy does not include the carbon cycle. Latitudinal changes in sun irradiation cause most of the horizontal air pressure fluctuations that generate wind energy. Friction at the Earth's surface dissipates most of the wind energy, which then transforms into heat, the final and least valuable component of the planetary energy hierarchy. This planetary energy cycle is not disrupted by the generation of electrical energy from the wind. Another near-surface frictional force is only introduced, and this only partially provides higher-valued electrical energy, as well as heat. Electricity is converted to heat when consumed by humans, completing the circle of energy around our globe. The global planetary energy cycle seems unaffected by wind energy generation, as

electrical energy may be used immediately, and the energy conservation law is not violated. Consequently, wind power is a renewable energy source that may be deemed environmentally friendly. But the entropy budget is also affected. The Earth's entropy rises as a result of large-scale wind energy generation, which may slow down air circulations. It is possible to determine the amount of wind energy that is globally accessible based on the chain of energy transformations in the atmosphere. At the top of the troposphere, the incoming solar power is around 174300 TW (342 W/m^2). Moreover half of this power is available in the form of kinetic energy, which will eventually be dispersed by radiation in the atmosphere. The boundary layer accounts for almost half of this dissipation (871 TW, or 1.75 W/m2). According to Bez' limit, wind turbines can potentially collect 56% of the energy available on Earth's surface, resulting in a 122 TW potential power output. 61 TW (1,925 EJ/year) of wind power is theoretically possible, although only approximately half of it is practical. According to other estimates that employ comparable methods, the total quantity of energy is around the same. In a more pessimistic assessment by de Castro et al. (2015), the global kinetic energy of the Earth's atmosphere is estimated to be 1200 TW. A 200-meter-deep surface layer contains 8.3% of this energy, resulting in a total power output of 100 TW. An extraction area of 20% of the land's surface may yield 20 TW of surface layer energy. To reduce this further, wind parks should only be built in locations with enough wind resources. It is estimated that just 10% of this energy can be accessed by wind turbines. It is estimated that just 1 TW (32 EJ/year) of wind energy can be extracted. the near-surface dissipation (here varying between 8 and 50 percent) of this kinetic energy and how much can be extracted from this kinetic energy because of technical aspects of the turbines are two critical assumptions in these calculations, even though the estimate of global kinetic energy in the atmosphere is fairly robust and yields probably over 1,000 TW (here varying between 10 and 50 percent). Wind energy from the Earth's atmosphere is likely to be in the single digits of TW, which is a reasonable estimate. Figures like this must be contrasted to the entire energy consumption of mankind, which is estimated to climb to 30 trillion kilowatts (947 trillion kilowatts) by the middle of the century and 45 trillion kilowatts (1420 trillion kilowatt-hours) by the year's end. This comparison shows that wind energy can only be a portion of the solution for a sustainable supply of renewable energy for humanity. Other renewable energy sources must be used in conjunction with wind and solar

power. In addition, it is projected that even 10% of the available wind energy will have a significant impact on the climate of the Earth [7].

1.8. PRESENT STATUS OF WIND ENERGY GENERATION

By the end of June 2015, the global wind energy conversion capacity had reached 370 GW, of which 32.1 GW had been added in the first six months of the year [7].

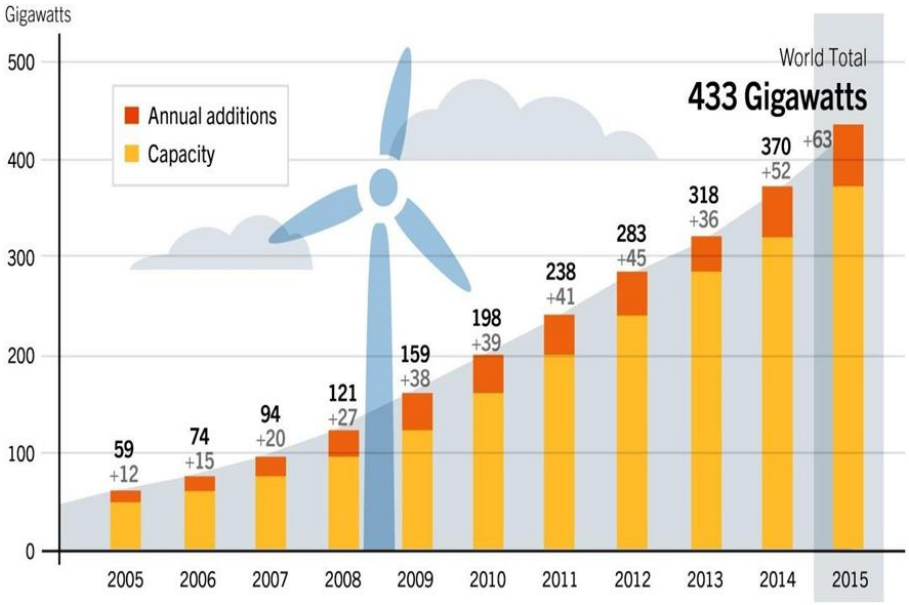

Figure 1.6. Wind power global capacity and annual addition 2005-2015 [7].

Following the United States (65.4 GW) and Germany (6.8 GW), China has built the most of this infrastructure (72.8 GW) (nearly 38 GW). Both Spain and India have an installed capacity of 31.2 GW. Since the end of 2009, China has more than quadrupled its production capacity. About 5.5% to 7.3% of the world's energy needs are met by this 370 GW. By the end of 2015, it accounted for 9.5% of net German electric energy consumption in Europe. These shares are expected to rise significantly during the next 20 years. Despite ambitious aspirations, offshore wind energy generation is still in its infancy. At the end of June 2014, the installed capacity in Germany was just 1.21 GW, or less than one percent. The global installed capacity of 370 GW is already a significant percentage of the wind energy that is now accessible. By extrapolating the data for the first half of 2015, we can estimate that this installed capacity is growing at

a pace of about 15% per year. In only six years, the value would have doubled, and in over 18 years, it would have increased tenfold. About 20–30 years into a constant rise in installed capacity of 15% per year, the anticipated limitations would be met. As a result, it is unlikely that the current growth rate will continue for an extended period of time [7].

1.9. TYPES OF WIND TURBINES

Wind turbines may be classified into two broad categories: horizontal-axis wind turbines (HAWTs) and vertical-axis wind turbines. There are many different types of turbines on the market today (VAWTs). In keeping with the name, the rotor shafts of each turbine are oriented in a certain way. The blade axis for HAWT machines is horizontal, but the axis for VAWT machines is vertical [8].

1.9.1. Horizontal Axis Wind Turbines (HAWT)

Wind turbines with a horizontal axis Wind turbines of the HAWT design category are what most of us picture when we think of them. The blades of a HAWT resemble those of a propeller and rotate horizontally, similar to those of a windmill. As seen in Figure 1.7, horizontal-axis wind turbines have their main rotor shaft and electrical generator located at the summit of a tower (Figure 1.7). As a general rule, big turbines are directed by wind sensors connected with a servo motor, whereas small turbines often employ a simple wind vane located square to the rotor (blades). Most big wind turbines contain a gearbox that converts the slow revolution of the rotor into a quicker rotation that is more suited to powering an electrical generator. Turbulence is created behind a tower, hence the turbine is normally positioned upwind of the tower to reduce this effect. Stiff wind turbine blades are designed to avoid being forced into the tower by heavy winds. In addition, the blades are positioned far from the tower and are occasionally slanted slightly upwards. However difficult it may be to maintain them aligned with the wind, downwind machines have been developed because to the fact that their blades may be permitted to bend during strong winds, reducing their swept area and hence their wind resistance. Turbulence can cause fatigue failures, which is why most HAWTs are located upwind [8-45].

Figure 1.7. Types of horizontal axis wind turbines [61].

1.9.2. Vertical Axis Wind Turbines (VAWT)

Wind turbines that have their axis of rotation perpendicular to the wind direction are known as vertical axis wind turbines. Because of this, they are more efficient than their horizontal axis counterparts. Figure 1.8 shows the various types of vertical axis wind turbines. In the next chapter, we'll studied the advantages of VAWTS, a more current version of the vertical axis wind [9-49].

Figure 1.8. Types of vertical axis wind turbines [60].

1.10. OBJECTIVES

Compared to other types of wind turbines, vertical axis turbines have various benefits. As an example, the VAWT doesn't require any yaw devices, and it may be erected in places where higher structures are not permitted. Furthermore, the VAWT may be lowered so that its moving components can be maintained more easily. To put it simply, the VAWT was chosen as the topic of this study because of these benefits. The aerodynamic design and performance analysis of the VAWT will be the focus of the research. Gharyan's representative meteorological station is used in the first phase of this study to examine the city's wind energy and wind evaluation. An aerodynamic analysis will be conducted in the second stage of this research to ensure that a suitable vertical axis wind turbine performs to specification. Actual field data from Gharyan city will be used to design this project. Calculations of average wind speed, design wind speed, and yearly energy will be made using the collected wind data. The information gathered here will be used as inputs in the design process. It will be studied in the third stage of this project thesis how different shape parameters affect the

performance of the Darrieus wind turbine for a variety of tip speed ratios ($0.1 < \lambda \leq 7$), using the blade element theory and momentum theory [21-43].

CHAPTER 2

VERTICAL AXIS WIND TURBINE

2.1. OVERVIEW

For VAWTs, the shaft of the rotor is placed vertically, making them known as VAWTs. Due to this configuration, the wind turbine does not have to be oriented toward the direction of the wind. In areas where the wind direction changes often or where there are turbulences, this can be advantageous. It is easier to maintain a tower with a vertical axis since the generator and other essential components may be situated near the ground. When rotating towards the wind, a VAWT's fundamental flaw is that it causes drag. Vertical-axis turbines are difficult to put on towers, thus they are generally installed closer to the ground or the roof of a structure. A smaller turbine might generate less power since the wind speed is slower at a lower height. Wind turbines with vertical axis may be roughly classified into three categories [21-24]:

- Darrieus type.
- Savonius type
- H-Rotor type

Brief descriptions of these VAWT types are given below.

2.2. DARRIEUS WIND TURBINE

Due to its resemblance to a gigantic Eggbeater, Darrieus wind turbines are often referred to as "Eggbeater" turbines. Their high efficiency is offset by substantial torque ripple and cyclic stress on the tower, which leads to a lower level of dependability. In addition, owing of the low beginning torque, they typically require an external power source or an extra Savonius rotor to begin rotating. As more blades are used, the rotor

becomes more solid and the torque ripple is decreased [9]. The area of the blades relative to the rotor area is one way to gauge the solidity of a machine. An exterior superstructure attached to the top bearing holds up the newer Darrieus type turbines, which do not use guy-wires. See Figure 2.1 [9-21].

Figure 2.1. Darrieus wind turbine [58].

2.3. SAVONIUS WIND TURBINE

Many items, such ventilation and anemometers, rely on Savonius drag type turbines because of their excellent dependability. It is because they are a drag type turbine that they are less efficient than a HAWT. When it comes to turbulence and self-starting, Savonius are the best. See Figure 2.2 [9].

Figure 2.2. Savonius wind turbine [58].

2.4. H-ROTORS

It was discovered that the intricate mechanisms used to feather Darrieus VAWT blades with straight blades were superfluous, which led to the development of H-Rotors in the UK throughout the 1970s and 1980s (Figure 2.3). It was discovered that the opposite blade's (in the flow of the wind) ability to move the entire blade arrangement forward would be limited by the drag/stall effect generated by a blade exiting the wind flow. As a result, the H-Rotor was able to maintain its ideal rotational speed regardless of the wind speed [9].

Figure 2.3. H-Rotor-type VAWT [58].

2.5. THE MAIN COMPONENTS OF DARRIEUS TYPE VAWT

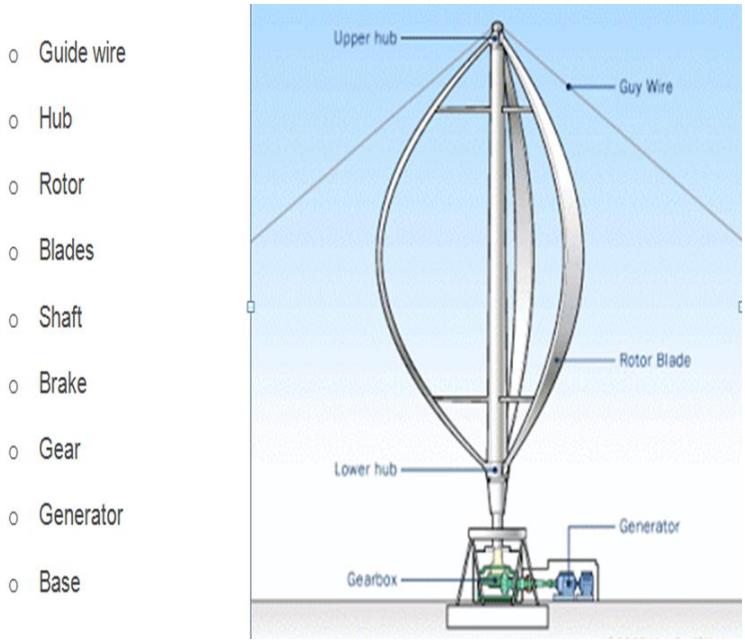

Figure 2.4. The main components of Darrieus type VAWT [16-48].

2.5.1. Guides Wire

Guide wires are often required for vertical axis wind turbines in order to hold the rotor shaft firmly in place and to minimize mechanical vibration [48].

2.5.2. Hub

When the rotor's blades are joined to the hub, it's called a hub. For the most part, cast iron or cast steel is utilized. Blades in VAWT are linked to VAWT's top and lower hubs at two places [48].

2.5.3. Rotor

A wind turbine's rotor is its beating heart, and it's made up of a hub and several rotor blades. Turbine components are responsible for capturing wind energy and converting it to mechanical motion. The rotor's ability to harvest more energy from the wind rises in direct proportion to its increased diameter. As a result, wind turbines are frequently constructed with a specific diameter rotor and a specific amount of expected wind energy [48].

2.5.4. Rotor Blades

When it comes to wind turbines, rotor blades are an essential and basic component. Aluminum, fiber glass, and carbon fiber are the most common materials because they offer the best strength-to-weight ratio. Additionally, the design of individual blades impacts the rotor's overall shape. The rotor blades "catch" the wind's kinetic energy and transform it into rotational energy for the hub. Blades for the Savonius wind turbine (VAWT) come in two flavors: drag force and lift force (Darrieus and giromill wind turbine) [48].

2.5.5. Shaft

The turbine blades turn the shaft, which is referred to as the "rotor." The generator, located inside the main housing, is connected to it through this cable [48].

2.5.6. Mechanical Braking

There are certain turbines that use a mechanical brake on a low-speed shaft between the turbine and transmission instead of the high-speed shaft between the transmission and generator. Wind turbines may be stopped in an emergency by using a mechanical drum brake or disk brake. As a backup to the rotor lock mechanism, this brake holds the turbine still for maintenance. In order to prevent a blaze in the nacelle, mechanical brakes are only utilized to slow the turbine down by 1 or 2 rotor RPM after the blades have been furled and electromagnetic braking has been applied. A brake applied at rated RPM increases turbine load. Hydraulic systems drive these mechanical brakes, which are then connected to the main control box [48].

2.5.7. Gear Box

For the generator to run faster, the gearbox must take the low shaft rotational speed and boost it to a higher level. Plantary, helical, parallel shaft, spore, and worm gear stages are all examples of gear stages. Gears of different sorts can be mixed and matched in various ways. Aluminum alloys, stainless steel, and cast iron are used in their construction [48].

2.5.8. Generator

Generating power from mechanical rotational motion is what a generator does. Over the years, several generator types have been employed in wind energy systems. The generator is located behind the turbine rotor hub in a nacelle on the top of a tower for large, commercial horizontal-axis wind turbines. Wind turbines often use asynchronous machines, which are directly connected to the grid, to create power. The normal rotation speed of a wind generator is 5-20 rpm, but the electrical speed of a directly linked machine is between 750-3600 rpm; this is because the speed of the wind generator is slower than the speed of the electrical network. An internal gearbox is therefore installed in-between each of these components. As a result, the generator's overall cost and weight are both reduced [48].

2.5.9 Base

The roof of the structure on which the VAWT is mounted serves as the typical base [16-48].

2.6. ADVANTAGES OF VERTICAL AXIS WIND TURBINE

A vertical axis wind turbine has the following advantages: It is possible to install the generator, gearbox, and other components on the ground, eliminating the need for the tower to support them and making maintenance easier. There are many places where the wind turbine may be installed: roofs, hills, mesas and passes, to name just a few. There's no need for a yaw mechanism to maintain the rotor pointing into the wind because the blades are already upright. When compared to a horizontal axis wind turbine, this one is noticeably more peaceful-sounding. A vertical axis wind turbine is particularly beneficial in residential and urban areas since it can be installed on roofs. Even in areas where higher constructions are forbidden, they can be erected. The highlands, where they can power mountain lodges in the worst of the weather, are a good fit for these generators [10].

2.7. DARRIEUS AND STRAIGHT BLADED ROTORS

Templin did some of the earliest theoretical work on the Darrieus turbine. To estimate the turbine's performance, he relied on the single stream tube model. Geometric and aerodynamic characteristics were tinkered with in order to see what would happen. Drag coefficient of the airfoil section. Figure 2.5(a) demonstrates the solidity of the turbine and Figure 2.5(b) the H/D ratio as well. Be aware that the power coefficient is defined as the quotient between the actual power and the highest possible Glauert value. Templin relied on this information to determine the portion of an aerofoil to utilize. Found in Eastman N. and Sherman's Jocobs [21-43].

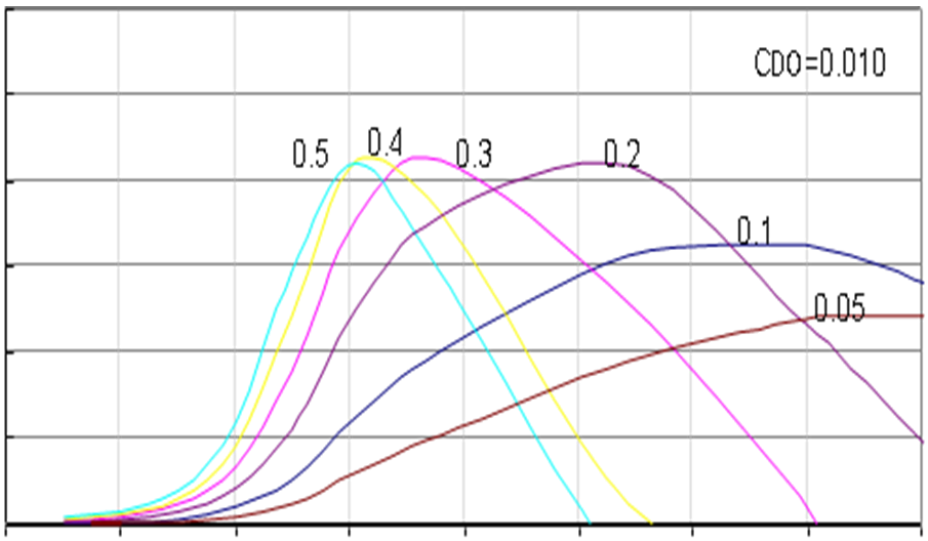

(a)

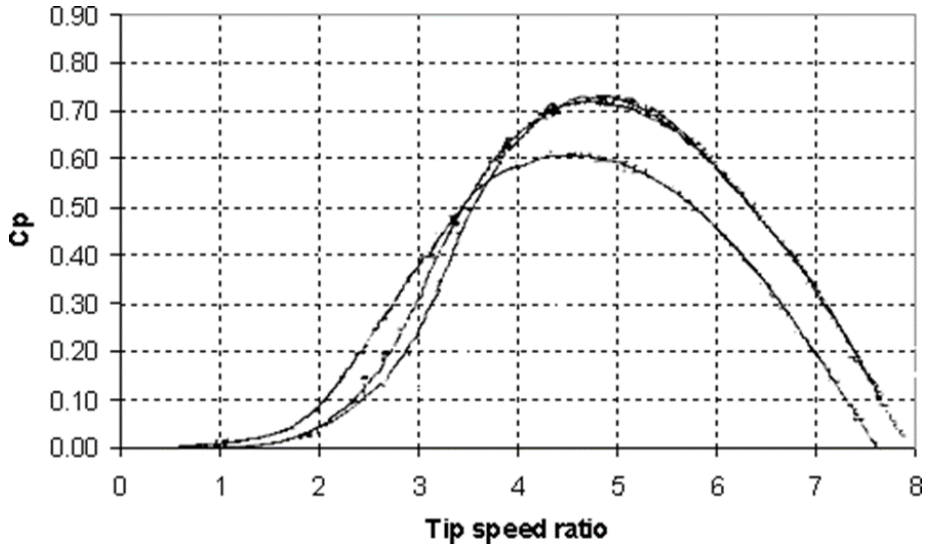

(b)

Figure 2.5. Effect of solidity NC/R (TEMPLIN) [21-43].

2.8. PREVIOUS RESEARCHES

Efficiencies of horizontal axis and vertical axis wind turbines are comparable. However, its modest initial torque is a significant drawback. Prior work on Durries and straight-blade rotors was discovered through a literature review. In 1974, Templin developed the first and most straightforward approach for predicting the performance parameters of a Durries-type VAWT [43]. A single stream tube is considered to

contain the whole turbine in this concept. This was the first model to combine the windmill actuator disc theory into a Durries-type VAWT analytical prediction model. By using the equation of stream wise drag with the change in the axial momentum of the disc, a constant induced flow velocity (rotor axial flow velocity) is achieved. r. Keep in mind that the power coefficient is defined as the ratio between the actual power and the maximum Gluer value, which can be found here. Templin [27] utilized aero foiled section data. In Jacobs, Eastman N. and Sherman [28], was taken. Low tip speed ratios were not addressed in this study. Walton and Jest [29] the influence of Reynolds number on the Durries turbine's aerodynamic performance was examined. This study's analytical framework is mostly derived from Templin [27]'s 1974 formulation. Performance estimation should take into account the influence of a fluctuating Reynolds number, according to this study. Using the single stream tube model, Noll and Ham published an analytical technique in 1980 for the prediction of performance of a cyclically pitched straight-bladed vertical-axis wind turbine. They incorporated the effects of strut drag, turbulent wake condition, and dynamic stall into their technique of analysis. – Wilson and Wiseman [15] improved on the single stream tube model in 1974 by introducing the multiple stream tube model. Fig. 8 depicts the aerodynamically independent parallel stream tubes used to split the swept volume of the turbine in this model. After that, for every stream tube, we apply the blade element and momentum theories. Because of this, they used a viscous and incompressible flow to calculate the induced velocity via the stream tube in their model. To calculate the induced velocity, just the lift force is included. Another multiple stream tube model for a Durries type VAWT was presented in 1975 by Strickland [16]. Only when a blade Reynolds number is similar to the test Reynolds number in Figure 2 does the multiple stream tube model exhibit strong agreement with test results (nearby 4 of tip speed ratio). Because he utilized just one constant representative blade Reynolds number, which really changes along the blade of DWT with rotational speed and incoming air velocity in the study, it exhibited a discrepancy with test results at other spots. As a result, investigating the DWT performance prediction while substituting a constant representative Reynolds number for the local blade Reynolds number is critical. For the same calculation, Wilson employed theoretical lift force exclusively, but Strickland included drag force as well. This is the primary difference between Wilson's model and that of Strickland. As compared to Strickland's model, Wilson's model

provides faster convergence because of its reduced complexity. Using numerous stream tube models, Maracas et al. offered another hypothesis that included the impacts of airfoil shape, support struts, blade aspect ratio, turbine solidity and blade interference, among other things. [14]. the flow across a flat plate is used to examine the impact of flow curvature. Using a flat plate with a changing angle of attack, they constructed an equation of lift distribution from the leading edge to the following edge points and averaged the dispersed lift force. For a small chord-to-radius ratio, the influence of flow curvature on performance parameters is negligible, according to them. When Sharpe published his report on the multiple stream tube concept in 1977, he went into great detail about the idea. Strickland's model has a lot in common with his model. The Reynolds number impact was also included into the equation [13]. Read and Sharpe introduced an updated version of their multiple stream tube model in 1980 [18]. A Darrieus rotor was studied by Sharpe, who did both an analytic and experimental research. He predicted the Darrieus rotor's performance over a wide range of Reynolds numbers using the multiple stream tube hypothesis. A DC motor was used in an open jet wind tunnel to allow the unloaded turbine to accelerate freely in a continuous flow of air, allowing the experiment to be carried out. Theory showed that the Reynolds number has an effect on the rotor performance [11]. For symmetrical airfoils, the multiple stream tube hypothesis was shown to predict superior results when Reynolds number data was used. At low Reynolds numbers, theoretical and experimental results were found to be in close agreement. The Darrieus rotor's performance may be predicted using different stream tube modes, which Shankar used. The results of this investigation were based on NACA 0012 section blades. Critzos et al. (1955) provided the assumed sectional parameters used in this study. A section Reynolds number of 3 x 105 is assumed for all calculations.

All forces operating on the blade were assumed as quasi-steady, and no interaction between the blades was neglected in the study.. Using a straight bladed vertical axis wind turbine, Healy investigated the effect of blade thickness on the turbine output. Reynold's number and tip speed ratios from 2.25 to 3.0 have been used to derive the power coefficients of NACA profiles 0009, 0012, 0015 and 0018, respectively [51-53]. The lift and drag coefficients for a particular angle of attack and blade Reynolds number were interpolated using a common subroutine to calculate the aerodynamic

coefficients from data. The multiple stream tube modal was used as the basis for the computer application. The computed findings showed that the greatest power coefficient for all profiles was attained at the maximum turbine Reynolds number and was about, at solidity around. Generally speaking, thicker profiles are better at lower Reynolds numbers because, at a given angle of attack, separation happens far more frequently from thin profiles than from thicker ones. Rotor performance at low speed ratios ($\lambda < 2.0$) is not shown in this result. A simple variable pitch mechanism was explored by Kirke and Lazauskas in order to obtain the required combination of strong beginning torque and good efficiency at running speed for straight bladed vertical axis wind turbines. An easy-to-use, low-cost pitch control system that relies on aerodynamic and inertial forces to regulate the blade pitch's amplitude was developed by the inventors. Theoretically lead to more performance gains. Straight bladed VAWT with a sailwing tested by Murai, Maruyama, and Tsukui by varying several parameters such as the tension of trailing edge wire, membrane material, and leading edge shape on the turbine performance is difficult to use with Darrieus turbines. They came to the conclusion that the tiny sailwing had better performance than a Savonius rotor, but was inferior to a huge Darrieus wind turbine. Even though it had a lesser tip speed ratio than a rigid-wing vertical-axis wind turbine, the maximum power coefficient was found to be smaller yet. Using these facts, small and medium-sized wind turbines can reduce the rotation speed and centrifugal force on the blade, which is the major structural issue. It is obvious from prior studies that the H-rotor wind turbine's performance at low tip speed ratios ($0 < \lambda < 1$) was not examined in any of the previous investigations [1-2-3].

CHAPTER 3

WIND ENERGY AND WIND ASSESSMENT

3.1. INTRODUCTION

The speed of the wind is the most important element affecting the amount of electricity generated by a wind energy conversion system. In light of the cubic connection between velocity and power, even a little change in wind speed may have an enormous effect. Identifying a good location for a wind energy project requires finding a location with strong and remarkable wind spectra [17].

3.1.1. Causes of the Wind Power

Even though the sun's heat is constantly being absorbed by the Earth, its release into the atmosphere is unevenly distributed. Where there's less heat released (cold air zones), atmospheric gas pressure rises; where there's more heat released (warm air zones), gas pressure lowers. Convective movements generate a macro-circulation as a result of this: heated air masses rise, reducing density as they do so, and suck colder air from below. Moving air masses produces a persistent high and low-pressure region in the atmosphere, which is also affected by the rotation of our planet (Figure 3.1). Wind is the movement of an air mass, either quickly or slowly, across locations of differing pressure. The faster the air moves and the stronger the wind, the bigger the pressure differential. with the low-pressure system, whereas in the northern hemisphere it veers toward Instead of blowing in a clockwise way around high pressure areas and counterclockwise around low pressure areas like you might expect, wind actually circulates in the other direction. To put it another way, in practice, a sailor who is facing the wind has the low pressure region *B* and the high pressure area *A* (Figure 3.2) [19].

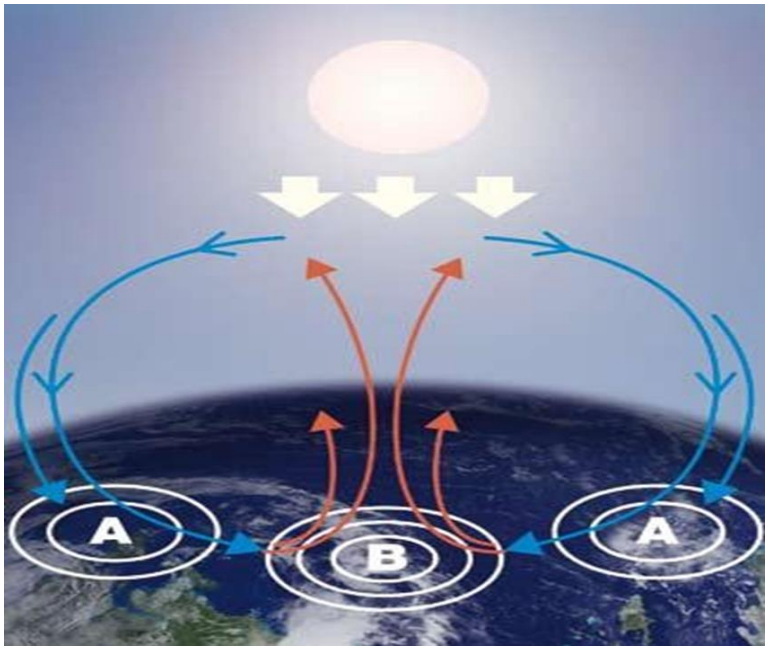

Figure 3.1. Wind flows [19].

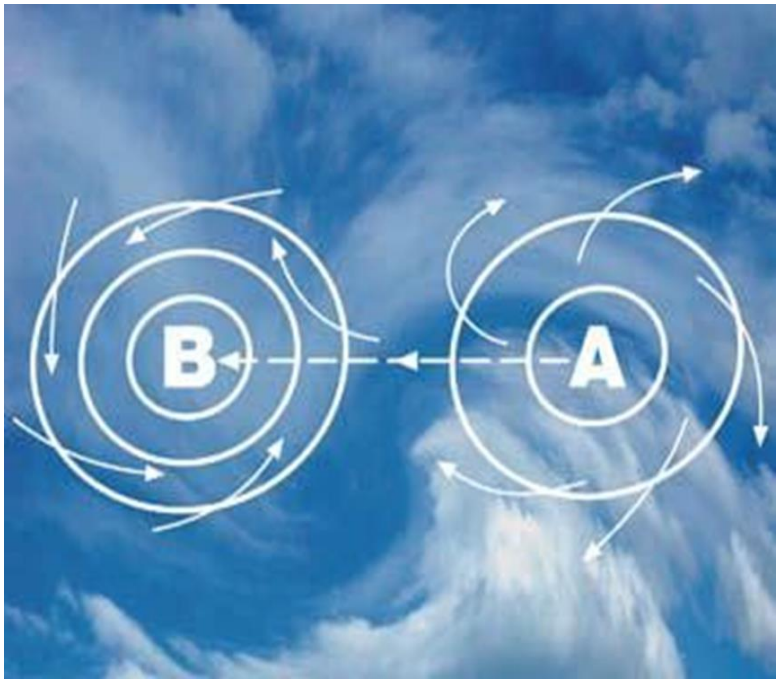

Figure 3.2. Global wind flows [19].

Instead, it's the other way around in the southern hemisphere. On a wide scale, at different latitudes, there is a cyclical movement of air masses that is affected by the seasons. Sea and earth breezes are formed because of a distinct difference in temperature between land and ocean masses. There are several factors that influence

how the wind behaves in a given area, including landform, topography, and weather. For example, big and flat areas like the sea tend to have a higher wind intensity because of this. For one thing, winds are more intense at the tops of hills or in valleys that are parallel to the primary wind's path, whereas they are slower and less powerful on uneven terrain like that found in cities or woods. Atmospheric stability also affects wind speed relative to altitude [19]. Wind is the name given to the movement of air masses in the atmosphere, which can have a variety of reasons. The sun's heat on the Earth is the first and most significant of them. As a result, wind energy consumption is a sort of solar energy usage in an indirect manner. It is the earth's surface that absorb and then return solar energy to the atmosphere above. Solar energy absorption varies with geographic location, time of day, and year since the earth's surface is not uniform (land, lake, desert, forest) and so the absorption of solar energy varies. Because of this non-uniform heat absorption, the air masses will migrate from one area to another because of the resulting changes in temperature, density, and pressure. There is a big difference in solar energy absorption between the tropical and the polar parts of our planet. As a result, the tropical regions warm up and the polarregions get colder, causing a powerful convection current to flow between them. As a result of the rotation's Coriolis forces, air masses in the northern hemisphere are deflected to the right, and those in the southern hemisphere to the left. The spiral motions of air equalization caused by this mechanism are well-known from cloud images of low pressure zones [20]. At a reasonable altitude, the Earth's rotational influence becomes noticeable. The angular momentum of each air particle is west-to-east oriented. The closer the particle gets to the axis of rotation of the Earth, the closer it gets to the poles. It is because of the law of conservation of momentum that the velocity component increases from west to east as we go nearer to the pole. West drift, the reverse of global wind direction, is caused by this phenomenon and is less severe nearer to the Equator (Figure 3.3). Surface friction lowers wind velocity close to the ground, which lessens the influence of the Coriolis forces as well. Therefore, geotropic winds are deflected less than wind near the earth. In addition to these large-scale equilibration motions in the atmosphere, small-scale topographic conditions also affect wind flows. Temperature rises faster on steep slopes facing the sun, for example. Large continuous forest areas have distinct heating and cooling patterns from those of water surfaces that are close by. Jet-like effects may be created by valley cuts that are designed to follow

the primary wind direction. If wind turbines are to be installed in the area, these factors must be taken into account when deciding where to put them. However, they may also be used to their benefit. The air travels in parallel lines of equal pressure at higher altitudes (isobars). Geotropic wind is the term used to describe the movement of air masses above a height of roughly 600 meters. There are no surface impacts on the airflow. Because of this, it is possible to sense Earth's surface at lower altitudes as well. The boundary layer refers to this portion of the atmosphere. The intensity of the geotropic wind, surface roughness, Coriolis effects, and temperature impacts are the primary determinants of boundary layer parameters [19-22].

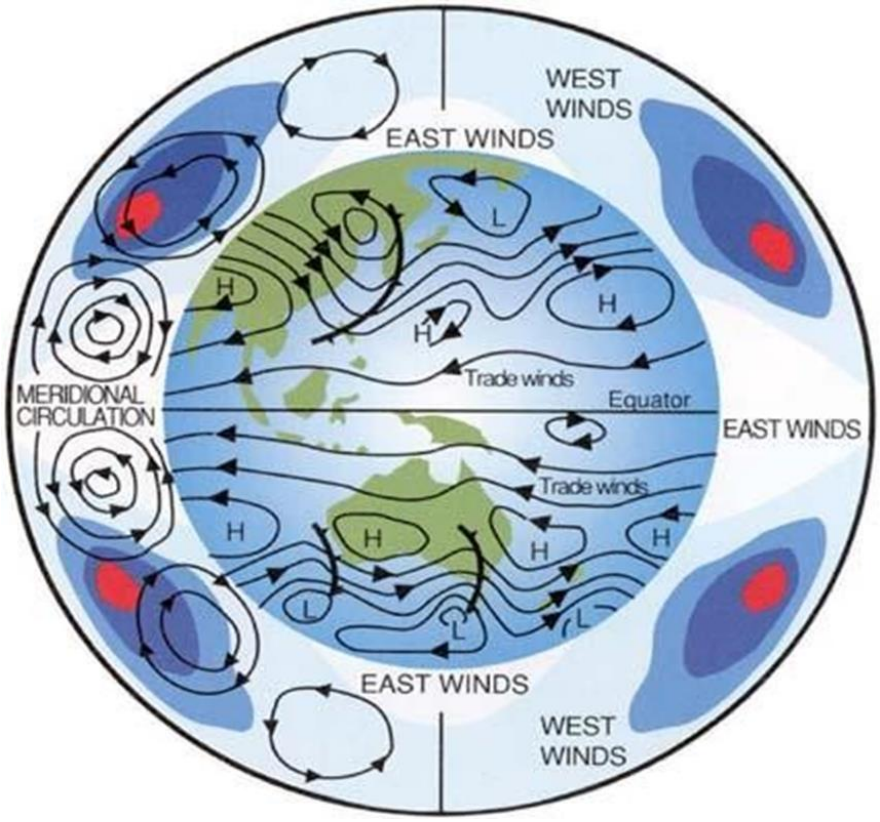

Figure 3.3. Wind flows circulation [22].

Only 2% of the $1.5\times1018\,kWh$ of solar energy that the earth's atmosphere collects each year gets turned into energy for air motion. Despite this, a wind power estimate of $4\times1012\,kWh$ is produced. This is a hundred times greater than the total output of all the power stations on the planet [22].

3.2. CHARACTERISTICS OF THE WIND

To correctly predict the performance of any wind turbine, it is required to have a thorough understanding of the characteristics of the wind and its velocity ($p \propto U_{\infty}^{3}$) [23].

Many variables must be understood about the wind, including its average speed, short-term fluctuations around that speed (called gusts), daily, monthly, and yearly peaks and valleys, and variations with altitude. Measurements taken over an extended period of time at a single location are the only way to accurately identify these site-specific factors. They are used to evaluate the economics and performance of a wind farm. We will be collecting, evaluating, and analyzing data that has already been collected [21-23].

3.2.1. Variation in Time

Wind speed changes may be broken down into the following categories based on time [54]:

- **Inter-annual variations**
  On a time scale longer than a year, these kinds of fluctuations in wind speed are common. An accurate assessment of a site's long-term average wind speed is equally critical to an accurate assessment of its interannual variability [54].

- **Seasonal and monthly variation**
  Latitude and position in relation to certain topographic features, such as land masses and water, influence the amount of seasonal variation in wind at a given location. While mid-latitude continental sites are prone to strong winds in winter and spring, coastal mountain passes are prone to strong winds in summer [54].

- **Diurnal variation**

Deferential heating of the Earth's surface throughout the daily variation cycle causes this sort of wind speed fluctuation. It is common for wind speeds to climb throughout the day and fall between midnight and daybreak as a normal diurnal fluctuation [54].

- **Short-term variations**

  Generally speaking, short-term variations are defined as changes that occur within 10 minutes or less. Since the wind speed changes constantly, so does the wind's energy content. In addition to turbulence and gusts, short-term wind speed fluctuations are of relevance [54].

The term "turbulence" refers to the random changes in wind speed that are imposed on the average wind speed. There are oscillations in all three directions (longitudinal, horizontal and vertical) in a turbulent wind field, whereas gusts are distinct events [54].

3.3. WIND DATA COLLECTION

The Gharyan station's hourly wind speed data from 2012 to 2016 has been statistically examined as part of this research. To make statistical analysis easier, the wind speed data in time series format are commonly organized in the frequency distribution format. Translated frequency distributions were created using the available time-series data sets. At the Gharyan station, a cup generator anemometer continually recorded the wind speed at a height of 10 meters or at actual height 50 meters. A three-hour average of the constantly collected wind speed data was used to calculate hourly values for this project [44].

3.4. WIND ASSESSMENT

Prior to doing any analysis of wind energy potential, it is necessary to choose a location for gathering wind speed and direction data. All-year-round data collection for a comprehensive wind resource evaluation is made possible only by using a network of anemometers connected to a computer network at wind resource monitoring stations. As this procedure takes some time, specialists also use earlier data to acquire a better

sense of the long-term wind patterns. In our situation, there are a number of credible data sources, like airports and climatological institute that may be used to obtain current weather information. Because high wind speeds are recorded on these areas, they may be added to existing data sets for the selection of possible turbine installation sites [54]. Figure 4.1 shows the several stations in that area where data was continually collected using a cup generator anemometer for this study's high points [44].

3.4.1. Wind Regime Analysis

In evaluating wind resources, analysis is an obvious next step after data gathering, since it aids in understanding current patterns in wind direction, duration, and amplitude.

$$V_m = \frac{1}{N}\sum_{i=1}^{N} V_i \tag{3.1}$$

(V_m) or the average/mean wind speed, may be used as a standard metric to demonstrate the wind's potential [1–41]. Here, N stands for the number of samples, and (V_i) is the wind speed recorded during the (i) observation. Using such a big sample, the wind speed data can be divided into intervals and a histogram may be generated to demonstrate the distribution of wind speed.

3.4.2. Power Exponent and Logarithmic Function

Because of the friction between the earth and the air, the wind speed is zero at the ground's surface. At higher altitudes, the wind's speed does not rise as quickly as it does closer to the earth. Wind speed varies by zero at 2000 meters of elevation. Different functions can theoretically depict this fluctuation in wind speed, but the following two functions best reflect the average wind speed variation as it relates to height [9–24]:

Power exponent function:

$$V(Z) = V_R \left(\frac{Z}{Z_R} \right)^{\beta} \tag{3.2}$$

At Z_r (above ground level), wind speed is represented by $V(Z)$, the altitude Z represents by Z, and the roughness of the terrain is represented by β as an exponent. Generally speaking, β is somewhere around 0.1.

Logarithmic function:

$$\frac{V(Z)}{V(10)} = \frac{\ln\left(\frac{Z}{Z_0} \right)}{\ln\left(\frac{10}{Z_0} \right)} \tag{3.3}$$

Wind speed at 10 meters height is represented by $V(10)$, while the length of roughness (Z_0) is shown in Table 3.1. The β and Z_0 parameters are used to depict different kinds of terrain [18].

Table 3.1. Different terrians' roughness [42-46].

Type of terrain	**Roughness level**	**Z_0 (m)**	**β**
Watery areas	0	0.001	0.01
Country areas with limited	1	0.12	0.12
Surface features	2	0.05	0.16
Farmlands, hedges and	3	0.3	0.28

When the average wind speed has previously been estimated at a reference height, these two functions are used to calculate the average wind velocity at certain elevations. The power exponent function with a value of 0.12 is used in this investigation. Our samples represent in Table 4.2 in next chapter. It shows the average monthly wind speed based on our data in 2016 [42-46].

3.4.3. Wind Statistics

Studies show that the non-cumulative Weibull distribution, which assumes the following equation, best describes the distribution of wind speed [25,26]:

$$PF(V) = \frac{k}{C}\left(\frac{V}{C}\right)^{k-1} \exp\left\{-\left(\frac{V}{C}\right)^{k}\right\} \tag{3.4}$$

Cumulative Weibull distribution is as follows:

$$F(v) = 1 - \exp\left\{-\left(\frac{V}{C}\right)^{k}\right\} \tag{3.5}$$

In this function, C stands for the scale parameter, and k shows the parameter shape. The Weibull distribution conveniently approximates distribution of continuous wind speed using discrete values, which are practically observed. Moreover, it is useful because in an area, the wind regime can be explained using just k and C, which are Weibull parameters [25-26].

Graphical Method (GM) is through plotting on a graph $\ln V$ (logarithmic function of V) against $\ln\left(-\ln\left(F\left(V\right)\right)\right)$. In this case, "ln" represents logarithm of base e that fits a straight line through the points. Here, k is the slope of this line while C equals $\exp\left(\ln V\right)$, or simply V. The $\ln\left(-\ln\left(F\left(V\right)\right)\right)$ equals 0. The logarithms of cumulative Weibull distribution are taken twice to implement this technique [14].

Empirical Method (EM) is considered as special case of the moment method, where the Weibull parameters, k and C, are given (3.6) and (3.7) equations respectively [13-25]. The scaling parameter C and the parameter shape k are represented in this function. Using discrete values that can be seen in the real world, the Weibull distribution may be used to approximate the continuous wind speed distribution.

Furthermore, the Weibull parameters k and C may be used to explain the wind regime in a region [16-26]. Plotting $\ln V$ (the logarithmic function of V) versus $\ln\left(-\ln\left(F\left(V\right)\right)\right)$ is a graphical method (GM). Logarithm of base e, "ln" fits a straight line between the locations in this example. Here, k is the line's slope, and C is equal to $\exp\left(\ln V\right)$, or just V. No matter how you look at it, it is equivalent to zero. For this strategy to work, the logarithms of the Cumulative Weibull Distribution are multiplied by two [14]. Empirical Method (EM) is a specific example of the Moment Method in which the Weibull parameters k and C are (3.6) and (3.7) [13-25]:

$$k = \left(\frac{\sigma}{V_m}\right)^{-1.086} \tag{3.6}$$

$$c \approx \frac{V_m k^{2.6674}}{0.184 + 0.816 k^{2.73855}} \tag{3.7}$$

Where, σ, is the standard deviation of the observed data defined as [27]:

$$\sigma = \sqrt{\frac{1}{N-1}\sum_{i=1}^{N}\left(v_i - V_m\right)^2} \tag{3.8}$$

3.5. ERROR ANALYSIS

There are a number of ways to get the Weibull curve, and each technique has its own method of calculating the curve's inaccuracy. It's done by multiplying the square of Weibull frequencies by real frequencies to get a coefficient of determination known as R^2. Root Mean Square Error (RMSE) and Mean Bias Absolute Error (MAE) are defined in Equation (3.9) [28, 29, 30].

$$R^2 = \frac{\left(\sum_{i=1}^{N}\left(y_i - z_i\right)^2 - \sum_{i=1}^{N}\left(y_i - x_i\right)^2\right)}{\sum_{i=1}^{N}\left(y_i - z_i\right)^2} \tag{3.9}$$

y_i is the real frequency, Weibull is the frequency, and z_i is the average wind speed, where N is the number of observations (the number of actual data). The difference between the Weibull frequency and the actual frequency is measured by the root mean square error, or RMSE. It is defined in Equation (3.10) [28, 29, 30].

$$RSME = \sqrt{\frac{1}{N}\sum_{i=N}^{N}\left(y_i - x_i\right)^2} \tag{3.10}$$

MBE, The Mean Bias Error, is a measure of how closely the Weibull frequencies much with actual frequencies. It is calculated from Equation (3.11) as [28, 29].

$$MBE = \frac{1}{N}\sum_{i=1}^{N}\left(y_i - x_i\right) \tag{3.11}$$

A further metric derived is the Mean Absolute Error, or *MAE* is another measure found from Equation (3.12) [28, 29, 30].

$$MAE = \frac{1}{N}\sum_{i=1}^{N}\left|y_i - x_i\right| \tag{3.12}$$

3.6. WIND POWER DENSITY

A region perpendicular to wind flow's direction has its wind power density measured. The wind power density equation is as follows:

$$P_w = \frac{1}{2}\rho U^3 A_s \tag{3.13}$$

This amount of wind power available per unit area is

$$WPD = \frac{1}{2}\rho U^3 \tag{3.14}$$

The cube of the wind speed is used in this formula, which means that the power is inversely proportional to the speed. On the other hand, we have an expression that is independent of the size of a wind turbine's rotor when we divide power by area. Wind speed and air density are all that matter to WPD. Wind turbine size, efficiency, or any other factor is irrelevant for calculating WPD [31-32].

3.7. OPERATIONAL CHARACTERISTICS

3.7.1. Power Performance

The power curve of wind turbine is a graph that indicates how large the electrical power output will be for wind turbine at different wind speeds. With such a curve it is possible to predict the energy production of a wind turbine without considering the technical details of its various components. The power curve gives the electrical power output as a function of the hub height wind speed [24-41].

The power curves are derived from field tests using standardized testing methods, it is also possible to estimate the power curve for a given machine by theoretical calculations. Figure 3.4 presents an example of a power curve for typical wind turbine, it is indicating the following parameter [31-32].

- Cut-in speed, the wind speed at which the turbine starts to generate power.
- Rated wind speed, the wind speed at the turbine reaches rated turbine power. This is often but not always the maximum power.
- The cut-out wind speed is the wind speed where the wind turbine stops production and turns out of the main wind direction. Typically, the cutout wind speed is in the range of 17 to 21 m/s [31-32].

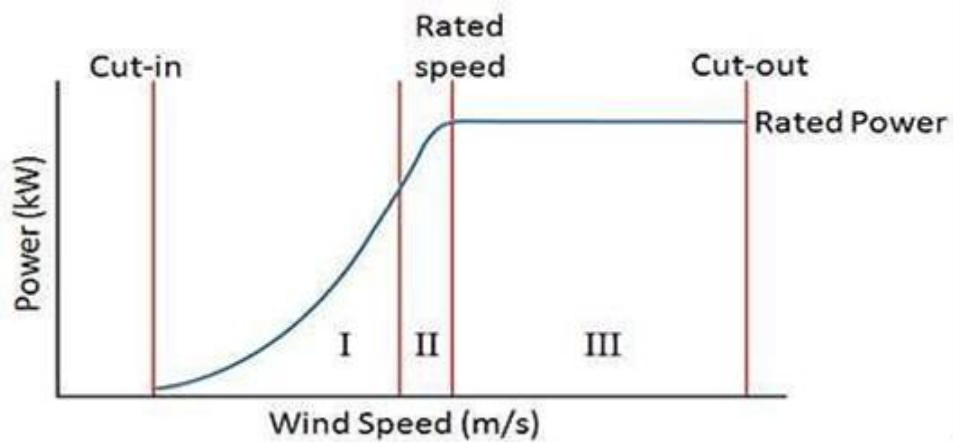

Figure 3.4. Power output from wind turbine as function of wind speed [31-32].

3.8. AVAILABILITY

The availability is the fraction of the time in a year that wind turbine is able to generate electricity. The times when a wind turbine is not available include down time for periodic maintenance or unscheduled repairs. The typical availabilities for modern wind turbines are 95-99 (%) better than many items of conventional generating plant. Useful power is only produced for wind speed between cut-in and cut-out wind speeds, depending on the wind conditions, the turbine will be operating at level than its availability [33].

Another measure is the capacity factor (Cf) is defined as the ratio of the actual annual energy output to the theoretical maximum output if the machine were running at its rated power during all the 8760 h of the year. The capacity factor is calculated as [33-41].

$$Cf\,(\%) = \frac{Actual\ Energy\ Output}{Rated\ Capacity \times 8760} x100 \tag{3.15}$$

There are several similar measures of power plant performance. To avoid confusion when comparing the performance of wind plant, the precise definitions of availability or load factor should be clearly understood [33].

3.9. ANNUAL ENERGY AND CAPACITY FACTOR

A wind turbine's yearly energy output is critical to determining the viability of a project, hence it must be estimated. Using long-term wind speed distributions and the turbine's power curve, we can estimate the amount of power generated at each wind speed across the year. Calculations should be done with a wind speed of 1 m/s for accurate results. the following formula may be used to express the annual energy production (AEP) of a wind turbine [37]. The wind speed, v_0 has a probability to fall between wind speeds v_i and v_{i+1}, which can be obtained through cumulative distribution function as given below:

$$F\left(v_i < v_0 < v_{i+1}\right) = \exp\left[-\left(\frac{v_i}{c}\right)^k\right] - \exp\left[-\left(\frac{v_{i+1}}{c}\right)^k\right] \tag{3.16}$$

Total yearly energy output is calculated as follows:

$$AEP = \sum_{i=1}^{N-1} \frac{1}{2}\left[P\left(v_{i+1}\right) + P\left(v_i\right)\right] \cdot F\left(v_i < v_0 < v_{i+1}\right) \cdot 8760 \tag{3.17}$$

$P\left(v_i\right)$ is the power output of a certain wind turbine at wind speed v_i and 8760 is the number of hours in the year [30-37].

In addition to generating real electricity, a wind turbine's capacity/load factor is a measure of how much energy it produces for a certain amount of time when the turbine is operating at its rated power level. For instance [15-28-29]:

$$Annual\ Load\ Factor = \frac{Energy\ Per\ Year\ (kWh)}{Rated\ Power\ (kW) \times 8760} \tag{3.18}$$

The power plant's performance may be assessed using a variety of approaches. A precise load factor and other characteristics should be taken into account when comparing the performances of various wind turbines. For computing Cf and AEP,

wind turbine specs and power curves must be supplied. In order to use Vestas (V60-850 kW), we'll need a low-rated wind speed and a 60-meter hub height (wind data is available for this height) [28-30,40]. The technical details of the turbine are listed in Table 3.2.

Table 3.2. Model wind turbine and its technical specifications [47].

Item		**Description**
Turbine		Vestas (V60- 850kW).
Configuration		3-blade vertical turbine
Rated Power	kW	850
Wind speed (cut-in)	m/s	3
Wind speed (rated)	m/s	13
Wind speed (cut-out)	m/s	20
Speed of rotor	rpm	14-29
Diameter of Rotor	M	60
Sweep area	m^2	2,828

Turbine power curve is demonstrated in Figure 3.5.

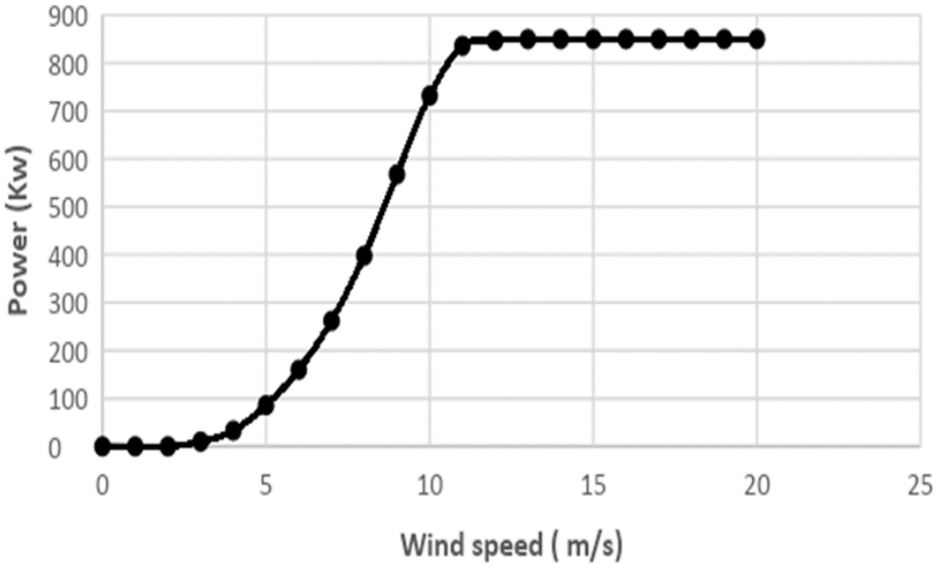

Figure 3.5. Vestas (V6050 kW) power curve [47].

3.10. COST AND ELECTRICITY PRICE

Using Equation (3.19) as a guide, evaluate each term's value to arrive at the present value cost (PVC). We used a procedure that has been used in other studies to calculate the numbers listed here [34, 35, 36].

$$PVC = I + C_{omr}\left[\frac{1+i}{r-i}\right]\times\left[1-\left[\frac{1+i}{1+r}\right]^{t}\right]-S\left[\frac{1+i}{1+r}\right]^{t} \tag{3.19}$$

Where, t is turbine life, I is investment, C_{omr} is eration, maintenance and repair cost, i is inflation rate, r is interest rate, S is scrap value.

From Equation (3.19), the price per kilowatt can be found by,

$$kWh\ price = \frac{PVC}{AEP\ X\ t}\times 100 \tag{3.20}$$

CHAPTER 4

STUDY AREA AND WIND CALCULATIONS

4.1. STUDY AREA

The feasibility of wind energy development depends on the particular social, economic, and physical characteristics of both study area and the wind resource. In this thesis one site is selected, as example to show wind energy availability in cost of Libya and to design a suitable by considering average wind velocity of Gharyan station, the location and properties of this site is shown in Figure 4.1 and Table 4.1 respectively.

Figure 4.1. The selected meteorological station [55].

Table 4.1. Physical features of the meteorological stations [44].

Station	Time Measurement	Elevation Above Sea Level (M)	Latitude (N)□	Longitude (E)□
Gharyan	2012-2016	693	32°10′01″	13°01′00″

4.2. MEAN WIND SPEED

The table and figures below show that at 50 m height, the maximum value (wind speed = 7.98 m/s) was measured at Gharyan 4. On the other hand, 5.43 m/s was the minimum value, which was observed at Gharyan 1. Table 4.2 shows the average monthly wind speed as meter per seconds and Table 4.3 shows the expected average monthly annual wind speed as meter per seconds and standard deviation as well. From Figure 4.2 to Figure 4.5, it shows comparing the average monthly wind speeds at our selected locations while Figure 4.6 shows the average wind speed per season. Figure 4.7 presents maximum frequency and mean wind speed of Gharyan 4 as well.

Table 4.2. Average monthly wind speed (m/s) [44].

Station	Jan.	Feb.	Mar.	Apr.	May	Jun.	Jul.	Aug.	Sep.	Oct.	Nov.	Dec.
Gharyan1	4.07	4.67	5.29	4.74	5.42	4.84	4.59	3.87	3.69	3.90	3.79	4.60
Gharyan2	4.42	4.66	5.40	4.90	5.17	4.98	4.61	4.24	3.94	4.31	4.44	4.66
Gharyan3	3.92	4.75	5.22	5.22	5.21	4.53	4.58	4.22	3.86	4.01	4.15	4.69
Gharyan4	4.52	4.84	4.47	5.05	5.22	5.43	5.41	5.09	5.12	4.84	4.58	5.38

Table 4.3. Expected average monthly annual wind speed (m/s), and standard deviation at height 50m for whole years [44].

Station	Jan.	Feb.	Mar.	Apr.	May	Jun.	Jul.	Aug.	Sep.	Oct.	Nov.	Dec.
Gharyan1	5.99	6.87	7.79	6.98	7.98	7.12	6.76	5.69	5.43	5.74	5.57	6.77
Gharyan2	6.5	6.85	7.94	7.2	7.61	7.32	6.78	6.23	5.79	6.34	6.52	6.86
Gharyan3	5.76	6.98	7.67	7.67	7.66	6.67	6.74	6.21	5.67	5.89	6.10	6.91
Gharyan4	6.65	7.12	8.04	7.43	7.67	7.98	7.95	7.49	7.53	7.12	6.74	7.91

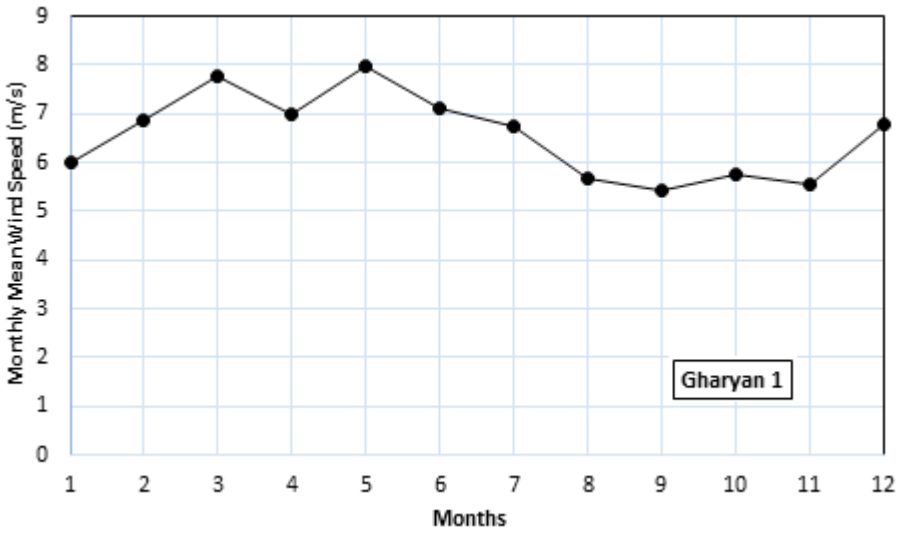

Figure 4.2. Monthly variation of wind speeds for Gharyan 1.

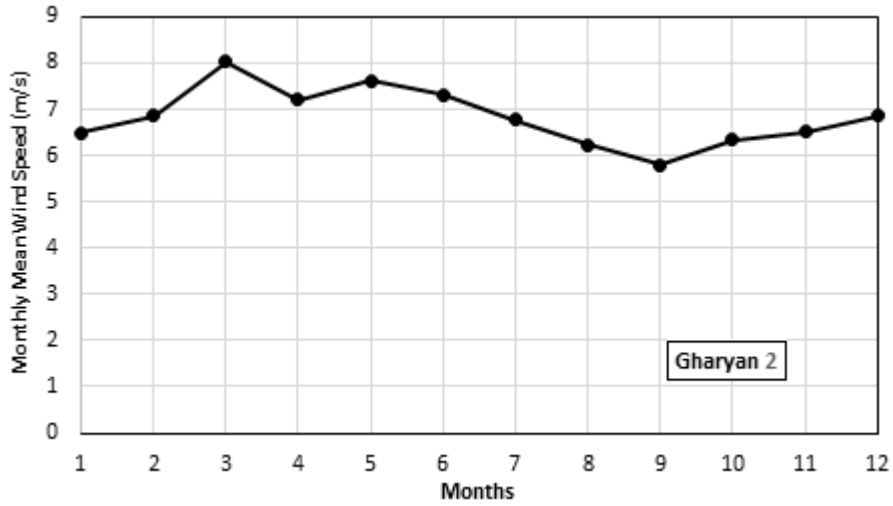

Figure 4.3. Monthly variation of wind speeds for Gharyan 2.

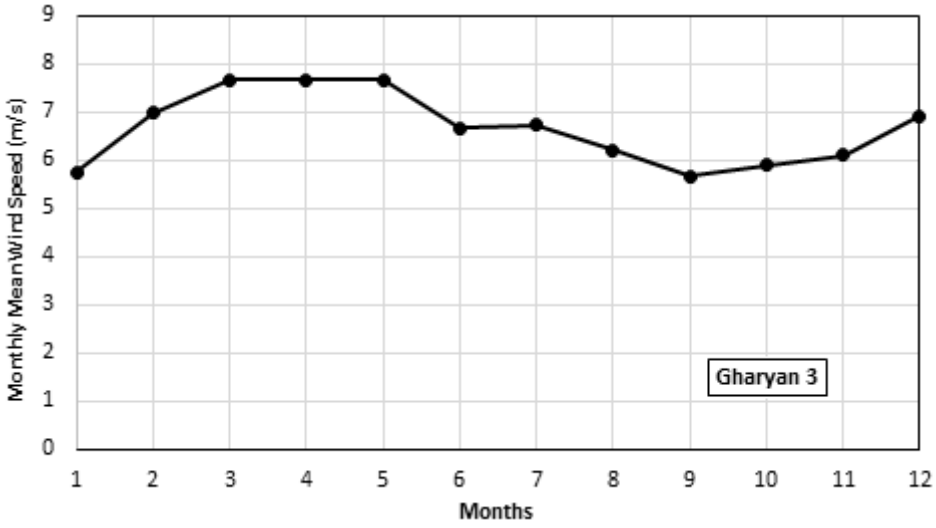

Figure 4.4. Monthly variation of wind speeds for Gharyan 3.

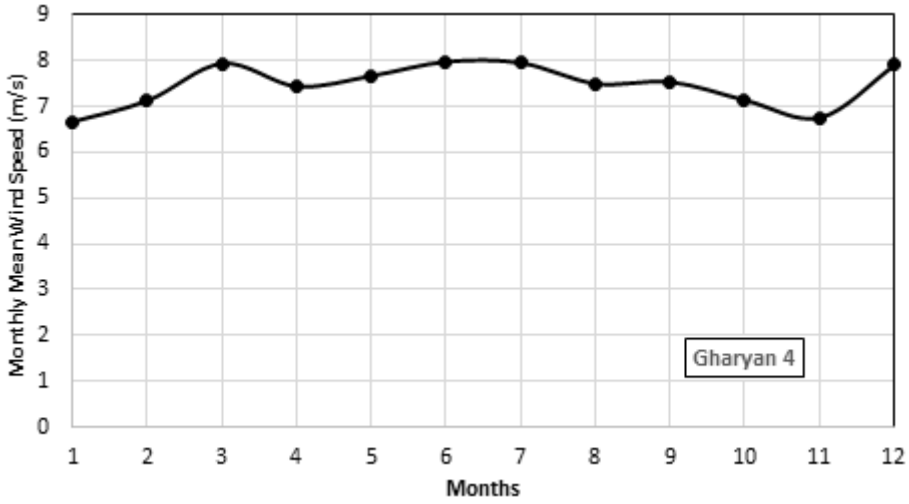

Figure 4.5. Monthly variation of wind speeds for Gharyan 4.

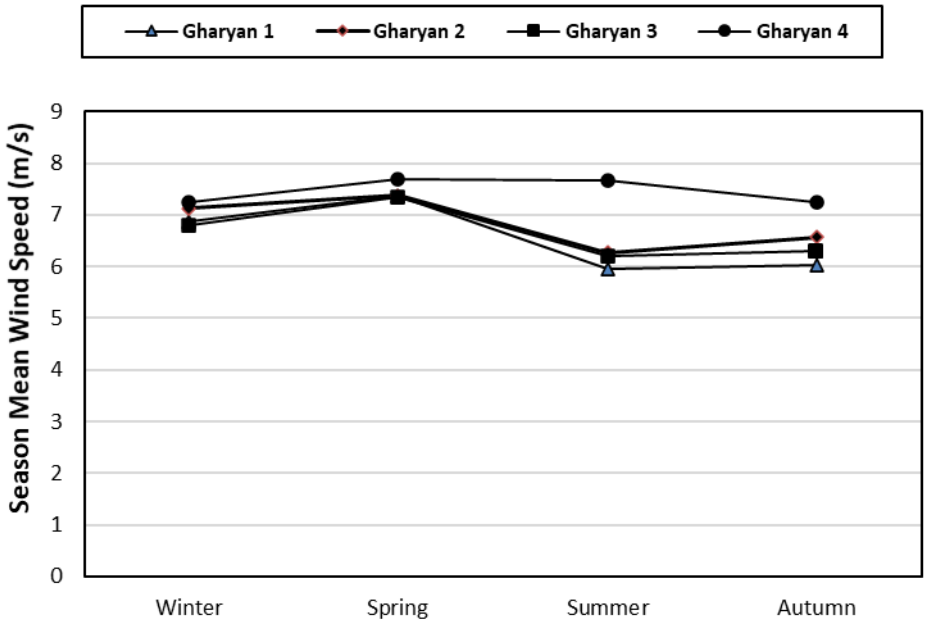

Figure 4.6. Seasons variation of wind speeds.

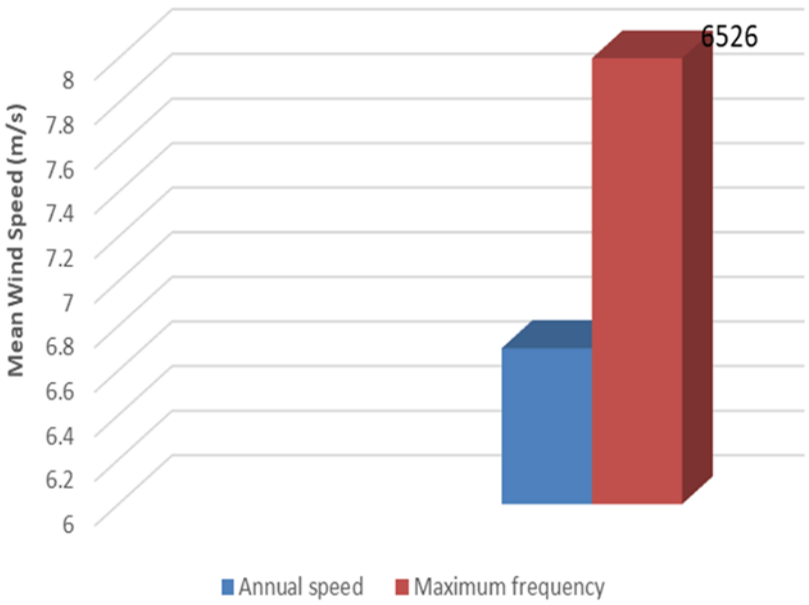

Figure 4.7. Maximum frequency and mean wind speed (Gharyan 4).

4.3. PROBABILITY DENSITY AND CUMULATIVE DISTRIBUTION FUNCTIONS

The Weibull frequency distribution is determined through initially determining the scale parameter C, and then the shape parameter k. For Gharyan 4 sample, Figure

4.8 shows how the parameters were determined: so, and the value of $C = 9.34 m/s$. The shape parameter is the slope of the straight line, $k = 3.23$, while cumulative weibull distribution is given in Figure 4.9. The scale factors, shape parameters, annual mean wind speed were computed for locations and are given in Table 4.4. Those values represent results for the different sites at 50 m height.

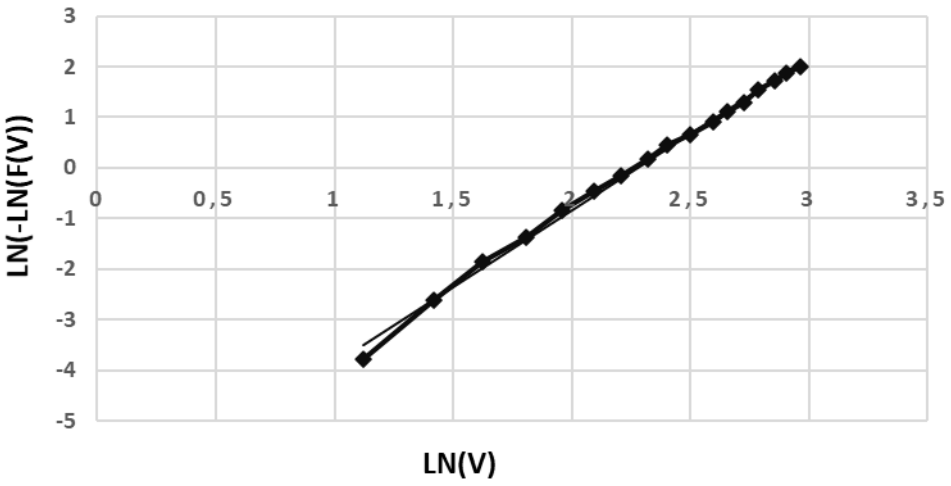

Figure 4.8. Weibull parameters (Gharyan 4).

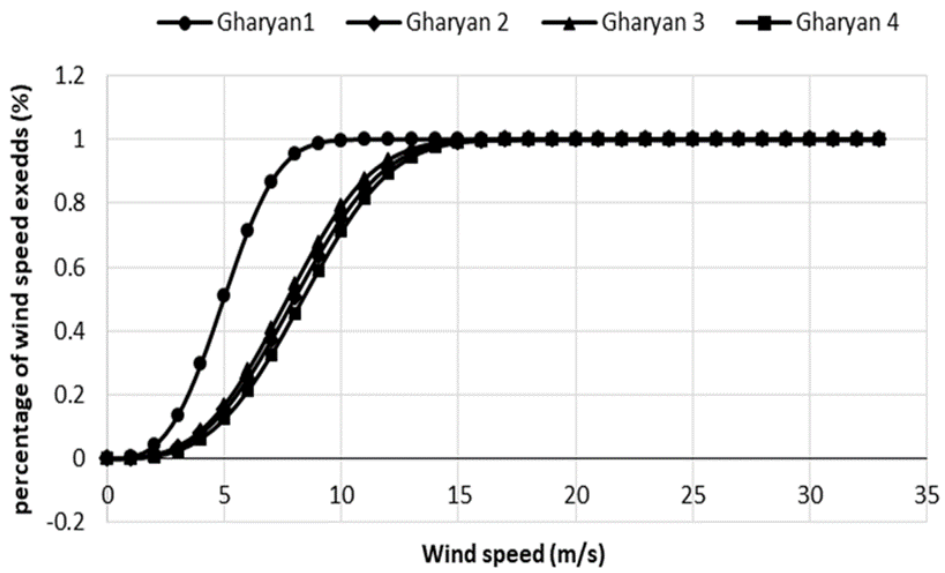

Figure 4.9. Cumulative Weibull distribution (all sites).

Table 4.4. Weibull parameters estimated by three methods at 50 m height.

Site	Methods			
	GM		EM	
	k	c	k	c
Gharyan 1	3.1199	5.5835	3.200	6.40
Gharyan 2	3.0912	8.9768	3.170	9.01
Gharyan 3	3.0828	8.6479	3.440	8.85
Gharyan 4	3.2300	9.3410	3.621	9.40

The errors associated with the different Weibull methods are calculated using Equation (3.9), Equation (3.10), and Equation (3.12) and for the example at 50 m the error results are shown in Table 4.5. The small values for *RSME* and *MAE* verifies that the methods for calculating the Weibull parameters in this study are accurate and can be used for wind energy assessment. Also, the R^2 values are close to 1.0 for all the methods in all the sites which proves the accuracy of the used methods once more.

Table 4.5. Error analysis result.

Site	Method	$R^2 \rightarrow 1$	$RSME \rightarrow 0$	$MBE \rightarrow 0$	$MAE \rightarrow 0$
Gharyan 1	GM	0.889389	0.01133	0.0001938	0.001665
	EM	0.864743	0.012529	0.0000986	0.001848
Gharyan 2	GM	0.963236	0.064188	0.0001153	0.001006
	EM	0.959998	0.066955	0.0000572	0.001044
Gharyan 3	GM	0.989971	0.047248	0.0001295	0.000706
	EM	0.983887	0.059887	0.0000781	0.000892
Gharyan 4	GM	0.89217	0.012481	0.0000996	0.001904
	EM	0.936468	0.095804	0.0000446	0.00148

4.4. ANNUAL WIND SPEED RESULTS

The measured annual wind speed frequency curves are plotted for all the sites in Figure 4.10. From Figure 4.10, we notice that the distribution curves of the sites have comparable patterns. They increase to arrive at a peak value and diminishing after that. The peak value is near the annual mean speed of the comparing site. The peak value of the frequency ranges between 13 % and 14 %.

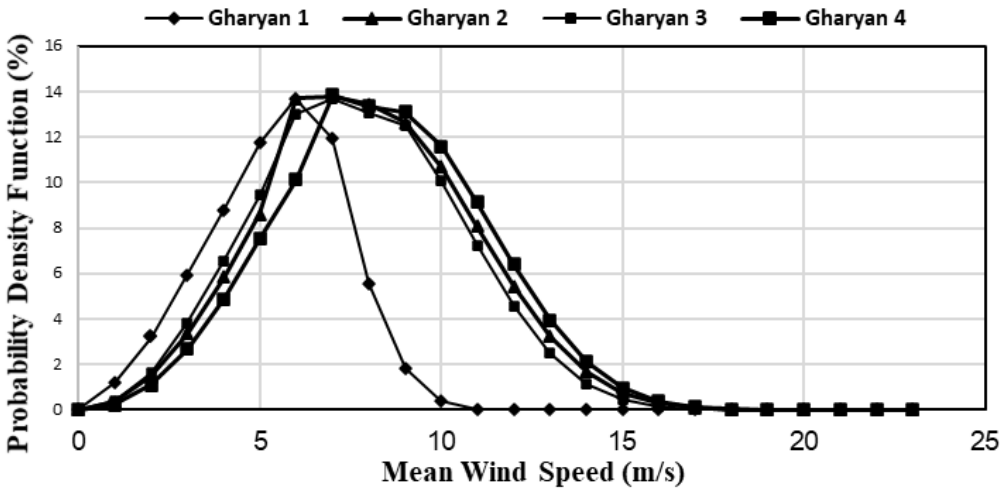

Figure 4.10. Measured annual frequency distribution.

The capacity factor and annual energy calculations for every considered site were done using the Ventis V60 wind turbine data with 60 m rotor diameter and 850 kW rated power. Figure 4.11 to Figure 4.14 demonstrate annual power generation for each location Gharyan 1 to Gharyan 4 respectively. Figure 4.15 shows Annual power generation for all sites. The annual power generation through Gharyan 4 is given, which clearly demonstrates that the maximum annual power generation is 2,187.34 MWh and minimum 1,434.12 MWh from Gharyan 1. The obtained values show that these wind turbines are appropriate for power generation in areas such as Gharyan 4. Table 4.6 summarizes the final results of the calculations.

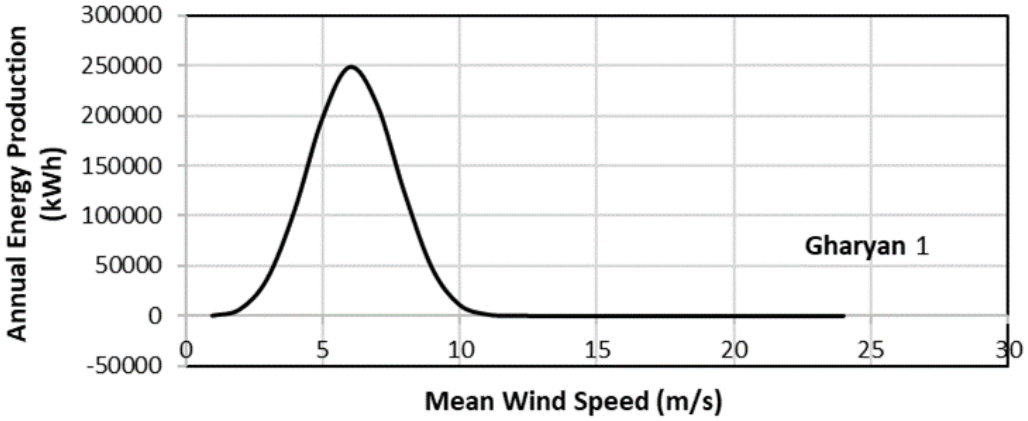

Figure 4.11. Annual power generation at Gharyan 1 at V60-850 kW.

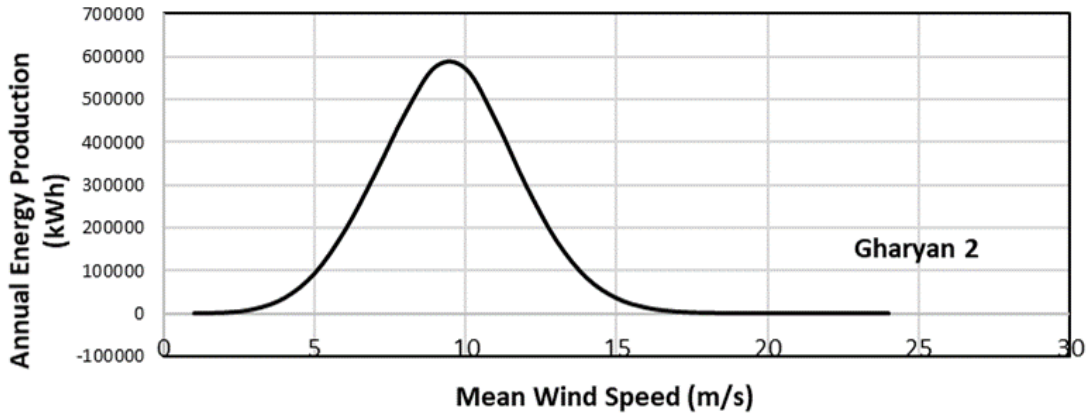

Figure 4.12. Annual power generation at Gharyan 2 at V60-850 kW.

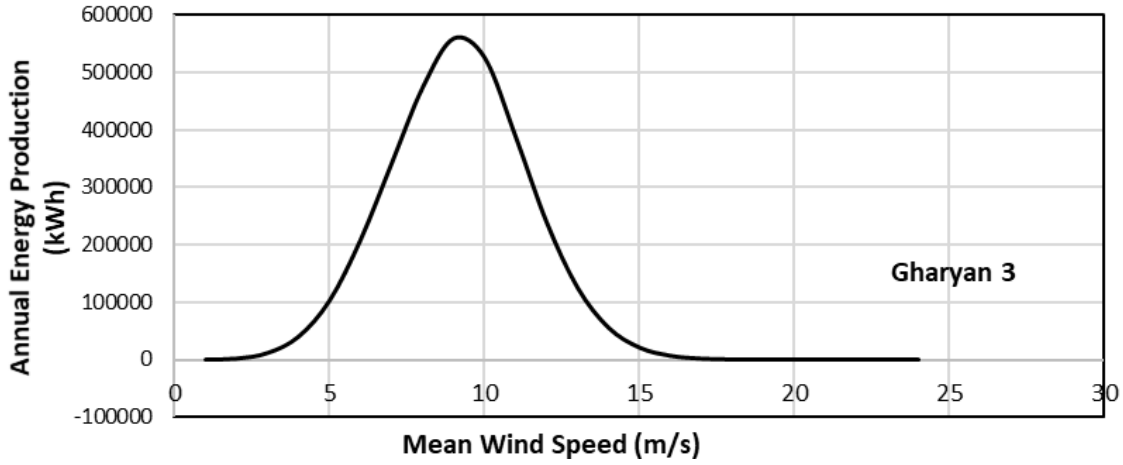

Figure 4.13. Annual power generation at Gharyan 3 at V60-850 kW.

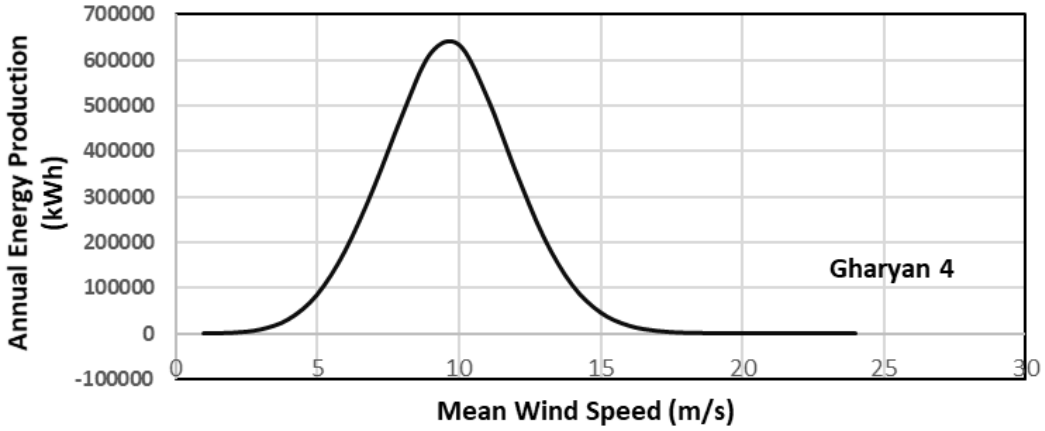

Figure 4.14. Annual power generation at Gharyan 4 at V60-850 kW.

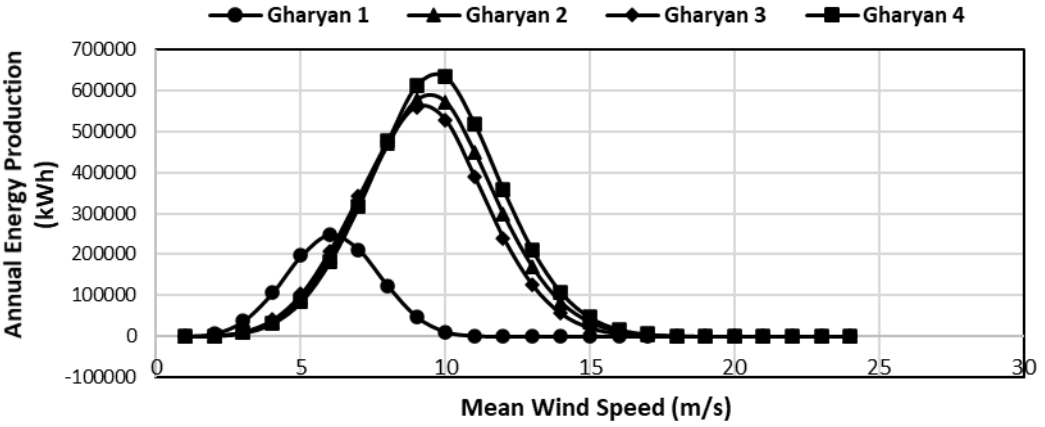

Figure 4.15. Annual power generation for all sites at V60-850 kW.

Table 4.6. Results of the areas under study.

Sites	Annual Mean Wind Speed (m/s)	Annual Energy (MWh)	Annual Capacity Factor (%)
Gharyan-1	6.3	1434.120	19.802
Gharyan-2	6.7	1877.500	25.923
Gharyan-3	6.5	1743.580	24.074
Gharyan-4	7.2	2187.340	30.201

4.5. RESULTS OF COST

The results of the electricity price for each site are shown in Table 4.7.

Table 4.7. Electricity cost of each kWh for each site.

Site	AEP (kWh)	Electricity (USD cent/kWh)
Gharyan 1	1434120	6.2630
Gharyan 2	1877500	4.7840
Gharyan 3	1743580	5.1510
Gharyan 4	2187340	4.1063

CHAPTER 5

WIND TURBINE THEORY

5.1. BACKGROUND

Rotating thin blades capture the wind's kinetic energy. When the blades are in motion, they pull energy from the airstream and transform it into productive mechanical or electrical work at the shaft. A wind power system's overall performance is determined by the wind turbines and load's specific characteristics. Stagnant air passes through the Darrieus rotor's blades, increasing the static pressure until it reaches atmospheric pressure. The turbine slows the flow of air in front of it, resulting in a rise in static pressure. Even though pressure has dropped downstream of the turbine, flow velocity has remained constant. This means that the static pressure does not differ between circumstances far upstream and far downstream. Models of stream tubes use time-averaged forces on blades to determine how fast the flow of momentum via a fixed stream tube may generate axial velocities at the rotor. Airfoil data on lift and drag coefficients and angle of attack and Reynolds number are used to determine forces depending on local velocity. For the sake of clarity, the Darrieus vertical axis turbine and its blade geometry and aerodynamics will be examined before the straight-bladed vertical axis turbine [38].

5.2. BLADE ELEMENT MOMENT THEORY (GEOMETRY)

Both straight-blade vertical axis turbines and Darrieus turbines can benefit from blade element theory, which examines forces and moments acting on the blade element in terms of local angle of attack and local change in velocity [43].

5.2.1. Straight Bladed Turbine

The straight bladed vertical axis wind turbine consists of blades having an airfoil cross-section the blades have a chord C, and the turbine rotates around vertical axis at angular velocity ω with radius R, and from the zero-lift direction or the chord line the azimuth angle β, and the blade pitch angle θ, are measured [40-43]. This geometry is shown in Figure 5.1.

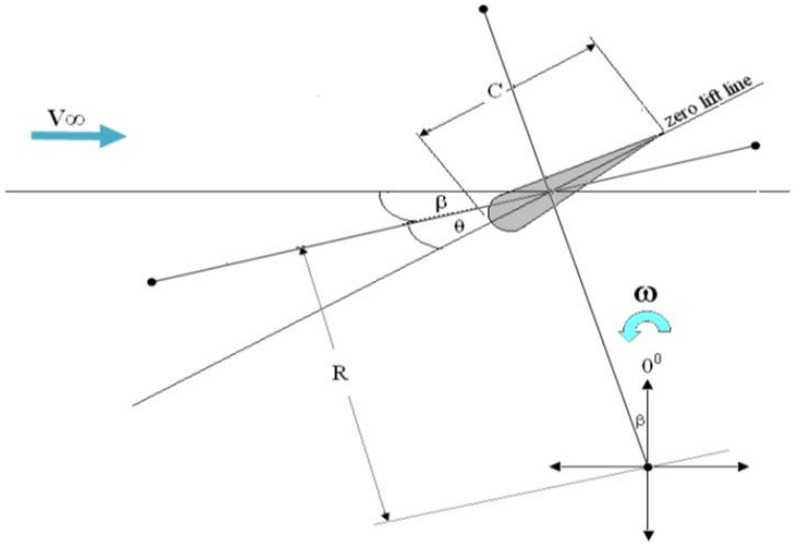

Figure 5.1. Blade element [43].

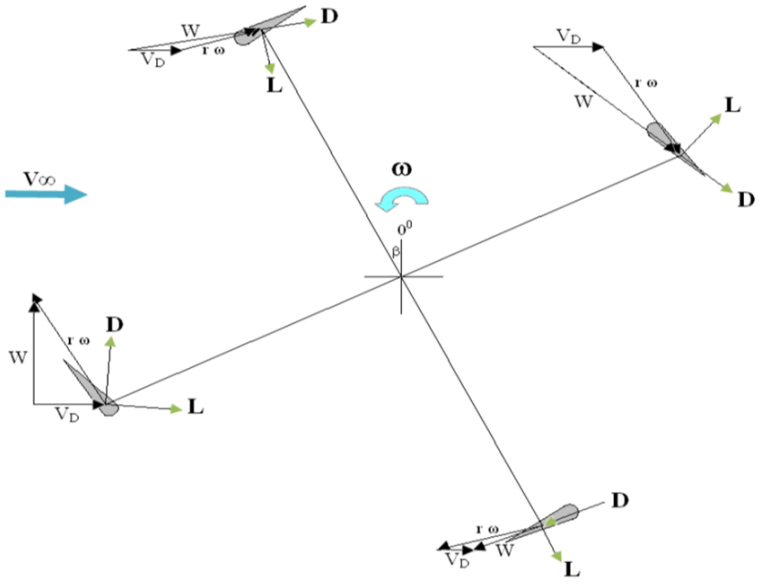

Figure 5.2. Blade forces and relative velocity [43].

The lift component is always in the forward direction of motion as seen in Figure 5.2 because the blade element creates lift and drag components that are normal and tangential to the resulting velocity W. Blade rotational speed, wind velocity, and generated axial swirl velocities all influence the flow's size and direction. Figure 5.3 shows how an arbitrary blade location yields the equations needed to derive the model [40-43].

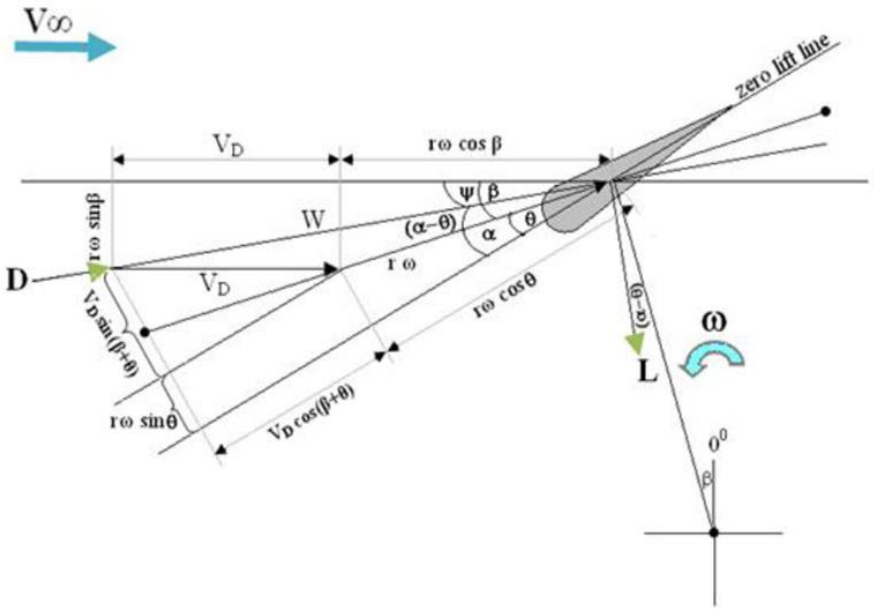

Figure 5.3. Blade element angles and velocity component [43].

In which V_∞ is the free stream velocity, V_D is the wind velocity through the turbine, α is the blade angle of attack, W is the magnitude of the resultant velocity vector and Ψ is the angle between the resultant vector and wind direction as shown in Figure 5.3. Resolving the velocity component, we get

$$\Psi = \tan^{-1}\left(\frac{R\omega\sin\beta}{R\omega\cos\beta + V_D}\right) \tag{5.1}$$

$$\Psi = \tan^{-1}\left(\frac{\lambda_D \sin\beta}{\lambda_D \cos\beta + 1}\right) \tag{5.2}$$

$$\alpha = \tan^{-1}\left(\frac{R\omega\sin\theta + V_D\sin(\beta+\theta)}{R\omega\cos\theta + V_D\cos(\beta+\theta)}\right) \tag{5.3}$$

Or,

$$\alpha = \tan^{-1}\left(\frac{\lambda_D\sin\theta + \sin(\beta+\theta)}{\lambda_D\cos\theta + \cos(\beta+\theta)}\right) \tag{5.4}$$

Where $\lambda_D = \frac{\omega R}{V_D}$ is the tip speed ratio across the disc based on the induced velocity,

$$\lambda_D = \frac{\omega R}{V_\infty} \tag{5.5}$$

is the overall tip speed ratio based on the free stream velocity [40-43].

However,

$$\alpha + \Psi = \beta + \theta \tag{5.6}$$

The local resultant velocity is given by [40-43]

$$W^2 = \omega^2 R^2 + V_D^2 + 2V_D\omega R\cos\beta \tag{5.7}$$

The relative dynamic pressure is given as follows [40-43]

$$\frac{W^2}{V_D^2} = \frac{\omega^2 R^2}{V_D^2} + \frac{2V_D\omega R\cos\beta}{V_D^2} + 1 = \lambda_D^2 + 2\lambda_D\cos\beta + 1 \tag{5.8}$$

And

$$W^2 = V_D^2\left(\lambda_D^2 + 2\lambda_D\cos\beta + 1\right) \tag{5.9}$$

5.2.1.1. Blade Element Forces

The force components on a blade element are shown in Figure 5.4, the azimuth angle, β is measured from the zero datum shown on this diagram [40-43].

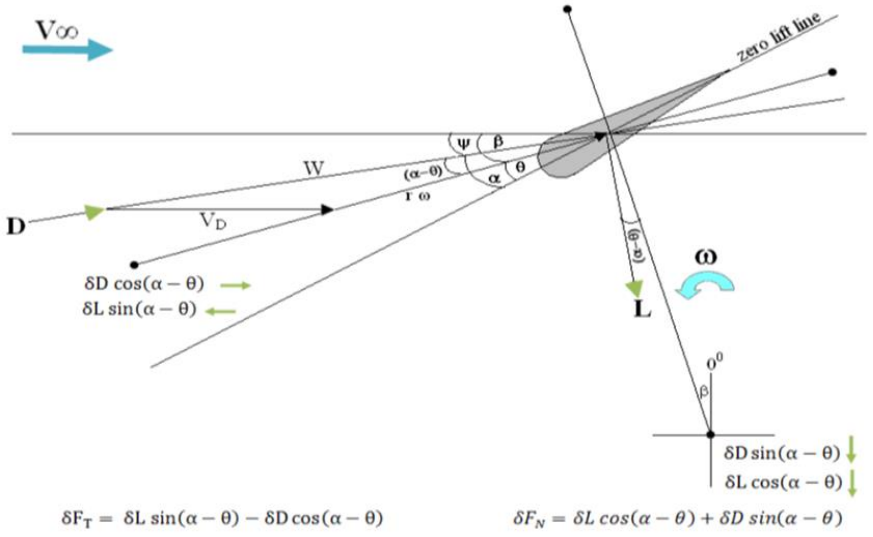

Figure 5.4. Blade tangential and normal force [43].

If the lift and drag coefficients C_L and C_D are known, the lift and drag forces on a blade element of span δy can be calculated as follows [40-43]

$$\delta L = \frac{1}{2}\rho W^2 C \delta_y C_L \tag{5.10}$$

$$\delta D = \frac{1}{2}\rho W^2 C \delta_y C_D \tag{5.11}$$

In Equation (5.10) and Equation (5.11), W is the local resultant velocity, C_L is the lift coefficient, C_D is the drag coefficient, C is the blade chord, δ_y is the blade element span [40-43].

The tangential and the normal force components of rotation are as following

$$\delta F_t = \delta L \sin(\alpha - \theta) - \delta L \cos(\alpha - \theta) \tag{5.12}$$

$$\delta F_n = \delta L \cos(\alpha - \theta) + \delta_D \sin(\alpha - \theta) \tag{5.13}$$

Taking the moments about the axis of rotation of the forces acting on unit length of blade the torque can be determined as shown in Figure 5.5 [40-43].

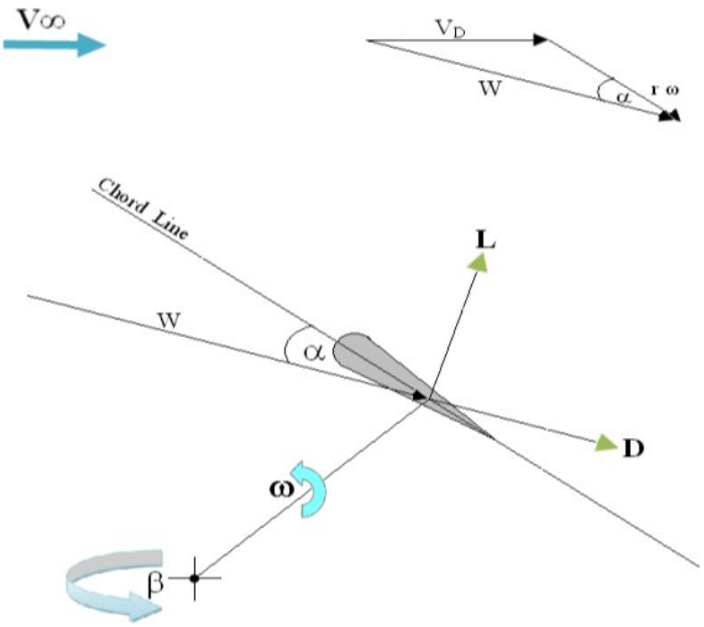

Figure 5.5. Aerodynamic forces acting on a rotating airfoil [43].

If δF_t is the net tangential force acting on the blade element, and δQ is the contribution of the blade element to torque [40-43], then

$$\delta Q = \delta F_t R \tag{5.14}$$

Thus,

$$\delta Q = 0.5 \rho W^2 R C \delta y \left[\sin(\alpha - \theta) - C_D \cos(\alpha - \theta) \right] \tag{5.15}$$

The torque coefficient, C_Q can be define as

$$C_Q = \frac{Q}{0.5\rho V_\infty^2 R A_t} \tag{5.16}$$

V_∞ is the freestream velocity and A_t is the swept area of the rotor, and if G is height /diameter ratio, i.e. $(H/2R)$

If N is the number of blades and L is the blade span and by integrating Equation (5.15) over the whole span, and for a complete revolution, the average torque on the whole turbine blade, can be determined as

$$Q = N\frac{C}{2\pi}\int_0^L\int_0^{2\pi}\frac{1}{2}\rho W^2\left[C_L\sin(\beta-\Psi)-C_D\cos(\beta-\Psi)\right]R\delta\beta\delta y \tag{5.17}$$

Hence,

$$Q = N\frac{C}{2\pi A_t}\int_0^L\int_0^{2\pi}\frac{W^2}{V_\infty^2}\left[C_L\sin(\beta-\Psi)-C_D\cos(\beta-\Psi)\right]\delta\beta\delta y \tag{5.18}$$

The power coefficient can be defined as

$$C_p = \frac{Power}{0.5\rho V_\infty^3 A_t} = \frac{Q\omega}{0.5\rho V_\infty^3 A_t} \tag{5.19}$$

Thus,

$$C_p = \frac{R\omega}{V_\infty}\frac{NC}{R}\frac{1}{2\pi A_t}\int_0^L\int_0^{2\pi}\frac{W^2}{V_\infty^2}\left[C_L\sin(\beta-\Psi)-C_D\cos(\beta-\Psi)\right]\delta\beta\delta y \tag{5.20}$$

5.2.2. Darrieus Blade Turbine

The Darrieus vertical axis wind turbine has airfoil-shaped blades linked to a vertical rotating shaft at both ends. Figures can be used to explain its working principle (Figure 5.6) [43].

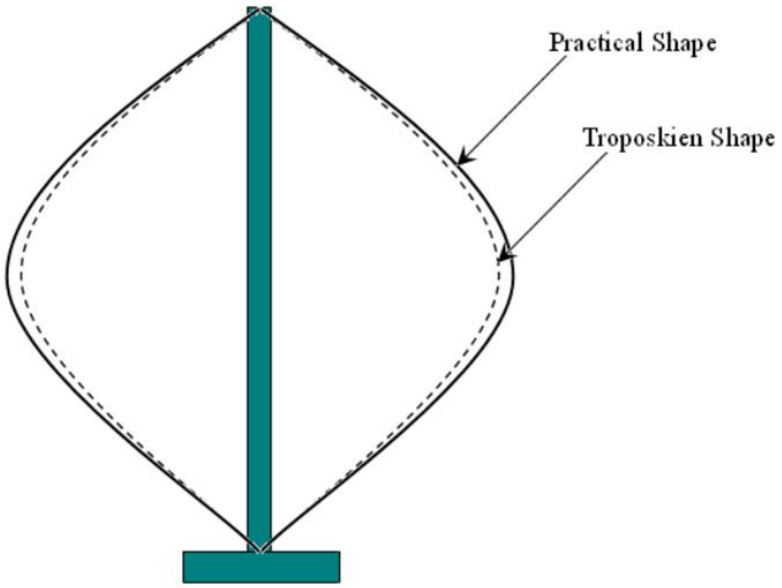

Figure 5.6. Schematic Darrieus VAWT [43].

The wind speed V_D and the turbine rotational speed $r\omega$ contribute to the flow of air across the airfoil's surface. The airfoil's lift force (L) and drag force (D) are determined by the angle of attack (α) of the wind speed (W). A positive torque is generated if the net force along the chord line is in the direction of rotation. During a wide range of wind speeds, the average torque for a cycle is positive, even if this condition does not occur at every rotating position [43].

As seen in Figure 5.7, the Darrieus turbine offers structural benefits over the straight-bladed version. It is possible to make blades under pure tension using a troposkien (turning rope) or parabola form. A mathematical representation of this form is unfortunately lacking. The troposkien can be approximated in two different ways. Darrieus Blade Geometry depicts two blades, one with a straight end and the other with a middle circular arc (Figure 5.7) [43].

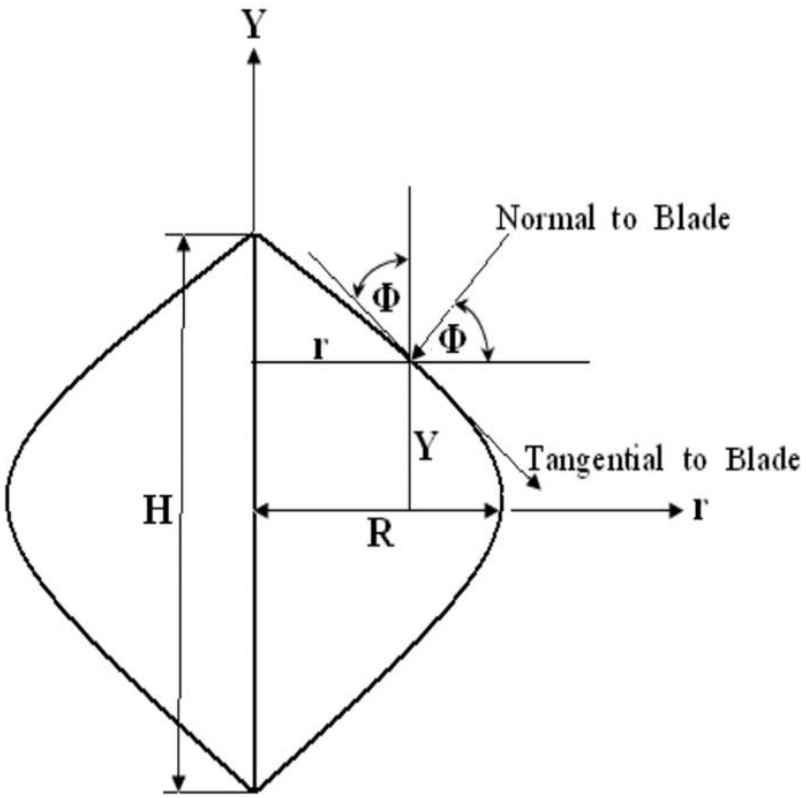

Figure 5.7. Darrieus blade geometry [43].

The equation of the parabola is of the form

$$Y^2 = A(m - r) \tag{5.21}$$

Where, A and m are constants [40-43].

The boundary conditions of the blade shape are as follows,

$$A, Y = 0 \quad ; \quad r = R \tag{5.22}$$

$$Y = H/2 \quad ; \quad r = 0 \tag{5.23}$$

The first boundary condition gives,

$$0 = A(m - R) \tag{5.24}$$

Since $A \neq 0$, thus $m = R$

The second boundary condition yield,

$$\left(\frac{H}{2}\right)^2 = A \tag{5.25}$$

Therefore,

$$A = \frac{H^2}{4R} \tag{5.26}$$

Substituting for A and m in Equation (5.21) yields,

$$Y^2 = \frac{H^2 R^2}{4R^2}\left(1 - \frac{r}{R}\right) \tag{5.27}$$

The general form of the blade shape is,

$$Y^2 = G^2 R\left(R - r\right) \tag{5.28}$$

Where, r is the local radius, measured from the axis of rotation; R is the equatorial radius; G is height/diameter ratio $\left(H/2R\right)$ [40-43].

5.2.2.1. Blade Inclination

The local angle Φ, which is the angle between the horizontal axis and the line normal to the blade chord as shown in Figure 5.8 can be determined by applying the relation of slopes between the tangent to the parabola and the perpendicular at the same point [40-43].

(r, Y).

Yields that

$$\tan\Phi = -\frac{1}{\frac{dy}{dr}} \tag{5.29}$$

Therefore,

$$\Phi(r,y) = \tan^{-1}\left[\frac{2Y}{G^2R}\right] = \tan^{-1}\left[\frac{4Y}{HG}\right] \tag{5.30}$$

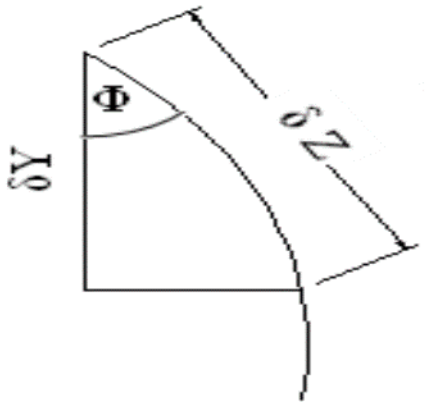

Figure 5.8. Shematic of local angle [40-43].

Velocity component along blade span [40-43],

$$\left[V_D \sin(\beta+\theta) + r\omega\sin\theta\right]\sin\Phi \tag{5.31}$$

Velocity component normal to chord [40-43],

$$\left[V_D \sin(\beta+\theta) + r\omega\sin\theta\right]\cos\Phi \tag{5.32}$$

The velocity components on a blade element are shown in Figure 5.9 [40-43].

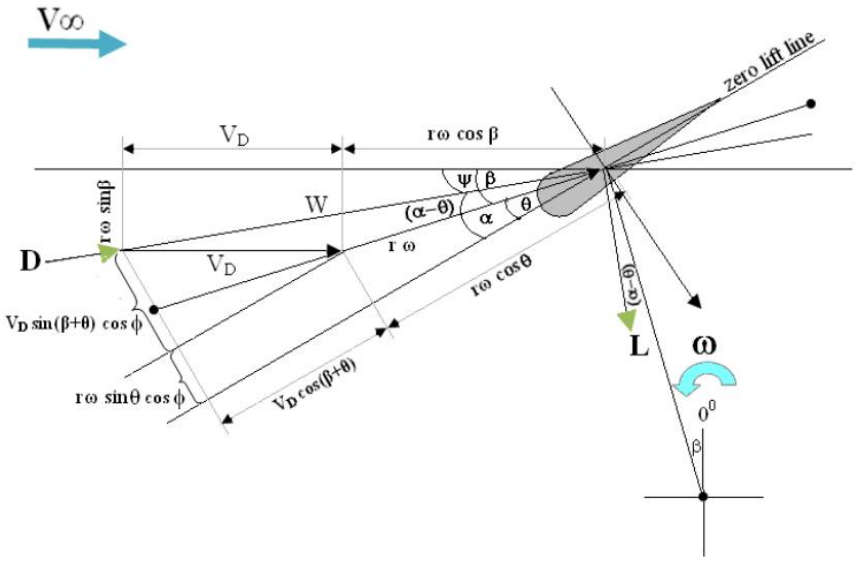

Figure 5.9. Darrieus blade velocity components [43].

5.2.2.2. Blade Element Angle of Attack

Because the angle affects the local velocity vortex, as seen in Figure 5.10. If a vector is perpendicular to the chord of a straight blade, it may be broken down into two components: a component parallel to the chord, which has no influence on the aerodynamics of a blade element. The blade element angle of attack is given as follows [40-43],

$$\alpha = \tan^{-1}\left(\frac{V_D \sin(\beta+\theta)\cos\phi + r\omega\sin\theta\cos\phi}{V_D\cos(\beta+\theta) + r\omega\sin\theta\cos\theta}\right) \tag{5.33}$$

Or,

$$\alpha = \tan^{-1}\left(\frac{\sin(\beta+\theta)\cos\phi + \frac{r\omega}{V_D}\sin\theta\cos\phi}{\cos(\beta+\theta) + \frac{r\omega}{V_D}\cos\theta}\right) \tag{5.34}$$

And the local relative resultant velocity W as follows,

$$W^2 = \left(R\omega\cos\theta + V_D\cos\left(\beta+\theta\right)\right)^2 + \left(r\omega\sin\theta + V_D\sin\left(\beta+\theta\right)\right)^2\cos^2\phi \tag{5.35}$$

The blade attack angle and the local relative consequent velocity are given by, when the blade pitch angle is zero [40-43].

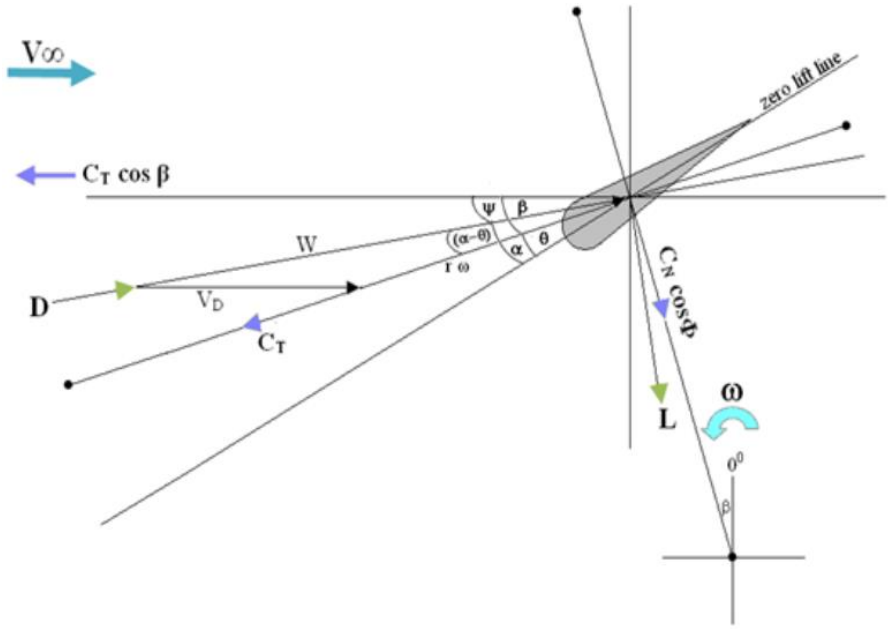

Figure 5.10. Blade element drag force [43].

$$\alpha = \tan^{-1}\left[\frac{\sin\left(\beta\right)\cos\phi}{\cos\left(\beta\right)+\dfrac{r\omega}{V_D}}\right] = \tan^{-1}\left[\frac{\sin\left(\beta\right)\cos\phi}{\cos\left(\beta\right)+\dfrac{rR\omega}{RV_D}}\right] \tag{5.36}$$

$$W^2 = \left[r\omega + V_D\cos\left(\beta\right)\right]^2 + \left[V_D\sin\left(\beta\right)\cos\phi\right]^2 \tag{5.37}$$

The relative dynamic pressure (DP) is given as follows

$$\frac{W^2}{V_D^2} = \left[\frac{r}{R}\lambda_D + \cos\beta\right]^2 + \left[\sin\beta\cos\phi\right]^2 \tag{5.38}$$

The local blade Reynolds number is given by [40-43],

$$\mathrm{Re} = \frac{\rho W C}{\mu} \tag{5.39}$$

Where, ρ is air density, μ is air viscosity, W relative resulting velocity, C blade chord.

5.2.3. Performance of Blade Element

The tangential coefficient C_T and normal coefficient C_N can be resolved from the lift and drag coefficient of Figure 5.4, as follows [40-43]

$$C_T = C_L \sin(\alpha - \theta) - C_D \cos(\alpha - \theta) \tag{5.40}$$

$$C_N = C_D \sin(\alpha - \theta) + C_L \cos(\alpha - \theta) \tag{5.41}$$

If the blade pitch angle $(\theta = 0^\circ)$, the tangential coefficient C_T and normal coefficient C_N are,

$$C_T = C_L \sin(\alpha) - C_D \cos(\alpha) \tag{5.42}$$

$$C_N = C_D \sin(\alpha) + C_L \cos(\alpha) \tag{5.43}$$

C_L and C_D are function of α and Re, and C_N and C_T can be calculated if C_L and C_D are known. The blade element tangential and normal forces are therefore given as follows [40-43],

$$\delta F_T = \frac{1}{2} \rho W^2 C_T \delta A \tag{5.44}$$

$$\delta F_N = \frac{1}{2} \rho W^2 C_N \delta A \tag{5.45}$$

5.2.4. Rotor Drag

The rotor drag force is obtained by resolving the blade element force s into a direction parallel to the ambient wind direction. This can be achieved using Figure 5.10, as follows [40-43].

$$\delta A = C\delta Z \tag{5.46}$$

$$\delta Z = \frac{\delta Y}{\cos\phi} \tag{5.47}$$

Where, δY is the blade element of thickness, and δA is the blade element area.

Thus:

$$\delta A = \frac{C\delta Y}{\cos\phi} \tag{5.48}$$

Substituting for δA into equations (5.44) and (5.45) yields

$$\delta F_T = \frac{0.5\rho W^2 C_T C\delta Y}{\cos\phi} \tag{5.49}$$

$$\delta F_N = \frac{0.5\rho W^2 C_N C\delta Y}{\cos\phi} \tag{5.50}$$

From Figure 5.10, the drag of the blade element is the sum of the components of δF_T and δF_N along the free stream direction [40-43]. Hence;

$$\delta D = \delta F_N \sin\beta - \delta F_T \cos\beta \tag{5.51}$$

Substituting for δF_T, δF_N from equations (5.49) and (5.50) into equation (5.51) yields,

$$\delta D = \frac{1}{2}\rho W^2 C\left(C_N \sin\beta - C_T \cos\beta\right)\delta y \tag{5.52}$$

The average value of the drag of the blade element over varies azimuth angle β and position y can be obtained by double integration of Equation (5.52) over the ranges,

$$\left(0 \le \beta \le 2\pi\right) \tag{5.53}$$

And

$$\left(\frac{H}{2} \le y \le -\frac{H}{2}\right) \tag{5.54}$$

Thus,

$$D = \frac{C}{2\pi}\int_{-\frac{H}{2}}^{\frac{H}{2}}\int_{0}^{2\pi}\frac{1}{2}\rho W^2\left(C_N \sin\beta - C_T \frac{\cos\beta}{\cos\phi}\right)\delta\beta\delta Y \tag{5.55}$$

For N number of blades,

$$D = N\frac{C}{2\pi}\int_{-\frac{H}{2}}^{\frac{H}{2}}\int_{0}^{2\pi}\frac{1}{2}\rho W^2\left(C_N \sin\beta - C_T \frac{\cos\beta}{\cos\phi}\right)\delta\beta\delta Y \tag{5.56}$$

Knowing that,

$$D = \frac{1}{2}\rho V_D^2 C_{DT} A_t \tag{5.57}$$

Where A_t is the swept area of the rotor,

$$A_t = \left(\frac{8}{3}\right) GR^2 \tag{5.58}$$

Where C_{DT} is the total rotor drag this yields,

$$D = \frac{4}{3} GR^2 \rho V_D^2 C_{DT} \tag{5.59}$$

Equating Equation (5.56), (5.59) yields,

$$C_{DT} = \frac{3}{8GR} N \frac{C}{R2\pi} \int_0^{2\pi} \int_{-\frac{H}{2}}^{\frac{H}{2}} \frac{W^2}{V_D^2} \left(C_N \sin\beta - \frac{C_T \cos\beta}{\cos\phi} \right) \delta\beta\delta Y \tag{5.60}$$

Due to the symmetry of the rotor above and below the equator allows simplification of the above integral equation.

Thus,

$$C_{DT} = \frac{6}{8GR} N \frac{C}{R2\pi} \int_0^{2\pi} \int_0^{\frac{H}{2}} \frac{W^2}{V_D^2} \left(C_N \sin\beta - \frac{C_T \cos\beta}{\cos\phi} \right) \delta\beta\delta Y \tag{5.61}$$

Equation (5.61) can be rewritten in non-dimensional from as,

$$C_{DT} = \frac{3}{4} \left(N \frac{C}{R} \right) \frac{1}{2\pi} \int_0^{2\pi} \int_0^{1} \frac{W^2}{V_D^2} \left(C_N \sin\beta - \frac{C_T \cos\beta}{\cos\phi} \right) \frac{\delta\beta\delta Y}{GR} \tag{5.62}$$

$$C_{DT} = \frac{3}{4} \sigma \frac{1}{2\pi} \int_0^{2\pi} \int_0^{1} \frac{W^2}{V_D^2} \left(C_N \sin\beta - \frac{C_T \cos\beta}{\cos\phi} \right) \frac{\delta\beta\delta Y}{GR} \tag{5.63}$$

$$\sigma = N \frac{C}{R} \tag{5.64}$$

Where, σ is called the rotor solidity [40-43].

5.3. AERODYNAMIC MODELING

5.3.1. Vortex Models

A variety of aerodynamic models, such as vortex theory, have found use in the development of aircraft propellers and wingtips. Although this theory is mathematically precise, the maximum angle of attack, and the effects of viscosity on airfoil stalling at low tip speed ratios cannot be easily included into it because of the theory's reliance on an inviscid analysis at high tip speed ratios. In order to accurately represent the non-linear aerodynamic near stall, numerical analysis is required [40-43].

5.3.2. Single Stream Tube (SST) Model

Templin was the first to model the aerodynamic performance of a Darrieus wind turbine by assuming that the rotor was an actuator disk surrounded in a single stream tube. Templin used this homogeneous induced velocity to calculate the forces on the airfoil blades. Flow velocity in the stream tube is connected to the free stream velocity by comparing the drag force on a rotor to the change in fluid momentum. With low tip-speed ratios (or low solidities) and relatively uniform induced velocities, this model works well for predicting overall performance, such as power coefficients. Air moving through the stream tube encounters pressure gradients as it passes through the turbine, which is represented by a uniform actuator disc. Newtonian mechanics may be used to describe a flow across a disc if the flow is considered to be constant, axial, and incompressible. As shown in Figure 5.11. Far upstream the pressure is atmospheric and is denoted by P_∞ and the velocity is V_∞. Just upstream of the disc, the air velocity relative to the disc is assumed to have decreased to $(V_\infty - V_1)$ while the pressure has been increased to P_1, in accordance with Bernoulli's theorem. This implies that the cross-sectional area of the stream tube has been increased. Just downstream of the actuator disc, the pressure has been reduced by a finite amount ΔP while the velocity

remains the same at (V_∞ -V_1). Far downstream of the disc, the pressure has returned to the atmospheric value P_∞, and the velocity at this stage is denoted by (V_∞ -V_2) [40-43].

Then, applying Bernoulli's theorem to the region ahead the disc, yields

$$P_\infty + \frac{1}{2}\rho V_\infty^2 = P_1 + \frac{1}{2}\rho\left(V_\infty - V_1\right)^2 \tag{5.65}$$

And similarly, for the region behind the disc

$$P_\infty + \frac{1}{2}\rho\left(V_\infty - V_2\right)^2 = P_1 - \Delta P + \frac{1}{2}\rho\left(V_\infty - V_1\right)^2 \tag{5.66}$$

Subtracting Equation (5.66) from Equation (5.65), yields

$$\Delta P = \frac{1}{2}\rho V_\infty^2 - \frac{1}{2}\rho\left(V_\infty^2 - 2V_\infty V_2 + V_2^2\right) \tag{5.67}$$

$$\Delta P = \frac{1}{2}\rho V_2\left(2V_\infty - V_2\right) \tag{5.68}$$

Since the drag force is determined by the integral of the pressure differential between the disc's back and front surfaces over the disc's whole surface area, this means:

$$Drag = \Delta P A = \frac{1}{2}\rho V_2 A\left(2V_\infty - V_2\right) \tag{5.69}$$

But the drag also equal to the rate of change of the momentum.

Thus,

$$Drag = \dot{m}\left(V_{in} - V_{out}\right) = \rho V_D A\left[V_\infty - \left(V_\infty - V_2\right)\right] \tag{5.70}$$

Where, $\dot{m}$ is the mass flow rate, V_{out} is the output velocity, V_{in} is the input velocity.

Hence,

$$Drag = \rho A(V_\infty - V_1)\left[V_\infty - (V_\infty - V_2)\right] \tag{5.71}$$

$$Drag = \rho A(V_\infty - V_2)V_2 \tag{5.72}$$

By comparing Equations (5.69) and (5.72). Thus,

$$2V_\infty - 2V_1 = 2V_\infty - V_2 \quad ; \quad V_2 = 2V_1 \tag{5.73}$$

Hence the velocity a head of the actuator disc is as shown in Figure 5.11 is as follow,

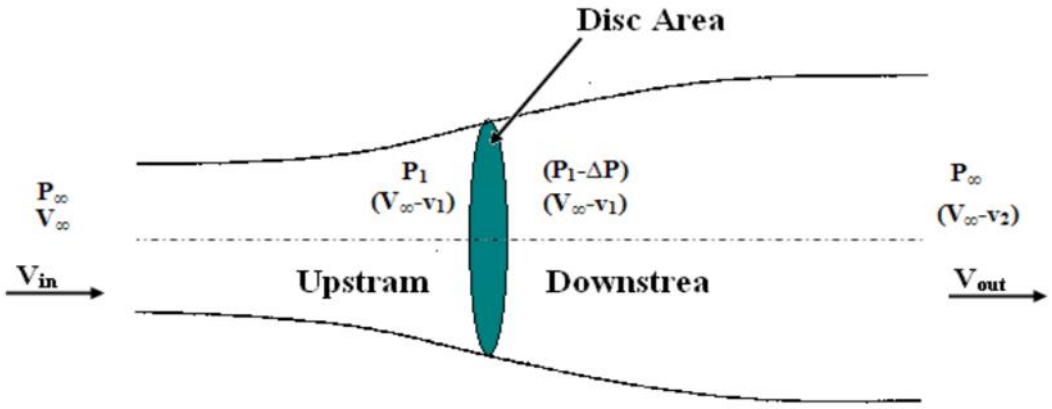

Figure 5.11. Actudiator disc theory [40-43].

$$V_D = V_\infty - V_1 = V_\infty\left(1 - \frac{V_1}{V_\infty}\right) = V_\infty(1-\alpha) \tag{5.74}$$

Or,

$$\frac{V_D}{V_\infty} = 1 - \alpha \tag{5.75}$$

Where $\alpha = \frac{V_1}{V_\infty}$ is the inflow factor. While the velocity for downstream is

$$V_{out} = V_\infty - V_2 = V_\infty \left(1 - \frac{V_2}{V_\infty}\right) = V_\infty \left(1 - 2\frac{V_1}{V_\infty}\right) = V_\infty (1 - 2\alpha) \tag{5.76}$$

Since the drag force on disc is equal to the change of the momentum through the disc [40-43].

Thus,

$$D = \rho A V_D \left[V_\infty - (V_\infty - 2V_1)\right] \tag{5.77}$$

Knowing that,

$$V_1 = V_\infty - V_D \tag{5.78}$$

Thus,

$$D = 2\rho A V_D \left[V_\infty - V_\infty\right] \tag{5.79}$$

5.4. TORQUE AND POWER

Taking the moments about the axis of rotation of the forces on unit length of blades as shown in Figure 5.4, the torque can be determined. If δF_T is the element tangential force, and δQ is the contribution of the blade element to the torque, then [40-43]

$$\delta Q = \delta F_T r \tag{5.80}$$

Where, r is the rotor radius, δF_T is the net tangential force acting on the blade element. Substituting about δF_T from Equation (5.49) gives,

$$\delta Q = \frac{1}{2}\rho W^2 \frac{C\delta Y}{\cos\phi} rC_T \tag{5.81}$$

Therefore the average torque on the whole turbine for N blades is given by the

$$Q = 2GR\frac{NC}{2\pi}\int_0^1\int_0^{2\pi} \frac{0.5\rho W^2}{\cos\phi} C_T r\delta\beta\delta\left(\frac{Y}{GR}\right) \tag{5.82}$$

Knowing that the total disc torque is given by

$$Q = \frac{1}{2}\rho V_\infty^2 A_t C_Q R \tag{5.83}$$

Where, C_Q is the torque coefficient, A_t is the rotor swept, R is the equator rad [40-43].

Hence, the rotor torque coefficient can be calculated using the following equation,

$$C_Q = \frac{Total\ Disc\ Torque}{0.5\rho V_\infty^2 A_t R} \tag{5.84}$$

Or,

$$C_Q = \frac{2GR}{0.5\rho V_\infty^2 A_t}\left(\frac{NC}{R}\right)\frac{1}{2\pi}\int_0^1\int_0^{2\pi} 0.5\rho W^2 \frac{C_T r}{\cos\phi}\delta\beta\delta\left(\frac{Y}{GR}\right) \tag{5.85}$$

Substituting for A_t and multiply by $\left(\frac{V_D}{V_D}\right)^2$ yields,

$$C_Q = \frac{3}{4}\left(\frac{V_D}{V_\infty}\right)^2 \sigma\frac{1}{2\pi} \tag{5.86}$$

And the power can be obtained by,

$$P = Q \cdot \omega \tag{5.87}$$

Hence,

$$P = 2GR\frac{NC}{2\pi}\omega\int_0^1\int_0^{2\pi}\frac{0.5\rho W^2}{\cos\phi}C_T r\delta\beta\delta\left(\frac{Y}{GR}\right) \tag{5.88}$$

A dimensionless power coefficient C_P can be defining as[40-43]:

$$C_P = \frac{Actual\ Power\ Generated\ by\ The\ Turbine}{Available\ Power\ in\ Wind\ With\ in\ The\ Swept\ Area} \tag{5.89}$$

Hence,

$$C_P = \frac{P}{0.5\rho V_\infty^3 A_t} \tag{5.90}$$

This yields,

$$C_P = \frac{3}{4}\sigma\frac{\omega R}{V_D}\left(\frac{V_D}{V_\infty}\right)^3\frac{1}{2\pi}\int_0^1\int_0^{2\pi}\frac{0.5\rho W^2}{0.5V_D^2}\frac{C_T}{\cos\phi}\frac{r}{R}\delta\beta\delta\left(\frac{Y}{GR}\right) \tag{5.91}$$

To solve Equation (5.91), it is required to know an expression for the term $\left(V_D/V_\infty\right)$ which could be obtained by equating the net blade force along the free stream direction and the thrust force calculated by the momentum equation [40-43].

Hence,

$$2\rho A_t V_D\left(V_\infty - V_D\right) = \frac{NC}{2\pi}2GR\int_0^1\int_0^{2\pi}\frac{1}{2}\rho W^2\left(C_N\sin\beta - \frac{C_T}{\cos\phi}\cos\beta\right)\delta\beta\delta\left(\frac{Y}{GR}\right) \tag{5.92}$$

Thus,

$$\frac{V_\infty}{V_D} = 1 + \frac{3}{16}\sigma \frac{1}{2\pi} \int_0^1 \int_0^{2\pi} \frac{0.5\rho W^2}{0.5\rho V_D^2} \left(C_N \sin\beta - \frac{C_T}{\cos\phi} \cos\beta \right) \delta\beta\delta \left(\frac{Y}{GR} \right) \tag{5.93}$$

Combining equation (5.93) with equation (5.61) yields

$$\frac{V_\infty}{V_D} = 1 + \frac{1}{4} C_{DT} \tag{5.94}$$

Knowing that the tip speed ratio based on the freestream velocity λ is related to the induced tip speed ratio λ_D as follows [40-43]

$$\lambda = \lambda_D \frac{V_D}{V_\infty} \tag{5.95}$$

Thus if λ_D is specified, λ can be calculated. The turbine performance can be calculated as

$$C_P = \lambda C_Q \tag{5.96}$$

The procedures of single stream tube model (SST) for carrying out computation on a specified stream tube to predict the rotor performance are as follows,

- Choose values of solidity σ, zero lift drag coefficient C_{Do}, and height/diameter ratio G.
- Assume initial value of the tip speed ratio, λ_D.
- Calculate the local blade angle, ϕ.
- Calculate the local angle of attack, α.
- Calculate the corresponding value, C_T, C_N.

- Calculate the relative dynamic pressure, $\frac{W^2}{V_D^2}$.
- Calculate the torque coefficient using Equation (5.86).
- Calculate the ratio $\left(\frac{V_\infty}{V_D}\right)$ using Equation (5.93).
- Calculate the power coefficient using Equation (5.91).

CHAPTER 6

ROTOR DESIGN AND PERFORMANCE ANALYSIS

6.1. INTRODUCTION

The results for the Darrieus vertical axis wind turbine using the both blade element model and the single stream tube model are discussed in this chapter, the blade element model results include the variation of angle of attack (α) and the variation of the torque and power coefficient as a function of both tip speed ratio (λ) and azimuth angle (β).The computer program (MATLAB) has been built taking into consideration the available input data and the required objective of the wind turbine [17-40-42]. The results also demonstrate the effect of varying various geometric parameters such as solidity (σ), height to diameter (H/R) and local radius ratio (r/R) on both torque and power of the rotor for high and low tip speed ratio [15-39-42].

6.2. ROTOR SIZING

Begin by deciding what required power output (Design Power) P_d is needed at a particular rated wind speed V_d first step in wind rotor design process is concerned with the determination of the rotor diameter. However, to do even this, one still required to know other design parameter, namely design power coefficient C_p, generator and gear-train efficiencies η_g and η_t, respectively. The available wind power in flow stream of cross section area A_s is given in Equation (3.13) not all of this power may be extracted. The actual electrical power is affected by the rotor coefficient C_p and by efficiency of the mechanical transmission system η_t and the generator itself η_g. Thus the actual electrical power P can be expressed in the form:

$$P_w = \frac{1}{2}\rho U_\infty^3 A_s C_p \eta_t \eta_g \tag{6.1}$$

Now, in almost any design procedure, a design operating point is normally selected. As far as wind rotor design concerned, this point is usually the design operating condition. Hence Equation (6.1) rewritten as:

$$P_d = \frac{1}{2}\rho V_D^3 A_s C_{pd} \eta_t \eta_g \tag{6.2}$$

Where the subscript d refers to the design condition. Therefore, the rotor area A_s can be easily determined once P_d, V_d, η_t and η_g are specified. As to C_{pd} a value is selected based on experience.

6.3. BLADE DESIGN PROCEDURE

The procedure begins with the choice of various rotor parameters as illustrate in Section 6.2 and the choice of an airfoil. An initial blade shape (chord length distribution and twist length distribution along the blade length) is then determined using the optimum blade shape. The final blade shape and performance are determined iteratively.

6.3.1. Input Design Data

In order to start the design process, a number of input data have to be specified, namely:

- **Design output power, P_d**
  The design output power (Power requirement) for the proposed rotor has been selected to be 500 W.

- **Design wind speed, V_d**

  By considering mean wind speed for Gharyan 4.88 m/s, then the suitable design wind speed is 7.32 m/s. Knowing that the design wind speed is usually 1.5 times the average wind speed, $V_d \approx 1.5V_a$ [43].

- **Blade cross-section**

  The airfoil NACA-0018 has been selected is shown in Figure 6.1. The lift coefficient and drag coefficient versus angle of attack (From 0° to 180°) of the NACA-0018 airfoil for different values of Reynolds number are shown in Figure 6.2 and Figure 6.3 respectively. It is shown that the maximum lift coefficient at stall increases as Reynolds number increases. The lift coefficient and drag coefficient are nearly independent of the Reynolds number at high incidence. The characteristics of the selected at $\mathrm{Re} = 0.7 \times 10^6$ are shown in Figure 6.4 [51-53].

- **Design tip speed ratio, λ_d**

  According to the application of wind turbine, the value of the design tip speed ratio should be in the range of $0.2 < \lambda_d < 10$. In this study, λ_d was taken as 4.5 [51-53].

- **Design power coefficient, C_{pd}**

  Based on the practical experience, the value of power coefficient, C_{pd} varies in the range 0.4 to 0.45. In the present wind rotor, C_{pd}, the design power coefficient has been selected to be as 0.4 [15].

- **Number of wind rotor blades, N**

  According to Table 6.1 the number of blades, N, was chosen as 2.

Table 6.1. Suggested blade number N for different tip speed ratio, $\lambda > 4$ [25].

TSR ($\lambda = \omega R/V_\infty$)	**Blade Number (N)**
1	8-24
2	6-12
3	3-6
4	3-4
>4	1-3

The mechanical transmission (Gear-train) efficiency η_t and the generator characteristics in items of the generator efficiency η_g would be taken into account. For the present wind rotor, it was assumed that:

$$\eta_t = \eta_g = 0.95 \tag{6.3}$$

The information is shown in Table 6.2 for the rotor design in terms of illustrate rotor size and blade design.

Table 6.2. Illustrate rotor size and blade design.

σ (Solidity)	0.25	**N**	2
Power (Watt))	500	**ρ (kg/m^3)**	1.225
A_s (m^2)	5.203	**V_a (m/s)**	4.88
V_d (m/s)	7.32	**C_p**	0.4

H	**R**	**C**	**G**	**H/C**
1	7.804802825	1.95120071	0.064063117	0.5125049
1.25	6.24384226	1.56096057	0.100098621	0.800789
1.5	5.203201884	1.30080047	0.144142014	1.1531361
1.75	4.459887329	1.11497183	0.196193297	1.5695464
2	3.902401413	0.97560035	0.25625247	2.0500198
2.25	3.468801256	0.86720031	0.324319532	2.5945563
2.5	3.12192113	0.78048028	0.400394484	3.2031559
2.75	2.838110118	0.70952753	0.484477326	3.8758186
3	2.601600942	0.65040024	0.576568057	4.6125445
3.25	2.401477792	0.60036945	0.676666678	5.4133334
3.5	2.229943664	0.55748592	0.784773189	6.2781855
3.75	**2.081280753**	**0.52032019**	**0.900887589**	**7.2071007**
4	1.951200706	0.48780018	1.025009879	8.200079
4.25	1.836424194	0.45910605	1.157140059	9.2571205
4.5	1.734400628	0.43360016	1.297278128	10.378225

4.75	1.643116384	0.4107791	1.445424087	11.563393
5	1.560960565	0.39024014	1.601577936	12.812623
5.25	1.48662911	0.37165728	1.765739674	14.125917
5.5	1.419055059	0.35476376	1.937909303	15.503274
5.75	1.357357013	0.33933925	2.11808682	16.944695
6	1.300800471	0.32520012	2.306272228	18.450178

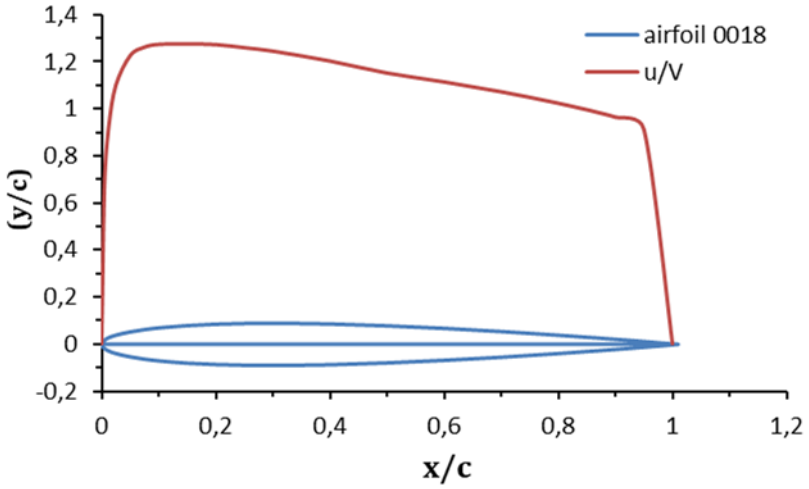

Figure 6.1. Geometric shape of the airfoil NACA 0018.

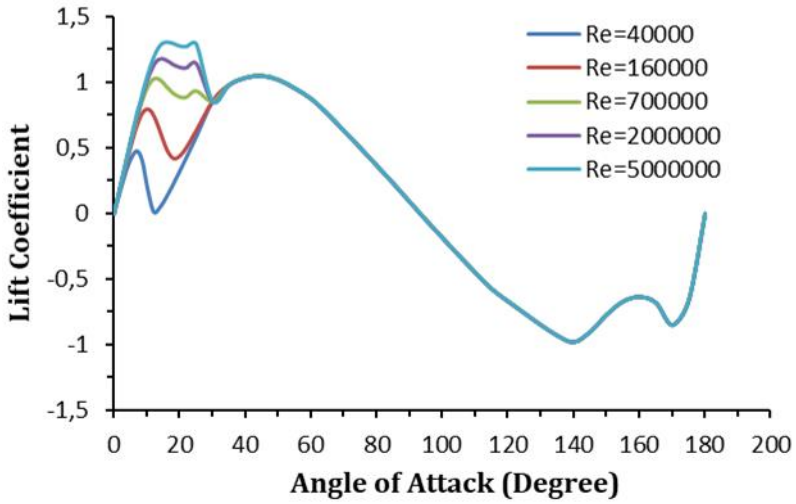

Figure 6.2. Lift coefficient versus incidence for NACA 0018 airfoil section.

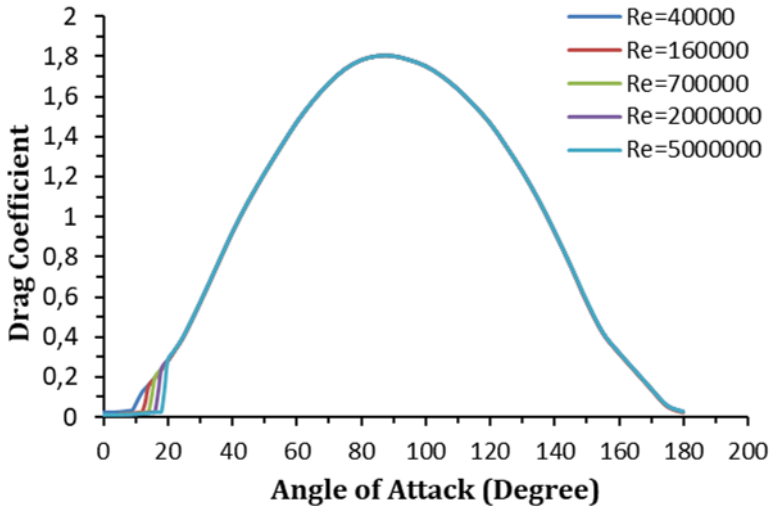

Figure 6.3. Drag coefficient versus incidence for NACA 0018 airfoil section.

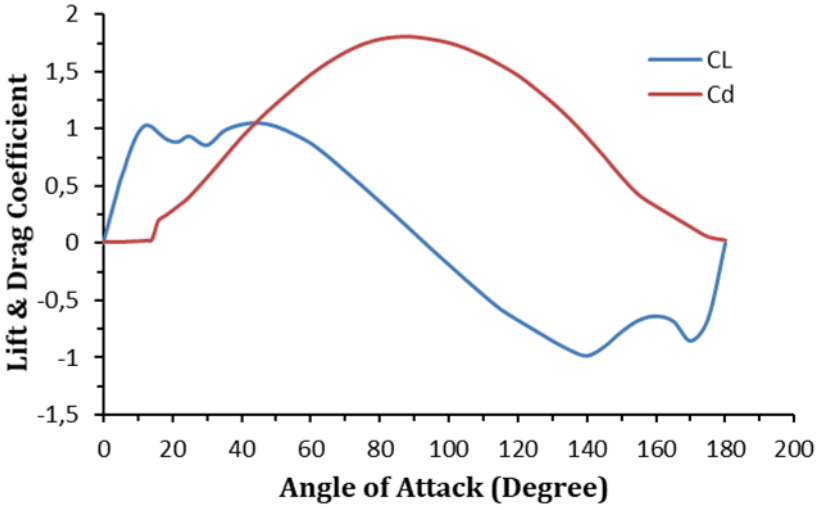

Figure 6.4. Airfoil 0018 characteristics for Reynolds number 7×10^{6} .

6.4. GENERAL SHAPE OF WIND TURBINE

The procedure begins with the choice of various rotor components. The blades how to contact with a shaft and dimensions of rotor and airfoil are shown in Figure 6.5. The height of the tower is 26.250 m. The top of the tower is a square shaped frame with a side length of one meter as seen in Figure 6.6.

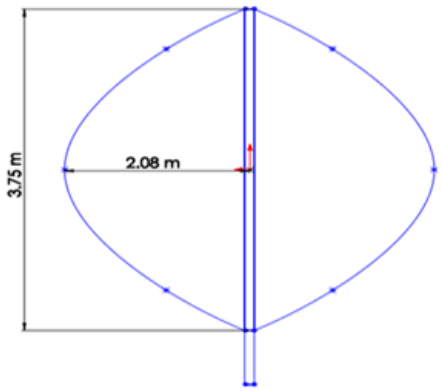

Figure 6.5. Rotor dimensions.

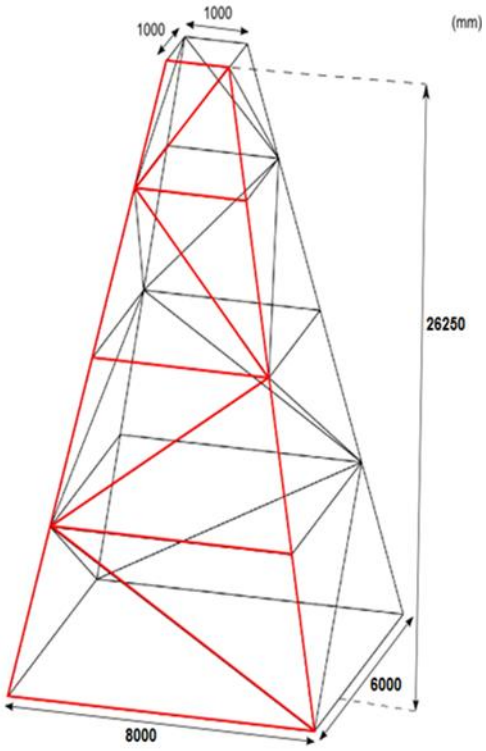

Figure 6.6. The tower model.

6.5. VARIATION OF THE BLADE ANGLE OF ATTACK

It is well known that the variation of the angle of attack effects the performance of the wind Turbines. The angle of attack depends on many parameters such as azimuth angle (β). Blade inclination angle (ϕ). Tip speed ratio (λ), local radius ratio (r/R). Figure 6.7, Figure 6.8, and Figure 6.9 show the variation of blade angle of attack as a function

of azimuth angle (β) for different values of tip speed ratio. $\lambda(0.1, 2, 7)$, and local radius ratio range of $r/R(0.51, 0.75, 0.99)$ respectively. It is clear from these figures that the angle of attack increases as the azimuth angle increases till it reaches its maximum value then it decreases as the azimuth angle increases. These figures also show that the angle of attack decreases as r/R increases. At all tip speeds ratios the angle of attack is positive in the upwind half of the cycle $(0 \le \beta \le 180)$ and negative in the downwind half $(180 < \beta < 360)$. The change from positive to negative incidence is very rapid at low tip speed ratio $(\lambda = 0.1)$ and low values of r/R. However as shown in Figure 6.8 and Figure 6.9, at higher values of tip speed ratio the angle of attack decreases as the tip speed ratio increases and this causes a negative thrust coefficient at higher values of tip speed ratio.

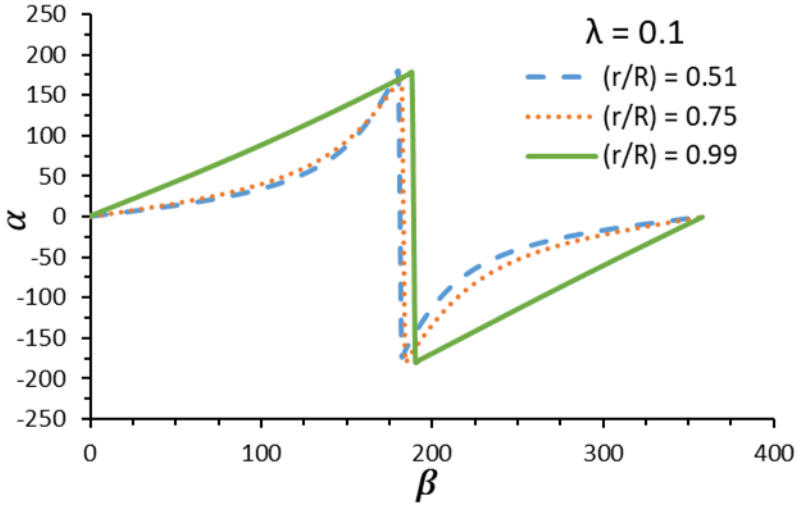

Figure 6.7. Variation of angle of attack versus the azimuth angle for (SST model) at $(r/R = 0.51, 0.75, 0.99); G = 0.5; \sigma = 0.4; C_{do} = 0.017; \lambda = 0.1.$

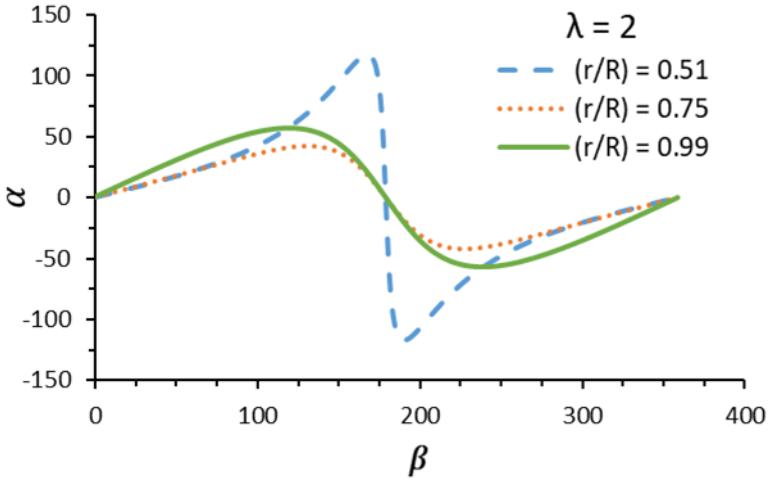

Figure 6.8. Variation of angle of attack versus the azimuth angle for (SSTmodel) at $(r/R = 0.51, 0.75, 0.99); G = 0.5; \sigma = 0.4; C_{do} = 0.017; \lambda = 2.0$.

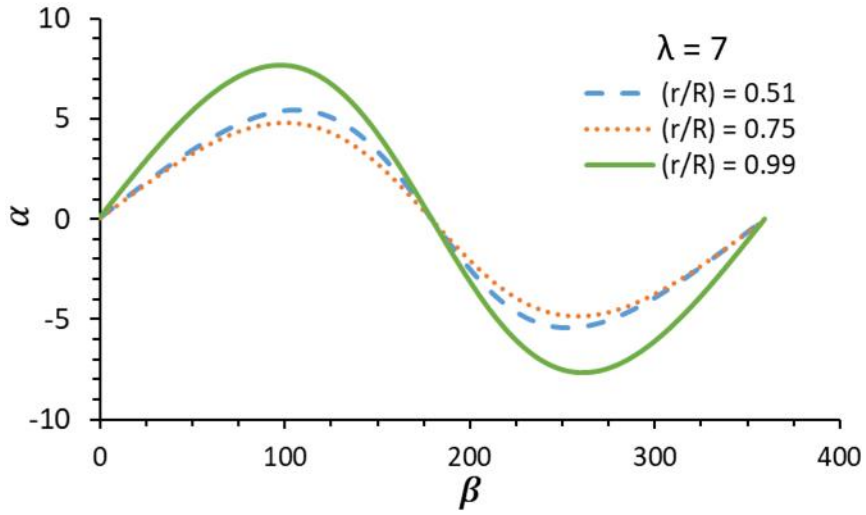

Figure 6.9. Variation of angle of attack versus the azimuth angle for (SST model) at $(r/R = 0.51, 0.75, 0.99); G = 0.5; \sigma = 0.4; C_{do} = 0.017; \lambda = 7.0$.

6.6. LOCAL AND AVERAGE RESULTS

The results of the variation of the local and average torque coefficients are indicated in Figure 6.10, Figure 6.11, and Figure 6.12. Figure 6.10 shows the variation of the local torque in case of low tip speed ratio ($\lambda = 0.1$). This figure indicates that for a fixed value of r/R, the torque coefficient increases as the azimuth angle (β) increases until the aerodynamic stall ($\alpha = \alpha_{stall}$). Beyond stalling, the value of the torque coefficient (C_q) becomes negative and reaches a minimum value at different azimuth

angles dependent on the value of the tip speed ratio(λ). Subsequently the torque coefficient increases and becomes positive. Due to the symmetry of NACA 0018 section the ($C_q - \beta$) curves almost repeat themselves in reverse from (180 to 360). Also it is clear that for fixed value of azimuth angle (β) the local torque coefficient increases as the local radius increases. Figure 6.11 shows the variation of local torque coefficient at higher tip speed ratio ($\lambda = 2$), these figures indicates that at tip speed ratio ($\lambda = 2$), the local torque coefficient is higher than in case of ($\lambda = 0.1$), which is represented in Figure 6.10, while Figure 6.12, shows that at higher values of tip speed ratio ($\lambda = 7$), the local torque coefficient becomes negative at most azimuth angle range and this is decreasing of the angle of attack as high value of the tip speed ratios.

6.7. VARIATION OF TORQUE COEFFICIENT

Figure 6.13 shows that the effect of varying the rotor height to diameter ratio on the torque coefficient of the whole turbine versus tip speed ratio, whilst keeping the solidity ($\sigma = 0.4$) and blade zero lift drag coefficient ($C_{do} = 0.017$) are constant. Figure 6.13 shows that for low range of tip speed ratio ($0.1 < \lambda < 7$), the values of the torque coefficient increases as (H/D) ratio increases from (0.51-0.99). However, for higher for values of tip speed ratios ($0.1 < \lambda < 7$), the torque coefficient decreases at the value of H/D increases. The effect of the rotor solidity on the average torque is as shown in Figure 6.14 show the effect of varying the rotor solidity. Whilst keeping the rotor height diameter constant at ($H/D = 1.0$), and with a blade zero-lift drag coefficient constant at $C_{do} = 0.017$. It is clear that the average torque increases as the tip speed ratio increases till it reaches its maximum value then it decreases as the tip speed ratio increases. This figure indicates that both the starting torque and maximum torque coefficient at ($NC/R = 0.6$) are higher than that the ($NC/R = 0.4$ and $NC/R = 0.2$). Thus the solidity may be useful in improving the possibility of self-starting. Figure 6.15 shows the effect of varying the blade airfoil zero-lift drag coefficient on the average torque coefficient of the (D_{cb}) while both the blade solidity (NC/R) and the height/diameter ratio are kept constant. It is shown that in the high tip speed ratio range of ($\lambda = 7$) the torque coefficient increases as the blade aerofoil

zero-lift drag coefficient decrease. However, at low tip speed ratio, ($\lambda < 7$) the effect of varying the zero-left drag coefficient is small and may be neglected because at the low tip speed ratio range the profile drag is a small fraction of the total drag.

6.8. VARIATION OF POWER COEFFICIENT

The rotor power coefficient is dependent on many parameters such as rotor solidity, height/diameter ratio, blade airfoil zero-lift drag coefficient. The influence of varying the rotor height/diameter ratio on the power characteristic is shown in Figure 6.16. The variation is similar to the effect of the (H/D) on the torque coefficient which has been discussed in Figure 6.13. Figure 6.15 indicates the effect of varying the blade solidity ($\sigma = 0.4$) on the wind turbine power coefficient, for values of whilst keeping the rotor height-diameter constant at ($H/D = 0.5$), and with a blade zero-lift drag coefficient ($C_{do} = 0.017$).The result indicate that for values of ($\lambda < 7$) the power coefficient increases as the solidity increase, while for ($\lambda > 7$) the effect on the value of the power coefficient is small and can be neglected. Figure 6.11 represents the effect of varying the blade airfoil zero-lift drag coefficient on the power coefficient while the blade solidity (NC/R), the height/diameter ratio are kept constant. It is shown that for ($\lambda > 7$) the power coefficient increase as the blade airfoil zero angle of attack decreases, while ($\lambda < 7$) the effect of the zero lift drag coefficient is very small and can neglected the effect of blade airfoil section on the performance of (D_{cb}) are shown in Figure 6.11.

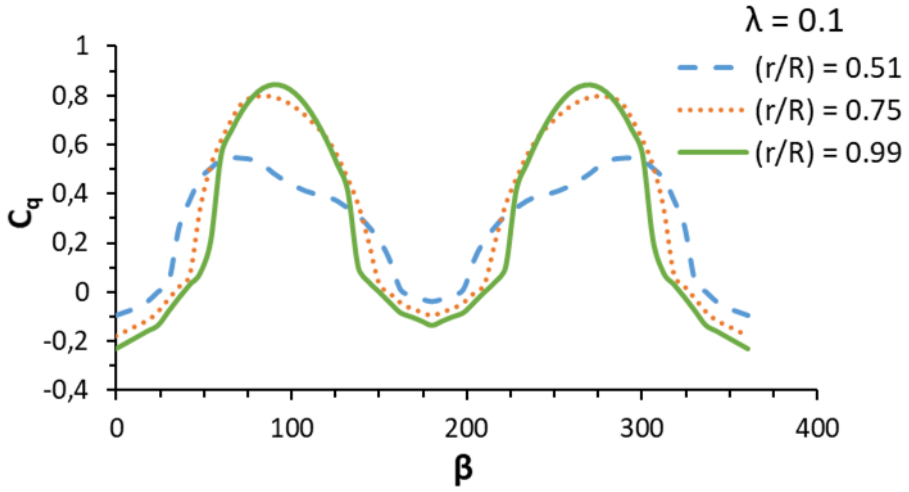

Figure 6.10. Variation of local torque coefficient versus the azimuth angle for (SST model) at $\left(r/R=0.51,0.75,0.99\right);\ G=0.5;\sigma=0.4;C_{do}=0.017;\lambda=0.1$

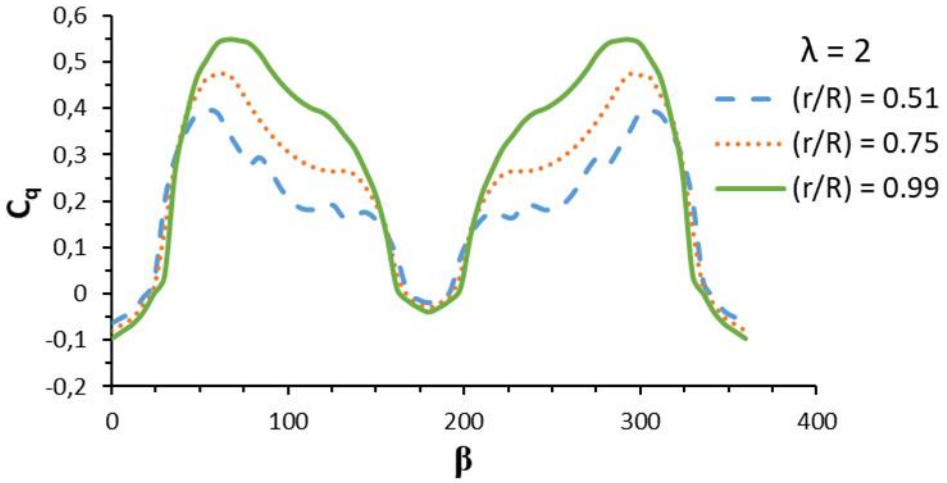

Figure 6.11. Variation of local torque coefficient versus the azimuth angle for (SST model) at $\left(r/R=0.51,0.75,0.99\right);\ G=0.5;\sigma=0.4;C_{do}=0.017;\lambda=2.0$

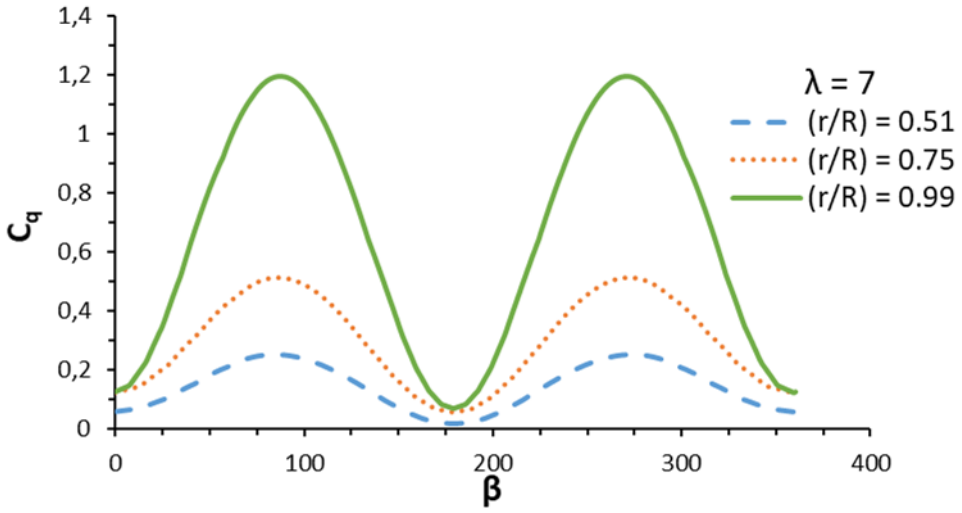

Figure 6.12. Variation of local torque coefficient versus the azimuth angle for (SST model) at $\left(r/R=0.51,0.75,0.99\right)$; $G=0.5;\sigma=0.4;C_{do}=0.017;\lambda=7.0$

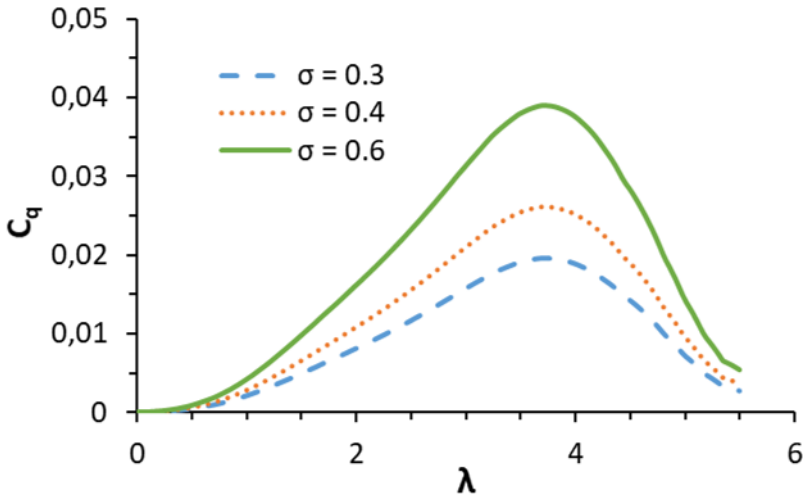

Figure 6.13. The effect of solidity on rotor torque coefficient for (SST model), $G=1.0;C_{do}=0.017;\sigma=0.3-0.6$.

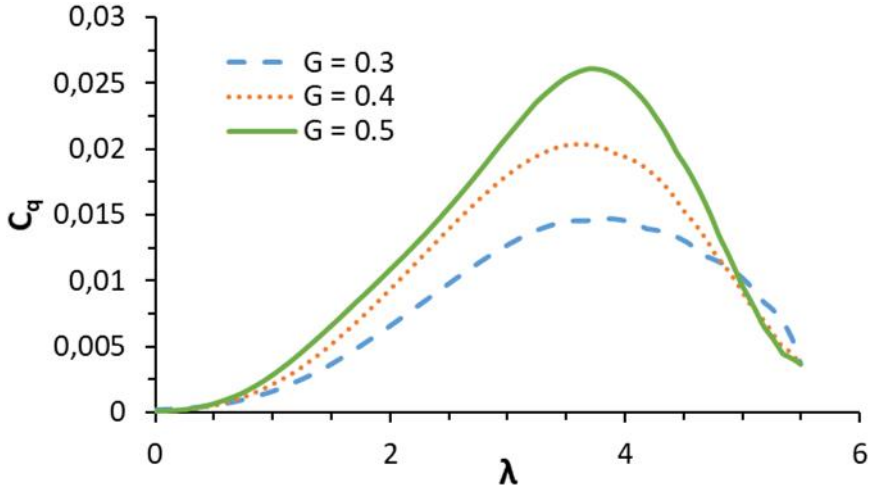

Figure 6.14. The effect of height/diameter on rotor power coefficient for (SST model), $S = 0.4; C_{do} = 0.017; G = 0.3 - 0.5$.

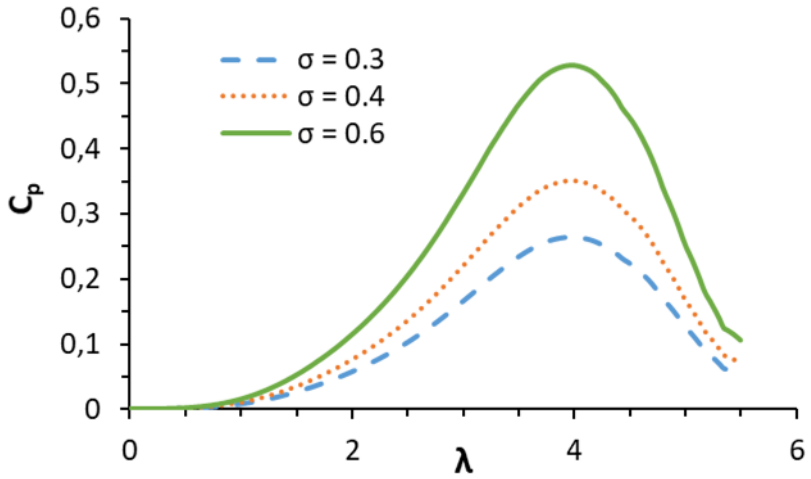

Figure 6.15. The effect of solidity on rotor power coefficient for (SST model), $G = 1.0; C_{do} = 0.017; \sigma = 0.3 - 0.6$.

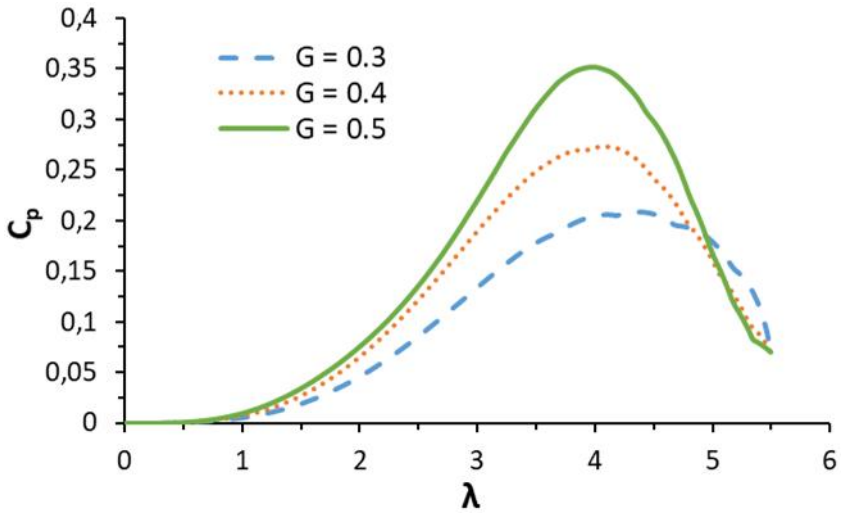

Figure 6.16. Rotor power coefficient versus tip speed ratio for (SST model), $\sigma = 0.4; C_{do} = 0.017; G = 0.3 - 0.5$.

CHAPTER 7

CONCLUSIONS AND FUTURE WORK

7.1. CONCLUSIONS

The principal conclusions as result of this study as follows:

- This study shows that the wind energy is available in Gharyan area. It could be used to generate electricity, also wind energy may be used for other applications like water sea desalination.

- Existing data resources indicate that the mean annual wind speed of over 4.88 m/s at Gharyan which promising to generate 530131 kWh at $C_p = 0.4$.

- Investigation of available wind power density at height 10 m and 50 m indicates Gharyan area have a good power density. This site is ideal for grid connection applications.

- The existing data resources indicates that the expected mean annual wind speed (at height 50 m) of over 7.32 m/s at Gharyan area with capacity factor exceeding 49.94%. These values indicate that Gharyan area could be generate 2187340 kWh per year.

- Tip speed ratio has an important influence on wind rotor performance.

- At low tip speed ratio, the angle of attack increases as the azimuth angle increases, this leads to the stall phase and flow separation which cause the self-starting problem.

- The starting torque of the rotor increases as the solidity increases this may help to improve the performance of the vertical axis wind turbines at low tip speed ratios.

- An increase in the rotor solidity will increase initially the maximum power coefficient, then it decreases, while both the value of λ corresponding to $C_{p,\max}$ and the operating range $\lambda_{\max}$ decreases continuously.

7.2. FUTURE WORKS

The following research points should be considered during the future studies.

- Begin to setup power plants using wind energy, particularly vertical axis wind turbine to overcome the problems on the ground.

- Study the effect of using variable pitch blade of flexible blades on the possibility of self-starting of the vertical axis turbine.

- An experimental work is required to validate the theoretical results this can be done using a wind tunnel or in the real fields.

REFERENCES

1. Wilson, R. E. and Lissaman, P. B. S., "Applied aerodynamics of wind power machines", ***Oregon State University***, California (1974).

2. Darrieus G.J.M., "Turbine having its rotating shaft transverse to the flow of the current", ***US Patent***, Patent No. 1835081 (1931).

3. İnternet: Office of Electricity Regulation UK, "Fifth Renewables Order for England and Wales", **https://www.ofgem.gov.uk/sites/default/files/docs/1998/09/fifth-renewable-order-for-england-and-wales_0.pdf** (1998).

4. Danish Ministry of Environment and Energy, "Energy 21", ***The Danish Government's Action Plan for Energy***, Copenhagen (1996).

5. Sofia, M. M., Farhat, I. A., and Kagilik, A. S., "Investment promotion in renewable energy in Libya; Vision & Methodology", ***AIUE Proceedings of the 2nd Energy and Human Habitat Conference***, 1(1): 1-6 (2021).

6. Ancona, D. F., "Encyclopedia of Architecture: Design, Engineering and Construction", ***John Wiley & Sons***, New York, 32-39 (1989).

7. American Wind Energy Association, "Energy and emission balance favours wind", ***Wind Energy Weekly***, 521 (1992).

8. Decoste, J., Smith, A., White, D., Berkvens, D., and Crawford, J., "Self-starting Darrieus wind turbine", ***Design Project Mech.***, 40 (20): 21-23 (2004).

9. Kirke, B. K., "Evaluation of self-starting vertical axis wind turbines for stand-alone applications", Ph.D. Thesis, ***Griffith University***, Australia, 10-20 (1998).

10. Gupta, R., Roy, S., and Biswas, A., "Computational fluid dynamics analysis of a twisted airfoil shaped two-bladed H-Darrieus rotor made from fiberglass reinforced plastic (FRP)", ***International Journal of Energy and Environment***, 1 (6): 953-968 (2010).

11. Hills, R. L., "Power from Wind: A History of Windmill Technology", ***Cambridge University Press***, London, 89 (1994).

12. Heymann, M., "The History of Wind Energy Utilization 1890-1990", ***Skiba, Martin***, Frankfurt (1995).

13. Wilson, R. E., "Wind-turbine aerodynamics", ***Journal of Wind Engineering and Industrial Aerodynamics***, 5 (4): 357-372 (1980).

14. Carrigan, T. J., Dennis, B. H., Han, Z. X., and Wang, B. P., "Aerodynamic shape optimization of a vertical-axis wind turbine using differential evolution", ***International Scholarly Research Notices***, 2012(1): 1-16 (2012).

15. Grylls, W., Dale, B., and Sarre, P. E., "A theoretical and experimental investigation into the variable pitch vertical axis wind turbine", ***2nd International Symposium on Wind Energy Systems***, Amsterdam, 2 (1): 122-138 (1978).

16. Migliore, P. G., Fritschen, J. R., "Darrieus wind-turbine airfoil configurations", ***U.S. Department of Energy Office of Scientific and Technical Information,*** United States (1982).

17. Drees, H. M., "The cycloturbine and its potential for broad application", ***2nd International Symposium on Wind Energy Systems***, Amsterdam, 2 (1): 81-88 (1978).

18. Putnam, P. C., "Power From The Wind", ***Van Nostrand Reinhold***, New York (1974).

19. Sustainable Energy Development Authority, "2000-2001 Annual Report", ***SEDA Report***, Malaysia, 23-31 (2002).

20. Conradsen, K., Nielsen, L. B., and Prahm, L. P., "Review of Weibull statistics for estimation of wind speed distributions", ***Journal of Climate and Applied Meteorology***, 23 (8): 1173-1183 (1984).

21. Murai, H., Maruyama, S., and Tsukui, M., "Experimental research on gyromill type vertical axis wind turbine using a sail wing", ***Journal of Wind Engineering***, 15 (1): 357-368 (1983).

22. Pasqualetti, M., Gipe, P., and Righter, R., "Wind Power in View-Energy Landscapes in a Crowded World", ***Academic Press***, San Diego (2002).

23. Justus, C. G., Hargraves, W. R., and Yalcin, A., "Nationwide assessment of potential output from wind power generators", ***Journal of Applied Meteorology and Climatology***, 15 (4): 673-678 (1976).

24. Johnson, G. L., "Wind Energy Systems", ***Prentice Hall***, New York (1985).

25. Manwell, J. F., McCowan, J. G., and Rogers, A. L., "Wind energy explained: Theory, design and application", ***Wind Engineering***, 30 (2): 169-175 (2006).

26. Manwell, J. F., McGowan, J. G., and Rogers, A. L., "Wind Energy Explained: Theory, Design and Application, ***John Wiley & Sons***, England (2015).

27. Yee, C. K. and Lai, F. C., "Effects of a porous manifold on thermal stratification in a liquid storage tank", ***Solar Energy***, 71 (4): 241-254 (2001).

28. Rocha, P. A. C., de Sousa, R. C., de Andrade, C. F., and da Silva, M. E. V., "Comparison of seven numerical methods for determining Weibull parameters for wind energy generation in the northeast region of Brazil", ***Applied Energy***, 89 (1): 395-400 (2012).

29. Baseer, M. A., Meyer, J. P., Rehman, S., and Alam, M. M., "Wind power characteristics of seven data collection sites in Jubail, Saudi Arabia using Weibull parameters", ***Renewable Energy***, 10 (2): 35-49 (2017).

30. Fazelpour, F., Markarian, E., and Soltani, N., "Wind energy potential and economic assessment of four locations in Sistan and Balouchestan province in Iran", ***Renewable Energy***, 10 (9): 646-667 (2017).

31. Rehman, S., Halawani, T. O., and Mohandes, M., "Wind power cost assessment at twenty locations in the kingdom of Saudi Arabia", ***Renewable Energy***, 28 (4): 573-583 (2003).

32. Kamal, F. M. and Islam, M. Q., "A theoretical investigation of the design and performance of a horizontal axis wind turbines at wind conditions of Bangladesh", ***Journal of Mechanical Engineering***, 1 (8): 33-51 (1995).

33. Burton, T., Sharpe, D., Jenkins, N., and Bossanyi, E., "Wind Energy Handbook", ***John Wiley & Sons***, Chichester (2001).

34. Izelu, C. O., Agberegha, O. L., and Oguntuberu, O. B., "Wind resource assessment for wind energy utilization in Port Harcout, River State, Nigeria, based on Weibull probability distribution Function", ***International Journal of Renewable Energy Research (IJRER)***, 3 (1): 180-185 (2013).

35. Olaofe, Z. O., "Assessment of the offshore wind speed distributions at selected stations in the south-west coast, Nigeria", ***International Journal of Renewable Energy Research (IJRER)***, 7 (2): 565-577 (2017).

36. Pachauri, R. K. and Chauhan, Y. K., "Assessment of wind energy technology potential in Indian context", ***International Journal of Renewable Energy Research (IJRER)***, 2 (4): 773-780 (2012).

37. Hansen, M. O. L., "Aerodynamics of Wind Turbines", 2th Edition, ***Earthscan Publications Ltd.***, London (2008).

38. DuPont, B. L., Cagan, J., and Moriarty, P., "Optimization of wind farm layout and wind turbine geometry using a multi-level extended pattern search algorithm that accounts for variation in wind shear profile shape", ***International Design Engineering Technical Conferences and Computers and Information in Engineering Conference***, Chicago, 3 (1): 243-252 (2012).

39. Wahl, M., "Designing an H-rotor type wind turbine for operation on Amundsen-Scott south pole station", M.Sc. Thesis, ***Uppsala Universitet***, Sweden (2007).

40. Elmaabrok, A. M., "The aerodynamic of vertical axis wind turbines", M.Sc. Thesis, ***Manchester School of Engineering (Aerospace Division)***, Manchester (1995).

41. Wilson, R. E., "Wind-turbine aerodynamics", ***Journal of Wind Engineering and Industrial Aerodynamics***, 5 (4): 357-372 (1980).

42. Claessens, M. C., "The design and testing of airfoils for application in small vertical axis wind turbines", M.Sc. Thesis, ***Delft University of Technology***, Netherlands (2006).

43. Templin, R. J. "Aerodynamic performance for the NRC vertical axis wind turbine", ***NASA STI/Recon Technical Report N76***, National Aeronautical Establishment, Ottawa (1974).

44. Renewable Energy Authority of Libya (REAOL), "Average monthly wind speed", ***Director of Projects Department Report***, Tripoli (2007).

45. Gasch, R. and Twele, J., "Wind Power Plants: Fundamentals, Design, Construction and Operation", ***Springer-Verlag Berlin***, Heidelberg (2012).

46. Thresher, R. W. and Darrell, M. D., "Trends in the evolution of wind turbine generator configurations and systems", ***Wind Energy***, 1 (1): 70-85 (1998).

47. İnternet: The Wind Power Wind Energy Market Intelligence, "Databases and Reports", **https://www.thewindpower.net/** (2021).

48. İnternet: Green Mechanic, "Vertical Axis Wind Turbine Parts", **https://www.green-mechanic.com/2013/03/vertical-axis-wind-turbine-parts.html** (2021).

49. DeCoste, J., McKay, D., Robinson, B., Whitehead, S., Wright, S., "Self-starting vertical axis wind turbine", Final Year Design Project, ***Dalhousie University***, Halifax (2006).

50. Manwell, J., Mcgowan, J., and Rogers, A. L., "Aerodynamics of wind turbines", ***Wind Energy Explained***, 1 (1): 91-155 (2009).

51. Sandia National Laboratories, "Innovative Design Approaches for Large Wind Turbine Blades", ***Sandia Report***, SAND2003-0723 (2003).

52. Giguere, P., Selig, M. S., and Tangler, J. L., "Blade design trade-offs using low-lift airfoils for stall-regulated HAWTs", ***Journal of Solar Energy Engineering***, 121 (4): 217-223 (1999).

53. Dahl, K. S., Fuglsang, P., "Design of the wind turbine airfoil family RISØ-A-XX", ***RISØ National Laboratory Report***, Denmark (1998).

54. Manwell, J. F., McGowan, J. G., and Rogers, A. L., "Wind Energy Explained: Theory, Design and Application, ***John Wiley & Sons***, England (2010).

55. İnternet: Google, “The Location of Gharyan”, **https://www.google.com.tr/maps/place/Garyan,+Libya/@32.1684619,13.0070164,15z/data=!3m1!4b1!4m5!3m4!1s0x13af3b6a069ddb81:0x1d7fd0b5875d190b!8m2!3d32.1717952!4d13.0184123** (2021).

56. İnternet: Polish Energy, “Polish Energy”, **http://www.polish-energy.com/teaserbox_2423576.jpg** (2021).

57. İnternet: Top Alternative Energy Sources, “The History of Wind Power”, **http://www.top-alternative-energy-sources.com/history-of-wind-power.html** (2021).

58. İnternet: Mechanic Love, “Wind Turbine Types”, **https://mechaniclove.com/wind-turbine-types** (2017).

59. İnternet: Wikipedia, “Location Libya”, **https://en.wikipedia.org/wiki/File:Location Libya** (2021).

60. İnternet: Alamy, “Wind Turbine in Canada”, **http://www.alamy.com/stock-photo-darrieus-windturbineat-government-of-canada-windmill-test-site-at-21252588.html** (2014).

61. İnternet: Auburn University, “Alternative Energy: Nuclear, Wind, and Solar Power”, **https://cla.auburn.edu/ces/energy/alternative-energy/** (2018).

APPENDIX A.

WIND SPEED VALUES

Table Appendix A.1. Shows the wind speed S (m/s) and direction D (°) at 10 meter height in January/2016.

Time	00:00		03:00		06:00		09:00		12:00		15:00		18:00		21:00	
Date	**D**	**S**	**D**	**S**	**D**	**S**	**D**	**S**	**D**	**S**	**D**	**S**	**D**	**S**	**D**	**S**
01-Jan	270	7.5	300	7.5	280	9	270	5	330	5	360	5	350	5	360	5
02-Jan	60	2.5	350	5	330	5	300	4	290	4	0	0	0	0	260	3
03-Jan	240	3	0	0	260	5	230	8	230	8	230	9	220	7.5	220	10
04-Jan	220	7.5	90	2.5	210	9	210	9	240	7.5	180	6	150	5	200	7
05-Jan	210	15	180	5	210	9	180	6	180	10	160	7	150	10	160	6
06-Jan	170	7	180	6	190	5	270	2.5	170	2.5	330	2	90	2	170	2
07-Jan	180	2	0	0	0	0	130	3.5	270	2.5	270	6	250	5	150	5
08-Jan	120	6.5	150	4	130	4	100	4	0	0	30	6	170	3	0	0
09-Jan	90	3	0	0	0	0	0	0	0	0	330	2.5	0	0	0	0
10-Jan	0	0	0	0	0	0	0	0	0	0	80	3	90	2.5	0	0
11-Jan	0	0	0	0	0	0	0	0	0	0	0	0	0	0	0	0
12-Jan	180	7.5	180	5	240	5	0	0	300	6	270	4	0	0	0	0
13-Jan	0	0	0	0	0	0	240	2.5	250	4	240	5	220	2.5	220	5
14-Jan	240	4	240	2.5	240	2.5	270	2.5	270	5	210	4	0	0	0	0
15-Jan	0	0	210	2.5	210	4	210	6	220	6	210	3.5	0	0	200	4
16-Jan	200	4	200	3.5	210	5	200	6	300	4	240	4	220	2.5	220	4
17-Jan	240	7	240	7	230	8	270	8	300	9	320	9	300	9	270	5
18-Jan	320	9	280	9	300	10	300	12.5	330	5	330	6	340	6	330	4
19-Jan	340	4	340	2.5	340	4	340	4	340	5	60	7	30	6	10	5
20-Jan	30	4	50	6	0	0	30	3.5	360	4	10	3.5	0	0	0	0
21-Jan	0	0	0	0	0	0	0	0	330	2.5	330	5	300	2.5	0	0
22-Jan	210	5	270	5	270	5	270	6	350	7.5	300	7.5	270	5	300	7.5
23-Jan	270	5	260	5	240	6	270	5	270	5	330	11	320	10	310	5
24-Jan	320	7	320	7.5	330	7.5	330	7	330	12	330	14	330	7.5	330	5
25-Jan	0	0	0	0	30	2.5	40	3.5	20	3.5	0	0	0	0	50	2.5
26-Jan	0	0	0	0	330	4	330	4	350	5	350	4	330	2.5	330	2.5
27-Jan	300	4	330	4	300	2.5	350	5	240	2.5	0	0	320	2.5	300	2.5
28-Jan	300	5	300	6.5	280	7.5	300	7	300	10	300	7	330	7	300	4
29-Jan	0	3.5	330	3	330	4	310	2.5	0	0	70	3	0	0	0	0
30-Jan	0	0	0	0	0	0	0	0	330	3	0	0	0	0	0	0
31-Jan	0	0	210	4	220	4	210	5	240	5	240	5	0	0	0	0

Table Appendix A.2. Shows the wind speed S (m/s) and direction D (°) at 10 meter height in February/2016.

Time	00:00		03:00		06:00		09:00		12:00		15:00		18:00		21:00	
Date	**D**	**S**	**D**	**S**	**D**	**S**	**D**	**S**	**D**	**S**	**D**	**S**	**D**	**S**	**D**	**S**
01-Feb	0	0	0	0	0	0	0	0	0	0	0	0	0	0	0	0
02-Feb	0	0	220	6	210	6	190	5	180	4	180	4	210	3	200	5
03-Feb	190	3	200	3	210	4	170	4	0	0	360	3	0	0	190	4
04-Feb	180	3	200	2.5	0	0	320	4	330	2.5	0	0	0	0	0	0
05-Feb	0	0	0	0	0	0	300	2.5	300	5	290	7	350	6	10	6
06-Feb	0	0	0	0	350	4	330	7.5	330	8.5	120	9	330	7.5	320	4
07-Feb	300	4	320	6	330	3.5	300	5	300	5	290	6.5	340	6	330	6.5
08-Feb	300	7	320	7.5	300	8.5	300	11	340	6.5	330	7.5	300	7.5	310	7.5
09-Feb	310	7.5	300	7.5	330	4	350	4	350	6	30	4	0	0	310	4
10-Feb	300	5	290	3	300	5	270	7.5	300	7.5	300	5	300	5	300	5
11-Feb	0	0	100	15	300	5	350	4	300	7.5	320	7.5	0	0	0	0
12-Feb	0	0	0	0	0	0	0	0	300	2.5	0	0	0	0	140	5
13-Feb	200	5	180	5	0	0	190	5	330	2.5	70	4	90	3	130	2.5
14-Feb	0	0	180	4	180	5	160	6	180	5	180	7	170	7	180	6
15-Feb	170	6	170	7	180	6	180	9	210	10	210	9	200	9	210	10
16-Feb	210	10	240	9	270	9	300	9	320	9	30	7.5	60	7	10	6
17-Feb	50	4	30	4	350	2.5	30	10	40	5	60	6	30	2.5	30	4
18-Feb	30	3	60	2.5	0	0	70	2.5	300	6	310	2.5	0	0	0	0
19-Feb	0	0	210	4	200	4	200	6	190	5	200	4	0	0	190	4.5
20-Feb	180	4	150	3.5	190	6	180	10	240	5	180	5	210	5	180	7.5
21-Feb	180	10	180	5	180	5	180	7.5	210	7.5	180	5	0	0	210	5
22-Feb	180	5	180	7.5	180	5	240	5	270	3.5	300	4	0	0	0	0
23-Feb	0	0	0	0	300	5	320	4	280	4	360	3	350	3	0	0
24-Feb	0	0	0	0	0	0	0	0	50	5	60	6	90	2.5	180	5
25-Feb	180	5	0	0	0	0	140	4	350	2.5	80	6	80	2	180	6
26-Feb	200	2.5	0	0	210	4	240	2.5	320	2.5	320	5	0	0	0	0
27-Feb	240	2.5	0	0	0	0	10	2.5	10	3	90	2.5	50	3	0	0
28-Feb	0	0	0	0	0	0	0	0	0	0	90	4	60	4.5	0	0
29-Feb	0	0	0	0	280	2.5	330	3.5	330	2.5	320	3	50	2.5	0	0

Table Appendix A.3. Shows the wind speed S (m/s) and direction D (°) at 10 meter height in March/2016.

Time	00:00		03:00		06:00		09:00		12:00		15:00		18:00		21:00	
Date	**D**	**S**	**D**	**S**	**D**	**S**	**D**	**S**	**D**	**S**	**D**	**S**	**D**	**S**	**D**	**S**
01-Mar	0	0	0	0	0	0	340	2.5	360	5	60	5	0	0	0	0
02-Mar	0	0	0	0	0	0	0	0	320	5	330	5	60	2.5	0	0
03-Mar	0	0	0	0	0	0	0	0	180	3	200	5	200	2.5	200	4
04-Mar	180	5	180	5	180	5	190	5	210	10	220	7.5	240	4	0	0
05-Mar	210	3.5	210	5	240	3.5	210	6	220	10	210	8	320	8	330	7
06-Mar	310	6	240	5	240	4	230	8	240	7.5	260	9	260	7	260	8
07-Mar	260	8	260	9	260	5	300	7.5	240	6.5	300	5	220	2.5	240	2.5
08-Mar	0	0	220	3.5	210	5	240	6	240	10	270	6	280	4	0	0
09-Mar	300	4	300	2.5	0	0	0	0	260	3	210	4.5	80	3	0	0
10-Mar	200	4	210	3.5	280	4	260	9	280	6	270	6.5	0	0	210	3
11-Mar	220	7.5	210	5	260	6	270	10	270	7.5	260	6	330	6	330	2.5
12-Mar	330	2.5	0	0	300	2.5	330	5	350	7.5	360	6	0	0	0	0
13-Mar	0	0	300	5	270	4	280	6	320	7.5	350	5	0	0	0	0
14-Mar	0	0	0	0	0	0	0	0	300	5	330	4	0	0	200	4
15-Mar	180	2.5	160	2.5	240	5	240	5	240	5	310	3.5	0	0	220	3.5
16-Mar	240	3.5	240	3.5	240	3.5	240	3	330	5	350	7	0	0	300	4
17-Mar	10	3	70	3	70	4	30	5	360	5	330	5	360	2.5	0	0
18-Mar	0	0	270	4	210	6.5	210	11	220	7.5	240	4	210	3	210	5
19-Mar	210	6	240	7.5	210	10	220	10	210	12.5	220	9	210	5	220	6
20-Mar	290	7.5	230	4	240	4	160	3.5	180	3	300	6	160	3.5	160	5
21-Mar	170	5.5	330	5	340	3.5	360	5	330	5	330	5	0	0	0	0
22-Mar	90	2.5	170	5	180	7.5	180	12.5	180	12.5	180	7.5	240	7.5	270	5
23-Mar	300	5	270	6	270	6	240	6	270	10	240	6	240	3.5	240	2.5
24-Mar	210	9	270	8	310	9	240	6	280	12.5	280	9	280	7.5	270	9
25-Mar	300	9	300	6	200	2.5	0	0	240	4	300	5	300	2.5	0	0
26-Mar	270	2.5	280	2.5	0	0	290	4	270	2.5	300	5	330	2.5	0	0
27-Mar	220	2.5	210	2.5	240	2.5	240	7.5	270	10	320	9	320	7.5	330	6.5
28-Mar	0	0	0	0	240	5	270	7.5	320	10	330	10	330	10	330	7.5
29-Mar	330	7.5	33	5	290	4	340	6	330	7.5	350	6.5	20	3	90	3
30-Mar	0	0	0	0	170	3.5	150	3	0	0	350	2.5	60	3	180	3
31-Mar	180	4	180	5	210	8	180	6	150	10	180	6	150	3.5	180	5

Table Appendix A.4. Shows the wind speed S (m/s) and direction D (°) at 10 meter height in April/2016.

Time	00:00		03:00		06:00		09:00		12:00		15:00		18:00		21:00	
Date	**D**	**S**	**D**	**S**	**D**	**S**	**D**	**S**	**D**	**S**	**D**	**S**	**D**	**S**	**D**	**S**
01-Apr	270	7.5	330	7	330	7.5	270	7.5	270	5	270	5	0	0	240	4
02-Apr	330	5	330	5	240	7.5	280	7	330	9	340	8	350	5	310	2.5
03-Apr	290	2.5	0	0	300	2.5	300	2.5	280	6	330	6	90	2	0	0
04-Apr	0	0	0	0	0	0	60	4	270	2.5	0	0	40	6.5	360	2.5
05-Apr	360	5	30	5	330	6	350	8	300	7.5	300	7	330	9	300	4
06-Apr	300	2.5	240	3.5	250	2.5	270	5	240	6	300	6	290	2.5	240	4
07-Apr	240	6	240	7	250	5	240	10	220	9	300	9	300	4	0	0
08-Apr	240	2.5	240	4	240	7.5	210	10	240	9	240	10	240	4	270	8
09-Apr	300	9	270	2.5	240	2.5	270	3.5	300	4	0	0	0	0	180	6
10-Apr	220	7	240	4	210	4	0	0	240	5	240	5	0	0	240	5
11-Apr	210	2.5	210	5	240	7.5	220	10	220	10	210	10	220	5	0	0
12-Apr	240	4	210	10	210	12.5	280	7	310	9	350	7	320	4	0	0
13-Apr	0	0	60	2.5	90	3	90	6	60	2.5	30	7.5	30	5	330	6
14-Apr	320	4	320	7	330	7.5	310	7	360	8	360	6	350	6	310	2.5
15-Apr	20	3.5	60	2.5	0	0	60	4	90	2.5	0	0	50	2.5	170	4
16-Apr	200	5	170	3	170	6	150	7.5	180	10	150	9	180	7.5	150	9
17-Apr	150	9	180	11	180	6.5	180	16	210	15	300	6	300	5	320	5
18-Apr	300	7.5	300	5	270	2.5	220	3	0	0	190	5	0	0	150	6
19-Apr	170	12.5	170	9	180	10	190	12.5	210	10	240	9	220	6	240	3
20-Apr	260	3.5	240	2.5	220	4	240	7.5	270	5	300	5	210	5	240	5
21-Apr	210	5	210	7.5	270	5	300	6	360	6	360	7.5	0	0	0	0
22-Apr	0	0	360	5	60	5	80	6	30	2.5	70	5	60	7.5	90	2.5
23-Apr	0	0	0	0	150	5	90	5	120	4	60	9	60	6	120	2.5
24-Apr	0	0	0	0	0	0	80	3.5	60	6	360	7	30	5	0	0
25-Apr	0	0	30	2.5	330	7	330	7	350	10	360	6	350	7.5	300	5
26-Apr	320	5	320	6	320	5	300	4	330	5	300	6.5	360	5	330	4
27-Apr	300	4	320	2.5	330	2.5	300	5	320	7	310	6	350	5	0	0
28-Apr	0	0	0	0	150	4	0	0	30	3	330	3	0	0	0	0
29-Apr	210	3.5	210	4	210	7.5	180	5.5	280	5	260	4	0	0	0	0
30-Apr	210	8	200	7.5	210	7	240	10	300	7.5	270	5	0	0	180	5

Table Appendix A.5. Shows the wind speed S (m/s) and direction D (°) at 10 meter height in May/2016.

Time	00:00		03:00		06:00		09:00		12:00		15:00		18:00		21:00	
Date	**D**	**S**	**D**	**S**	**D**	**S**	**D**	**S**	**D**	**S**	**D**	**S**	**D**	**S**	**D**	**S**
01-May	180	5	180	5	210	7.5	210	7.5	180	7.5	180	6	0	0	150	6
02-May	180	10	180	10	180	7.5	280	5	300	9	300	8	290	3	300	5
03-May	290	8	290	8	280	7	330	9	330	6	330	6	0	0	300	2.5
04-May	310	4	0	0	150	2.5	30	2.5	320	3.5	350	4	90	2.5	170	2.5
05-May	170	5	0	0	0	0	260	2	10	4	330	2.5	340	2.5	170	4
06-May	170	3	170	2.5	160	2.5	180	9	320	6	300	4	350	4	100	2.5
07-May	170	2.5	240	2.5	0	0	330	5	60	5	360	4.5	0	0	180	3.5
08-May	180	5	180	5	180	8	180	7.5	120	5	130	5	150	10	150	11
09-May	160	15	170	12.5	170	15	180	12.5	180	12.5	180	12.5	180	9	210	7.5
10-May	190	9	210	12.5	220	5	300	7.5	270	7.5	330	7.5	330	4	0	0
11-May	0	0	0	0	0	0	90	5	90	5	90	7.5	90	7.5	120	6
12-May	180	9	180	7.5	150	9	170	6	310	5	320	6	320	6	290	7
13-May	290	5	290	6	300	5	330	7	330	8	300	6	30	2.5	0	0
14-May	0	0	0	0	330	2.5	300	4	320	5	360	5	60	5	150	4
15-May	150	5	160	5	180	5	180	5	60	2.5	0	0	160	6	160	5
16-May	180	6	180	7	180	9	170	10	150	12.5	150	10.5	150	12.5	160	7.5
17-May	150	12.5	160	11.5	170	9	210	5	270	7	240	5	240	5	270	2.5
18-May	270	3.5	270	2.5	240	2.5	210	4	210	7.5	0	0	220	12.5	220	10
19-May	210	9	210	7.5	240	12.5	240	9	270	7.5	290	6	290	7.5	290	3
20-May	290	2.5	0	0	270	5	240	5	140	5	240	7.5	0	0	0	0
21-May	0	0	180	5	180	7.5	180	7.5	220	7.5	60	7.5	60	5	90	5
22-May	120	4	180	3.5	180	7.5	190	6	330	5	350	5	70	5	100	2.5
23-May	170	7	170	5	180	6	90	4	30	6	90	5	120	7	150	5
24-May	150	7.5	180	6	180	7.5	160	5	170	4	180	2.5	150	3.5	100	5
25-May	160	11	150	11	150	10	160	12.5	160	12	170	10	90	5	150	5
26-May	170	7	160	8	180	7.5	180	12	180	10	150	8	150	7	170	11
27-May	180	10	170	10	180	9	210	11	180	13	180	7	60	9	160	8
28-May	180	9.5	160	6	180	10	170	11	200	12.5	180	9	150	7.5	160	7.5
29-May	200	7.5	270	6	280	6	290	6.5	330	5	330	6	30	4	0	0
30-May	0	0	0	0	90	4	90	5	90	7.5	90	7.5	90	5	120	2.5
31-May	0	0	180	5	150	5	0	0	60	6	90	7.5	120	5	150	5

Table Appendix A.6. Shows the wind speed S (m/s) and direction D (°) at 10 meter height in June/2016.

Time	00:00		03:00		06:00		09:00		12:00		15:00		18:00		21:00	
Date	**D**	**S**	**D**	**S**	**D**	**S**	**D**	**S**	**D**	**S**	**D**	**S**	**D**	**S**	**D**	**S**
01-Jun	180	7.5	150	10	180	10	150	10	180	10	180	9	180	5	180	7.5
02-Jun	160	8	180	9	180	12	200	10	300	9	330	7	310	6	60	2.5
03-Jun	300	2.5	300	5	300	7	300	7	350	5	360	6	330	2.5	330	3.5
04-Jun	360	4	0	0	50	2.5	0	0	360	2.5	360	2.5	80	4	0	0
05-Jun	190	6	190	5	170	8	180	8.5	270	6	0	0	90	3	160	3
06-Jun	0	0	280	3	350	4	40	5	320	5	40	5	60	6	100	2.5
07-Jun	0	0	0	0	140	5	360	4	90	2.5	30	6	60	4	90	3
08-Jun	90	5	90	3	120	5	160	5	170	6	120	4	120	6	150	4
09-Jun	120	5	150	5	100	7.5	90	7.5	180	10	90	6.5	90	7.5	150	6.5
10-Jun	160	5	160	8.5	50	6.5	120	4	90	7.5	90	9	90	6	0	0
11-Jun	180	6	0	0	0	0	80	5	80	4	100	4	90	6	190	6
12-Jun	190	7	180	7.5	180	4	180	7	330	6	330	5	330	4	320	5
13-Jun	300	4	330	4	330	5	60	2.5	60	5	60	5	30	5	90	2.5
14-Jun	60	4	60	5	90	2.5	90	5	70	5	50	9	60	4	90	3
15-Jun	0	0	160	2.5	160	3	150	5	60	8	80	3.5	60	5	120	3.5
16-Jun	170	6.5	180	7	180	6.5	150	9	170	5	200	5	160	7.5	150	10
17-Jun	160	8	150	9	160	7.5	180	9	170	7.5	180	7.5	140	7.5	170	9
18-Jun	170	10	160	7.5	180	7	180	11	200	5	170	5	230	3	330	5
19-Jun	290	6	290	6	300	3	300	7.5	300	5	330	7.5	330	5	330	2.5
20-Jun	0	0	0	0	0	0	330	2.5	0	0	360	6.5	30	7.5	0	0
21-Jun	0	0	0	0	0	0	340	3	0	0	60	6	60	5	0	0
22-Jun	0	0	0	0	70	3	30	2.5	90	4	120	4	120	2.5	120	7.5
23-Jun	150	5	150	5	150	2.5	90	5	90	7	60	9	90	7	0	0
24-Jun	150	4	170	2.5	170	4	70	2.5	90	6	170	3	90	7	90	6
25-Jun	160	2.5	170	2.5	160	4	0	0	130	2.5	330	3.5	60	6	100	5
26-Jun	170	3.5	180	2.5	180	3.5	280	0	330	4	40	7.5	60	6	0	0
27-Jun	160	5	180	4	180	5	180	3.5	330	3	90	2.5	60	7	0	0
28-Jun	160	0	160	3	0	0	0	0	210	3	340	6	60	5	90	4
29-Jun	0	3.5	0	0	100	4	90	10	150	3	150	4	120	5	150	5
30-Jun	150	5	150	5	150	5	150	5	120	6	150	7.5	150	12.5	120	5

Table Appendix A.7. Shows the wind speed S (m/s) and direction D (°) at 10 meter height in July/2016.

Time	00:00		03:00		06:00		09:00		12:00		15:00		18:00		21:00	
Date	**D**	**S**	**D**	**S**	**D**	**S**	**D**	**S**	**D**	**S**	**D**	**S**	**D**	**S**	**D**	**S**
01-Jul	120	12.5	120	7.5	120	5	130	8	160	7	130	4	90	7	100	4
02-Jul	100	5	120	2.5	0	0	30	4	50	7	50	12.5	80	5	0	0
03-Jul	130	2.5	0	0	180	4	300	3.5	330	1.5	350	7	60	3.5	0	0
04-Jul	180	2.5	200	2.5	200	3.5	0	0	330	5	60	9	30	7.5	0	0
05-Jul	180	6	0	0	210	2.5	280	5	330	8	350	5.5	320	4	0	0
06-Jul	0	0	0	0	350	3.5	30	6.5	330	5	360	5	0	0	0	0
07-Jul	180	4	150	2.5	0	0	20	3	0	0	60	6	90	4	180	4
08-Jul	0	0	0	0	0	0	30	3.5	90	4	60	6	40	4	0	0
09-Jul	180	5	0	0	0	0	300	5	320	5	330	5	360	5	0	0
10-Jul	0	0	0	0	330	5	330	5	350	5	360	5	360	5	0	0
11-Jul	0	0	0	0	0	0	300	2.5	300	6	340	6	30	3.5	160	3.5
12-Jul	190	6	0	0	230	4	30	3	10	3	330	5	50	5	160	6
13-Jul	170	7	170	6	180	7	170	8	180	7	0	0	150	5	170	8
14-Jul	180	10	180	4	0	0	360	1.5	360	2.5	360	7.5	320	3.5	0	0
15-Jul	150	6	240	4	0	0	0	0	300	5	90	5	30	6.5	0	0
16-Jul	0	0	0	0	0	0	330	4	330	5	30	6	60	4	0	0
17-Jul	0	0	180	2.5	160	5	300	3	340	2.5	30	2.5	0	0	0	0
18-Jul	180	4	0	0	0	0	360	3	0	0	360	2.5	40	3	60	3
19-Jul	180	5	200	6	210	5	270	5	270	10	320	5	360	5	270	5
20-Jul	300	5	0	0	0	0	360	4	30	3.5	360	7.5	30	5	0	0
21-Jul	0	0	0	0	0	0	90	3.5	60	5	90	2.5	40	5	0	0
22-Jul	0	0	0	0	0	0	60	3.5	10	5	40	6	40	5	70	5
23-Jul	0	0	10	5	300	3	330	5	330	5	40	2.5	30	3.5	30	4
24-Jul	0	0	0	0	0	0	30	2.5	60	6	330	5	30	2.5	0	0
25-Jul	0	0	0	0	0	0	330	3.5	350	5	320	4	0	0	210	2.5
26-Jul	190	7	180	6	240	5	320	4	270	6	260	4	60	2.5	330	2.5
27-Jul	0	0	310	3	310	4	320	5	340	6	350	6	350	5	0	0
28-Jul	340	2.5	340	2.5	0	0	320	2.5	330	6	300	5	10	5	0	0
29-Jul	0	0	0	0	320	2.5	360	5	60	5	360	2.5	60	5	0	0
30-Jul	0	0	60	5	150	5	0	0	40	6	60	7.5	60	6	90	5
31-Jul	90	5	150	4	150	4	270	5	90	3.5	60	5	60	6	0	0

Table Appendix A.8. Shows the wind speed S (m/s) and direction D (°) at 10 meter height in August/2016.

Time	00:00		03:00		06:00		09:00		12:00		15:00		18:00		21:00	
Date	**D**	**S**	**D**	**S**	**D**	**S**	**D**	**S**	**D**	**S**	**D**	**S**	**D**	**S**	**D**	**S**
01-Aug	150	5	180	2.5	120	2.5	0	0	70	2.5	90	7	160	7.5	150	2.5
02-Aug	160	2.5	0	0	0	0	90	5	60	5	90	6	60	5	0	0
03-Aug	0	0	0	0	0	0	330	5	300	5	360	5	30	3.5	0	0
04-Aug	0	0	0	0	330	3.5	360	5	60	6.5	40	7.5	40	4	0	0
05-Aug	0	0	0	0	180	2.5	90	3.5	330	2.5	360	6	70	5	0	0
06-Aug	180	3.5	180	3.5	0	0	360	5	330	5	0	0	30	5	0	0
07-Aug	180	2.5	0	0	0	0	60	5	360	5	60	5	60	6	0	0
08-Aug	0	0	0	0	0	0	0	0	350	6	20	6	60	4	0	0
09-Aug	180	2.5	0	0	0	0	350	2.5	30	7	30	5	70	4	0	0
10-Aug	0	0	0	0	330	3	330	3	300	6	330	3.5	60	4	0	0
11-Aug	0	0	0	0	0	0	150	4	60	5	60	7	80	4	180	5
12-Aug	180	5.5	180	6	180	3.5	270	2.5	0	0	0	0	50	4	180	4
13-Aug	180	2.5	0	0	0	0	320	4	30	7.5	360	9	60	5	0	0
14-Aug	180	5	0	0	320	2.5	300	2.5	90	5	90	2.5	30	5	0	0
15-Aug	0	0	0	0	0	0	0	0	50	5	30	6	60	4	0	0
16-Aug	0	0	0	0	60	2.5	0	0	340	5	30	5	60	4	70	5
17-Aug	0	0	0	0	0	0	0	0	0	0	10	2.5	70	3	150	4
18-Aug	180	6	0	0	0	0	200	4	0	0	320	5	60	7	150	5
19-Aug	180	7.5	180	2.5	180	4	0	0	240	3.5	60	7	60	6	90	3
20-Aug	0	0	0	0	0	0	360	5	40	7.5	40	5	60	5	0	0
21-Aug	0	0	0	0	0	0	30	2.5	90	4	50	5	50	6	0	0
22-Aug	0	0	0	0	0	0	350	3.5	360	3	350	5	0	0	0	0
23-Aug	0	0	0	0	270	2.5	360	5	300	4	330	4	60	5	0	0
24-Aug	0	0	0	0	0	0	280	5	0	0	30	2.5	80	3	0	0
25-Aug	0	0	200	5	240	5	300	4	30	5	20	2.5	0	0	0	0
26-Aug	0	0	0	0	90	2.5	80	4	0	0	60	7	60	5	90	2.5
27-Aug	90	2.5	0	0	160	2.5	60	2.5	90	6	70	6.5	60	5.5	150	7.5
28-Aug	170	9	160	6	240	2.5	0	0	330	4	30	2.5	80	2.5	150	7.5
29-Aug	200	5	0	0	0	0	260	4	0	0	60	5	60	4	110	6
30-Aug	130	5.5	0	0	150	3	120	5	120	5	90	5	90	10	0	0
31-Aug	0	0	0	0	0	0	30	5	30	4	60	7.5	60	5	0	0

Table Appendix A.9. Shows the wind speed S (m/s) and direction D (°) at 10 meter height in September/2016.

Time	00:00		03:00		06:00		09:00		12:00		15:00		18:00		21:00	
Date	**D**	**S**	**D**	**S**	**D**	**S**	**D**	**S**	**D**	**S**	**D**	**S**	**D**	**S**	**D**	**S**
01-Sep	180	5	180	4	180	4	140	2.5	110	7	30	4	60	7	140	3
02-Sep	170	4	0	0	180	2.5	0	0	350	6	10	4	0	0	180	4
03-Sep	180	6	180	5	180	5	0	0	0	0	300	2.5	0	0	0	0
04-Sep	0	0	200	5	210	5	210	3	350	6	310	4	70	2.5	0	0
05-Sep	0	0	210	2.5	210	4	0	0	40	4	60	6	40	3	0	0
06-Sep	0	0	180	5	0	0	150	3.5	30	5.5	60	3.5	120	5	160	6
07-Sep	180	5	180	6	0	0	90	2.5	150	2.5	60	5	90	2.5	150	2.5
08-Sep	180	2.5	0	0	150	2.5	0	0	90	5	80	6	70	5	0	0
09-Sep	0	0	0	0	0	0	0	0	30	4	30	8	0	0	0	0
10-Sep	0	0	0	0	0	0	330	5	350	7	360	5	0	0	0	0
11-Sep	0	0	0	0	0	0	20	4	20	5	20	5	20	5	150	5
12-Sep	180	2.5	0	0	0	0	0	0	330	2.5	30	4	0	0	0	0
13-Sep	180	5	180	6	210	6	170	2.5	220	5	220	2	0	0	160	5
14-Sep	170	5	190	7.5	210	7.5	210	12.5	210	10	340	7.5	350	5	30	6
15-Sep	350	5	20	6	30	5	60	6	330	4	330	6	330	5	60	4
16-Sep	0	0	0	0	0	0	160	2.5	270	2.5	240	3	80	4	120	2.5
17-Sep	170	2.5	240	3	0	0	0	0	30	3.5	300	4	0	0	0	0
18-Sep	180	5	170	3	180	5	180	5	180	6	180	5	180	5	170	9
19-Sep	170	5.5	180	5.5	180	5	60	3	330	4	330	2.5	0	0	0	0
20-Sep	60	3.5	60	4.5	360	5	340	5	330	7.5	340	6	340	7	330	6
21-Sep	330	5	350	4	220	4.5	330	5	300	5	360	6.5	0	0	0	0
22-Sep	0	0	240	2.5	220	7.5	210	8	280	5	300	6	90	2.5	180	3.5
23-Sep	180	5	240	6	240	4	240	5	270	5	240	5	0	0	270	5
24-Sep	240	10	240	5	300	5	270	5	270	10	360	6	60	4	0	0
25-Sep	0	0	0	0	0	0	0	0	340	7	50	7	60	4	60	3
26-Sep	0	0	0	0	0	0	0	0	280	3	330	5	80	3	160	2.5
27-Sep	180	6	160	6	170	4	150	5	150	9	180	5	60	6	60	7.5
28-Sep	70	2.5	90	5	120	2.5	90	2.5	90	6	70	4	70	4	70	3
29-Sep	150	2.5	150	5	170	5	170	6	0	0	60	3.5	90	3	170	5
30-Sep	180	6	210	4	270	6	150	6.5	190	5	240	3.5	0	0	0	0

Table Appendix A.10. Shows the wind speed S (m/s) and direction D (°) at 10 meter height in October/2016.

Time	00:00		03:00		06:00		09:00		12:00		15:00		18:00		21:00	
Date	**D**	**S**	**D**	**S**	**D**	**S**	**D**	**S**	**D**	**S**	**D**	**S**	**D**	**S**	**D**	**S**
01-Oct	210	3.5	210	3.5	0	0	300	5	270	6.5	240	7.5	210	5	210	5
02-Oct	240	5	220	6	180	6.5	220	5	320	4	300	7.5	0	0	330	3.5
03-Oct	0	0	0	0	0	0	240	5	270	4.5	360	7	0	0	180	3.5
04-Oct	210	5	210	4.5	240	6	210	7	210	5	270	5	40	5	60	5
05-Oct	60	7.5	90	5	140	2.5	90	5	90	5	90	5	90	2.5	150	5
06-Oct	180	5	180	5	180	5	180	6	0	0	120	2.5	90	5	120	5
07-Oct	180	5	120	5	180	5	180	8	270	8	180	5	180	4	180	4
08-Oct	180	3	0	0	180	7	200	6	220	3	190	5	170	2.5	180	3
09-Oct	160	3	170	2.5	160	6	180	9	90	10	180	7	100	4	120	4
10-Oct	150	10	160	10	150	10	150	12.5	0	9	120	7	140	9	150	7.5
11-Oct	150	8	150	9	170	9	170	9	170	5	120	3	150	6.5	150	5
12-Oct	170	3	150	3	90	6	60	4	270	6	30	5	160	7.5	60	3
13-Oct	30	3	30	4	360	5	40	7.5	180	6	40	6	30	4	0	0
14-Oct	0	0	0	0	330	2.5	320	3	100	4	0	0	90	2.5	120	2.5
15-Oct	210	3	0	0	180	4	210	3.5	170	5	210	4	0	0	180	3.5
16-Oct	210	6	210	5	180	4.5	270	3.5	60	5	0	0	0	0	0	0
17-Oct	0	0	240	5	220	6	240	5	360	7.5	180	7.5	240	5	270	5
18-Oct	0	0	170	5	150	2.5	180	3.5	300	2.5	60	4	90	3.5	0	0
19-Oct	150	3.5	180	3.5	170	5	140	5	180	2.5	120	5	120	3	160	9
20-Oct	180	7	180	7	190	7.5	200	9	240	6	0	0	200	3	200	6
21-Oct	210	7.5	220	6	220	10	240	7.5	270	10	270	6	350	6	290	3
22-Oct	290	2.5	310	2.5	0	0	210	3.5	330	4	330	4	90	2.5	150	6
23-Oct	160	7.5	180	7.5	150	7.5	180	5	100	5	330	4.5	320	5	300	3.5
24-Oct	310	3	310	2.5	0	0	300	3.5	240	3.5	320	4	70	2.5	0	0
25-Oct	0	0	180	3.5	180	5	160	6.5	260	4	150	2.5	150	4	180	7.5
26-Oct	180	6.5	170	10	180	9	180	9	300	5	150	2.5	170	3.5	170	5
27-Oct	170	6	180	5	190	5	240	5	330	6	0	0	90	2.5	180	7
28-Oct	180	10	180	10	240	10	200	10	360	10	210	8	180	5	180	9
29-Oct	180	10	210	15	220	7	100	2.5	120	10	210	10	180	7.5	180	5
30-Oct	210	5	210	5	220	7.5	220	7.5	170	6	270	5	180	4	240	7.5
31-Oct	220	5	180	5	180	5	170	7	210	11	190	11	190	10	200	6

Table Appendix A.11. Shows the wind speed S (m/s) and direction D (°) at 10 meter height in November/2016.

Time	00:00		03:00		06:00		09:00		12:00		15:00		18:00		21:00	
Date	**D**	**S**	**D**	**S**	**D**	**S**	**D**	**S**	**D**	**S**	**D**	**S**	**D**	**S**	**D**	**S**
01-Nov	260	2.5	0	0	0	0	190	3	320	3	70	2.5	110	2.5	180	4
02-Nov	170	7	180	6	180	10	180	11	180	7	210	4	180	3.5	190	5
03-Nov	200	7.5	180	4	210	9	240	3.5	210	7	190	5	170	2.5	150	6.5
04-Nov	180	5	180	9	190	12	180	7.5	180	12.5	270	6	70	2.5	60	2.5
05-Nov	0	0	0	0	0	0	360	3.5	60	5	60	7	90	3	90	3
06-Nov	90	2.5	60	2.5	360	3.5	300	5	300	5	300	7	300	2.5	300	2.5
07-Nov	300	2.5	300	5	300	5	350	4	350	6	340	5	360	5	0	0
08-Nov	0	0	0	0	0	0	30	4	70	5	90	2.5	70	4	0	0
09-Nov	150	2.5	0	0	0	0	70	3.5	80	2.5	10	5	40	3.5	0	0
10-Nov	0	0	350	2.5	330	5	190	6	330	3	330	2.5	0	0	170	2.5
11-Nov	170	4	290	4	300	3.5	0	0	330	5	330	3.5	0	0	0	0
12-Nov	0	0	0	0	240	3	180	4	180	4	180	3	0	0	150	5
13-Nov	150	6.5	150	7.5	200	6	210	6	240	8	270	4	270	3	0	0
14-Nov	0	0	0	0	300	3	30	2.5	270	5	300	5	300	5	300	2.5
15-Nov	330	2.5	240	2.5	240	2.5	240	7.5	270	4	300	5	300	4	0	0
16-Nov	0	0	0	0	0	0	230	4	230	2.5	300	2.5	300	3	0	0
17-Nov	0	0	0	0	250	3	240	7	280	9	290	5	280	4	280	4
18-Nov	270	2.5	270	4	280	9	280	5	300	5	300	5.5	290	6	290	4.5
19-Nov	290	3	280	4	300	3	270	3.5	300	5	330	4.5	0	0	0	0
20-Nov	180	3.5	160	3	180	2.5	150	7.5	150	4	210	3.5	210	4	10	4
21-Nov	180	2.5	180	2.5	210	4	190	5.5	240	5.5	240	3	0	0	300	2.5
22-Nov	280	5.5	300	5.5	240	7	300	15	300	7.5	300	10	270	7.5	300	7.5
23-Nov	270	10	270	10	240	5	330	7.5	270	5	300	4	0	0	0	0
24-Nov	0	0	180	12.5	180	7.5	220	7	300	5	300	9	290	5	240	4
25-Nov	240	4	250	5	260	6	240	9	260	7.5	240	9	230	6	240	6
26-Nov	240	4	240	3	0	0	0	0	230	3	190	3.5	190	4	180	5
27-Nov	180	5	180	7	170	8	170	11	150	12.5	150	11	170	12.5	160	10
28-Nov	150	7	150	6.5	0	0	240	6	240	6.5	240	9	270	6	280	7.5
29-Nov	280	6.5	280	7.5	270	5	240	5	270	6	0	0	240	5	0	0
30-Nov	210	3.5	210	3	240	4	210	7.5	150	5	180	7.5	180	10	180	7.5

Table Appendix A.12. Shows the wind speed S (m/s) and direction D (°) at 10 meter height in December/2016.

Time	00:00		03:00		06:00		09:00		12:00		15:00		18:00		21:00	
Date	**D**	**S**	**D**	**S**	**D**	**S**	**D**	**S**	**D**	**S**	**D**	**S**	**D**	**S**	**D**	**S**
01-Dec	270	5	300	5	300	5	30	6	0	0	0	0	0	0	210	3.5
02-Dec	180	4	210	6	210	7.5	200	7	230	5	0	0	210	3	230	5
03-Dec	240	5	260	4	0	0	320	4	300	9	250	4	270	10	270	10
04-Dec	270	10	250	7.5	260	6	290	7.5	260	6	280	3.5	0	0	0	0
05-Dec	0	0	0	0	170	3.5	170	2.5	290	2.5	10	2.5	270	2	300	5
06-Dec	310	2.5	320	5	270	5	300	7	320	10	300	10	280	7.5	280	5
07-Dec	270	4.5	270	5.5	300	3	300	3.5	280	5	300	4	300	2.5	250	2.5
08-Dec	280	2.5	0	0	330	3.5	220	2.5	330	5	360	3	0	0	0	0
09-Dec	150	4	150	3	160	6.5	150	10	180	10	150	5	180	5	150	5
10-Dec	150	10	160	5	180	10	180	10	180	7.5	170	12.5	170	13.5	170	13
11-Dec	160	8	180	7.5	210	7	240	5	270	12.5	300	11	300	12.5	270	9
12-Dec	270	4	240	7.5	270	5	270	6	290	8	270	7	0	0	270	3
13-Dec	270	2.5	270	2.5	0	0	320	4	0	0	270	2.5	200	2.5	210	7.5
14-Dec	220	5	0	0	0	0	240	4	210	8	210	5.5	200	3	210	7.5
15-Dec	190	8	180	5	170	6	180	7	210	6.5	210	3.5	210	7	180	4
16-Dec	240	6	210	4.5	0	0	0	0	320	5	360	2.5	0	0	0	0
17-Dec	0	0	0	0	300	3.5	300	7.5	270	10	270	7.5	270	7.5	240	5
18-Dec	240	7.5	270	9	220	10	270	8	320	7.5	270	6	330	2	0	0
19-Dec	0	0	310	2	300	2.5	300	5	300	7.5	300	7.5	300	2.5	240	5
20-Dec	270	7.5	300	5	300	10	300	7	320	8	320	8	360	6	330	5
21-Dec	320	6	330	7	330	5	350	7.5	340	6	350	5	330	2.5	330	5
22-Dec	350	3	350	4	270	6	290	6	300	8	330	7.5	340	5	320	7
23-Dec	290	3	0	0	290	3	0	0	0	0	0	0	0	0	0	0
24-Dec	0	0	0	0	0	0	0	0	0	0	0	0	0	0	0	0
25-Dec	0	0	210	4	210	3	200	7.5	230	6	180	4	190	4	200	5
26-Dec	220	5	210	5	210	7	210	5.5	280	5	300	4	0	0	0	0
27-Dec	240	3	210	2.5	240	2.5	240	5	270	4	300	3.5	0	0	300	5
28-Dec	240	5	0	0	0	0	220	3.5	240	2.5	210	5	210	2.5	180	5
29-Dec	180	4.5	210	4.5	180	6	180	10	170	9	150	10	170	7.5	170	5
30-Dec	180	10	210	5	210	5	150	7	0	0	90	5	150	3.5	0	0
31-Dec	0	0	0	0	0	0	60	4	0	0	0	0	0	0	150	6

APPENDIX B.

MEAN MONTHLY AND YEARLY WIND SPEED

Table Appendix B.1. Monthly average wind speed (m/s) measured by Gharyan station.

Month / Year	Jan	Feb	Mar	Apr	May	Jun	Jul	Aug	Sep	Oct	Nov	Dec	Average
2012	5.19	4.11	4.73	5.05	5.20	4.60	4.79	3,81	5.55	5.46	5.21	6.00	**4.93**
2013	5.38	5.68	4.54	5.41	4.24	3.88	3.86	3.52	4.10	4.84	5.03	4.94	**4.60**
2014	4.87	5.31	4.92	4.93	4.83	3,89	4.11	3.44	4.05	4.07	4.99	5.27	**4.54**
2015	4.16	5.27	4.83	5.96	4.48	3.98	4,13	3.78	5.05	5.02	4.25	5.78	**4.75**
2016	4.52	4.84	5.41	5.05	5.22	5.43	5.41	5.09	5.12	4.84	4.58	5.38	**5.03**
	4.81	**5.01**	**4.87**	**5.20**	**4.67**	**4.35**	**4.44**	**4.08**	**4.75**	**4.83**	**4.79**	**5.49**	

Table Appendix B.2. Expected monthly average wind speed (m/s) in Gharyan at 50 meter height.

Month / Year	Jan	Feb	Mar	Apr	May	Jun	Jul	Aug	Sep	Oct	Nov	Dec	Average
2012	7.68	6.08	7.00	7.47	7.70	6.81	7.09	5.65	8.21	8.08	7.71	8.88	**7.31**
2013	7.96	8.41	6.72	8.00	6.28	5.75	5.72	5.22	6.07	7.16	7.44	7.31	**6.83**
2014	7.20	7.85	7.28	7.29	7.15	5.78	6.09	5.10	6.00	6.03	7.38	7.80	**6.74**
2015	7.16	7.80	7.14	8.40	6.63	5.90	6.12	5.59	7.47	7.43	6.29	8.55	**7.04**
2016	6.65	7.12	7.94	7.43	7.67	8.04	7.95	7.49	7.53	7.12	6.74	7.91	**7.47**
	7.13	**7.45**	**7.22**	**7.72**	**6.93**	**6.46**	**6.59**	**6.06**	**7.05**	**7.16**	**7.11**	**8.15**	

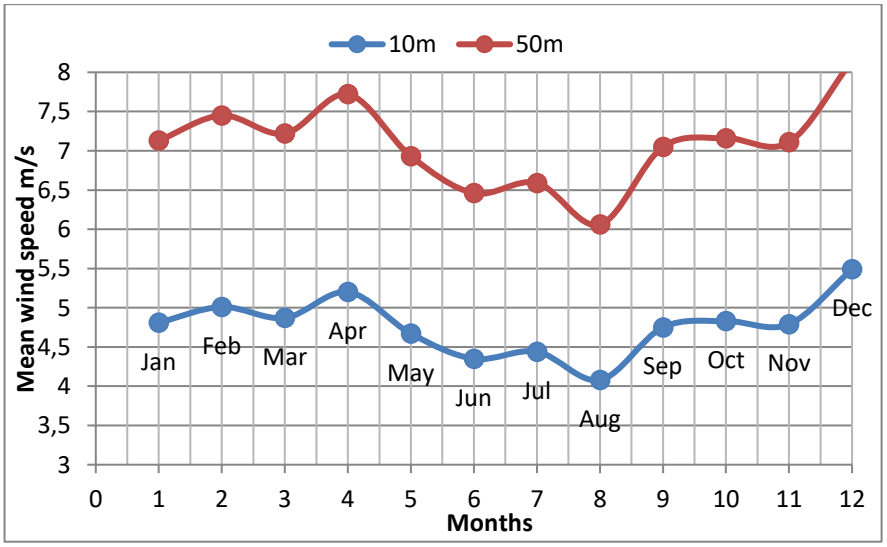

Figure Appendix B.1. Monthly mean wind speed for the station.

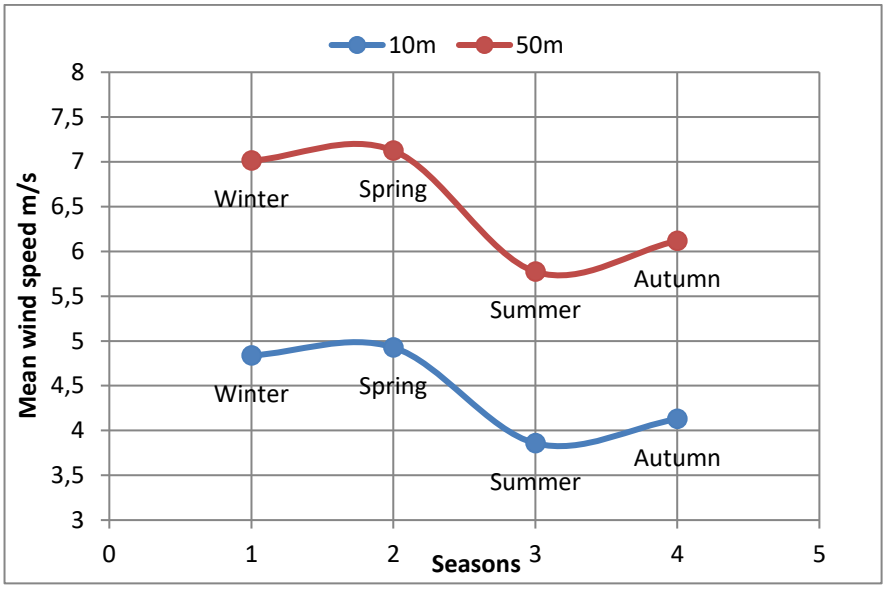

Figure Appendix B.2. Mean wind speed for different seasons of the year.

APPENDIX C.

FREQUENCY OF WIND SPEED

The Results were calculated at 10 meter and 50 meter height respectively. The probability and Weibull histogram are calculated for long period of time from 2012 to 2016 for this station. As a sample I show the calculation for Gharyan station. The frequency of wind speed is show in Table Appendix C.1.

Table Appendix C.1. Frequency of wind speed in interval 1ms.

Wind speed bin (m/s)	**Frequency of wind speed**		**Percentage of frequency wind speed (%)**	
	At 10 m	**At 50 m**	**At 10 m**	**At 50 m**
0-1	1156	670	0.079177330	0.045890411
1-2	362	115	0.024811185	0.007876712
2-3	1705	280	0.116753012	0.019178082
3-4	2651	1750	0.181574184	0.119863014
4-5	2178	2965	0.149147993	0.203082192
5-6	2785	2150	0.190749641	0.1472602740
6-7	1539	2720	0.105392922	0.186301370
7-8	941	1570	0.064446664	0.107534247
8-9	408	1040	0.027932089	0.071232287
9-10	372	465	0.025497784	0.031849315
10-11	296	285	0.020254666	0.019520548
11-12	103	310	0.007053243	0.021232877
12-13	74	95	0.005087073	0,006506849
13-14	11	100	0.000780226	0,006849315
14-15	8	30	0.000530554	0,002054795
15-16	6	25	0.000405717	0.001712329
16-17	5	15	0.000342466	0,001027397
Total	**14600**	**14600**	**1**	**1**

Table Appendix C.2. Determination of Weibull parameters.

Wind speed (m/s)	**Percentage of time wind speed exceeds**	**ln(v)**		**ln(-ln(p(v)))**	
	V(P(V))	**At 10 m**	**At 50 m**	**At 10 m**	**At 50 m**
1	1	0	-0.06918	-4.56286	-1.56326
2	0.920823	0.693147	0.873840	-2.49510	-1.55764
3	0.896012	1.098612	1.312317	-2.20908	-1.47835
4	0.779267	1.386294	1.601134	-1.38869	-0.80171
5	0.597709	1.609438	1.816855	-0.66427	-0.35666
6	0.448580	1.791759	1.989104	-0.22106	0.218858
7	0.257860	1.94591	2.132499	0.304051	0.441422
8	0.152487	2.079442	2.255332	0.631632	0.582969
9	0.088054	2.197225	2.362768	0.887810	0.890052
10	0.060129	2.302585	2.458241	1.033633	1.040495
11	0.034639	2.397895	2.544149	1.212770	1.319232
12	0.014390	2.484907	2.622237	1.444848	1.389769
13	0.007339	2.564949	2.693809	1.592190	1.424589
14	0.002254	2.639057	2.759870	1.807460	1.638457
15	0.001474	2.70805	2.850308	1.874806	1.645414
16	0.000944	2.772589	2.905706	1,940952	1.706988
17	0.000504	2.833213	2.950398	2.018465	1.864759

From Table Appendix C.2 by plotting **ln(v)** at 10 meter height in the x axis against **ln(-ln(P(V)))** at 10 meter height in the y axis, fitting straight line to the points and deduce the best fit equation as a shown in Figure 4.8. The resulting equation for the plot is **y = 1.5506x – 2.8116.** Then by comparing this equation with Equation (3.5), the scale parameter k determined for the given location as **k=1.5506**, similarly we have **k lnc =2.8116**, then the shape parameter can be solved as **C=6.13024.**

With the same method, when we apply the previous part on 50 meter height, the resulting equation for the plot is **y = 3.23x – 7.21715.** The scale parameter k determined for the given location as **k= 2.9283**, and the shape parameter C can be solved as **C= 9.341.**

APPENDIX D.

ANNUAL ENERGY CALCULATION

Annual energy calculation for the year of 2016 is based on a constant value of power coefficient, $C_p = 0.4$ and rotor diameter, $D = 4.16$ m. The calculation results of Weibull histogram and annual energy for the year of 2016 are shown in Table Appendix D.1 and Table Appendix D.2.

Table Appendix D.1. Frequency of wind speed.

Wind speed bin (m/s)	**Frequency of wind speed**		**Percentage of frequency days (%)**	
	At 10 m	**At 50 m**	**At 10 m**	**At 50 m**
0	222	135	0.07602739726	0.04623287671
1	185	82	0.06335616438	0.02808219178
2	130	98	0.04452054794	0.03356164383
3	428	113	0.14657534246	0.03869863013
4	390	150	0.13356164383	0.05136986301
5	561	212	0.19212328767	0.07260273972
6	249	230	0.0852739726	0.07876712328
7	158	428	0.05410958904	0.14657534246
8	239	395	0.08184931506	0.13527397260
9	126	291	0.04315068493	0.09965753424
10	97	234	0.03321917808	0.08013698630
11	38	209	0.01301369863	0.07157534246
12	26	130	0.00890410958	0.04452054794
13	33	80	0.01130136986	0.02739726027
14	10	52	0.00342465753	0.01780821917
15	14	30	0.00479452054	0.01027397260
16	6	13	0.00205479452	0.00445205479
17	5	18	0.00171232876	0.00616438356
18	3	7	0.00102739726	0.00239726027
19	0	3	0	0.00102739726
Total	**2920**	**2920**	**1**	**1**

Annual energy calculated for year 2016 for this stations are based on **Vestas (V60-850 kW) 500W** wind turbine power curves. As a sample Table Appendix D.2 shows the calculations of annual energy for Gharyan station.

Table Appendix D.2. Calculation of annual energy of 2016 based on Vestas (V60-850 kW) 500 kW

Wind Speed (m/s)	**Hours per year**		**Power Output (kW)**	**Energy (kWh)**	
	At 10 m	**At 50 m**		**At 10 m**	**At 50 m**
0	1571	1571	0	0	0
1	1050	23	0	0	0
2	557	33	5	2785	165
3	1545	27	16	24720	432
4	1404	1254	37	51948	46398
5	1613	453	58	93554	26274
6	357	1204	282	100674	339528
7	190	266	294	55860	78204
8	211	1602	388	81868	621576
9	85	583	399	33915	232617
10	47	348	447	21009	155556
11	55	591	482	26510	284862
12	31	206	498	15428	102588
13	13	151	500	6500	75500
14	10	244	500	5000	122000
15	7	75	500	3500	37500
16	3	78	500	1500	39000
17	2	19	500	1000	9500
18	3	9	499	1497	4491
19	5	21	493	2465	10353
20	1	2	398	398	796
21	0	0	0	0	0
22	0	0	0	0	0
23	0	0	0	0	0
Total	**8760**	**8760**		**530131**	**2187340**

The annual capacity factor for 500 kW Vestas (V60-850kWh) turbine at 10 meters and 50 meters height respectively can be calculated as the followings;

$$C_f = 530131/(500 \times 8760) = 12.104\%$$

$$C_f = 2187340/(500 \times 8760) = 49.939\%$$

APPENDIX E.

COMPUTER PROGRAM TO DESIGN AND PERFORMANCE ESTIMATION OF DARRIEUS (CURVED BLADES) WIND TURBINE

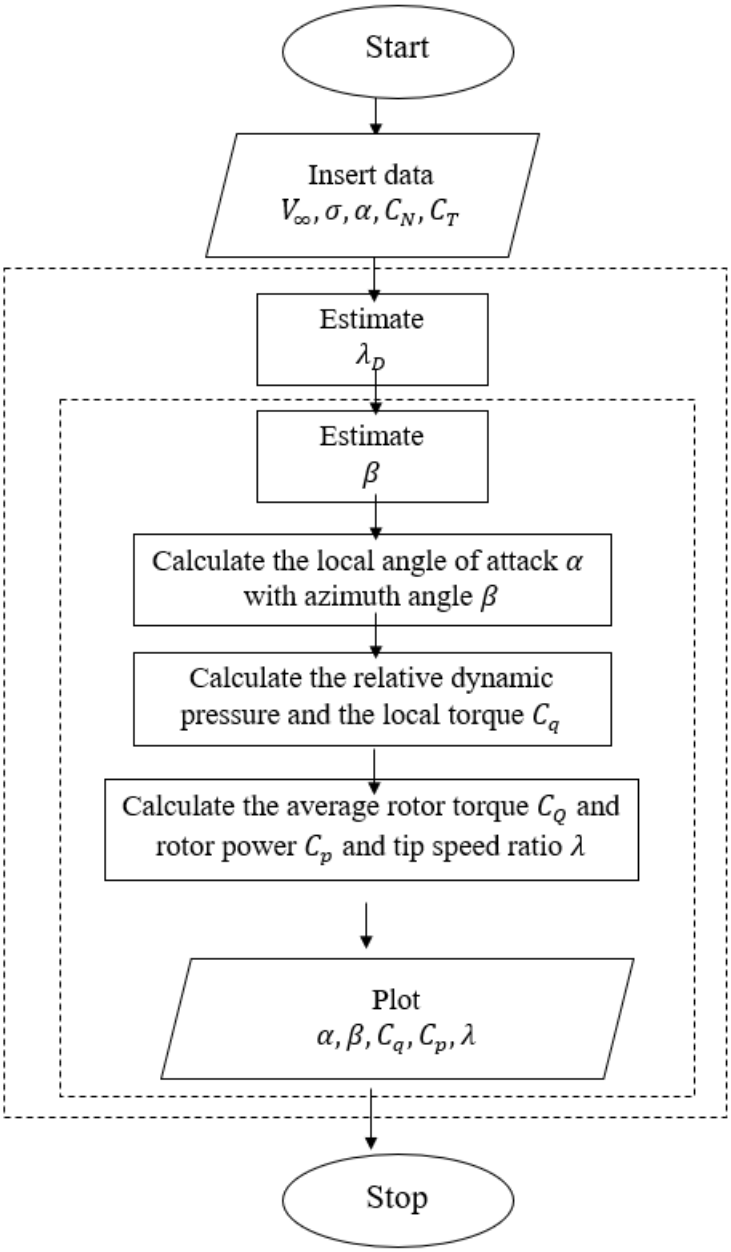

Figure Appendix E.1. Flow chart of calculation procedure.

COMPUTER PROGRAM TO DESIGN AND PERFORMANCE ESTIMATION OF DARRIEUS (CURVED BLADES) WIND TURBINE

```
C    THIS PROGRAM CALCULATES THE POWER AND THE TIP SPEED RATIO USING
C     THE SINGLE STREAM TUBE THEORY

      REAL*8 A(77),CN(77),CT(77)
      OPEN(5,FILE='da4')
C      OPEN(3,FILE='CP D9')
C      OPEN(33,FILE='CP D99')
C        OPEN(34,FILE='CP D994')
C        OPEN(35,FILE='CP D995')
C        OPEN(36,FILE='CP D996')
C        OPEN(22,FILE='CP D992')
C        OPEN(23,FILE='CP D993')
C        OPEN(24,FILE='CP D944')
         OPEN(25,FILE='CP D925')


C        OPEN(4,FILE='CQ&D9')
C        OPEN(44,FILE='CQ&D94')
c        OPEN(45,FILE='CQ&D95')
C        OPEN(46,FILE='CQ&D96')
C        OPEN(42,FILE='CQ&D942')
C        OPEN(43,FILE='CQ&D943')
C        OPEN(44,FILE='CQ&D944')
C        OPEN(51,FILE='CQ&D951')
C        OPEN(52,FILE='CQ&D952')
C        OPEN(53,FILE='CQ&D953')
         OPEN(54,FILE='CQ&D954')

C        OPEN(6,FILE='DAA9')
```

```
C       OPEN(66,FILE='DAA99')
        OPEN(77,FILE='DAA77')

C       OPEN(8,FILE='BETA. CQ9')
C       OPEN(81,FILE='BETA. CQ91')
c       OPEN(82,FILE='BETA. CQ92')
        OPEN(83,FILE='BETA. CQ93')
C    OPEN(7,FILE='DAR7')
     G=0.925
     F=(3.1415)/180.0
     S=0.25
     CD0=0.017
c    DO 4 I=1,77
c    READ(9,*)A(I),N(I),T(I)
c 4  CONTINUE
c    CALL E01BAF(77,A,N,K1,C1,81,WRK,478,0)
c    CALL E01BAF(77,A,T,K2,C2,81,WRK,478,0)
     PRINT*,'    L       CP'
C    DO 6 M=1,2
C    G=M*0.5
C    WRITE(3,*)W
    DO 1 I= 1,20

     DL=I*0.5
     SUM1=0.0
     SUM2=0.0
     DO 3 K=1,1
     HR=(K-1)/10.0
C    HR=0.0
C    RR=1.0
     RR=1-HR**2
C    WRITE(7,*)RR
     DO 2 J=1,61
```

```
      BETA=(J-1)*4.0*ATAN(1.0)/30.0
C     DO 2 J=1,37
C     BETA=(J-1)*4.0*ATAN(1.0)/18.0
      W=0.0*F
      DELTA=ATAN(2.0*HR/G)
C     DALTA=0.0
C     ALPHA=+ATAN(SIN(BETA)*COS(DELTA)/(RR*DL+COS(BETA)))
      Y=SIN(BETA)*COS(DELTA)
      X=+RR*DL+COS(BETA)
      ALPHA=+ATAN2(Y,X)
C         WRITE(6,*)ALPHA,BETA
C         WRITE(66,*)ALPHA,BETA
          WRITE(77,*)ALPHA,BETA
C     IF(BETA.LE.4.0*ATAN(1.0).AND.ALPHA.LT.0.0)THEN
C     ALPHA1=(ALPHA)+4*ATAN(1.0)+W
C     ELSE IF(BETA.GT.4*ATAN(1.0).AND.ALPHA.GT.0.0)THEN
C     ALPHA1=ALPHA-4*ATAN(1.0)+W
C     ELSE
      ALPHA1=ALPHA+W
C     ENDIF
      REWIND 5
   13 DO 15 M=1,77
      READ (5,*) A(M),CN(M),CT(M)
      DA=ALPHA1-A(M)
      IF(DA.LT.0.0)THEN
      CN2=(CN(M)+CN(M-1))/2.0
      CT2=(CT(M)+CT(M-1))/2.0
      GO TO 14
      ELse
      ENDIF
      GO TO 15
   15 CONTINUE
C     ENDIF
```

```
 14  DP=(RR*DL+COS(BETA))**2+(SIN(BETA)*COS(DELTA))**2
     DCN=CN(M)-CN(M-1)
     DA=A(M)-A(M-1)
     DCT=CT(M)-CT(M-1)
     CT2=CT(M-1)+(DCT/DA)*(ALPHA1-A(M-1))
     CN2=CN(M-1)+(DCN/DA)*(ALPHA1-A(M-1))
C    CALL E02BBF(81,K1,C1,ALPHA1,CN,0)
C    CALL E02BBF(81,K2,C2,ALPHA1,CT,0)
     IF(ABS(ALPHA1).LE.0.26)THEN
     E=CD0*COS(ALPHA1)
     ELSE
     E=0.0
     ENDIF
     CT2=CT2-E
C    WRITE(3,*)BETA,CT
C10  FORMAT(4F8.4)
     CT1=CT2
     CN1=CN2
C    CT1=CT
C    CN1=CN
     F1=DP*(CN1*SIN(BETA)-CT1*COS(BETA)/COS(DELTA))
     SUM1=SUM1+F1
     F2=DP*CT1*RR/COS(DELTA)
        DCQ=(3*S*F2/(4*((1+0.25*CDD)**2)))
C       WRITE(8,*)BETA,DCQ
C       WRITE(81,*)BETA,DCQ
c       WRITE(82,*)BETA,DCQ
        WRITE(83,*)BETA,DCQ
     SUM2=SUM2+F2
C    WRITE(3,*)BETA,CT1
  2  CONTINUE
  3  CONTINUE
     F1M=SUM1/60.0
```

```
      F2M=SUM2/60.0
      CDD=0.75*S*F1M
      CP=(81*S*DL*F2M/(64*((1+0.25*CDD)**3)))*(16.0/27.0)
      D=DL/(1+0.25*CDD)
C     Z=1.0-(D/LD)
      CQ=CP/D
C     DSA=0.33333*D
C      WRITE(3,*)D,DL ,CP
C         WRITE(33,*)D,DL ,CP
C         WRITE(34,*)D,DL ,CP
C         WRITE(35,*)D,DL ,CP
C         WRITE(36,*)D,DL ,CP
C         WRITE(22,*)D,DL ,CP
C         WRITE(23,*)D,DL ,CP
C         WRITE(24,*)D,DL ,CP
          WRITE(25,*)D,DL ,CP

C     WRITE(4,*)D,DL,CQ
C         WRITE(44,*)D,DL,CQ
c         WRITE(45,*)D,DL,CQ
C         WRITE(46,*)D,DL,CQ
C         WRITE(42,*)D,DL,CQ
C         WRITE(43,*)D,DL,CQ
C         WRITE(44,*)D,DL,CQ
C         WRITE(51,*)D,DL,CQ
C         WRITE(52,*)D,DL,CQ
C         WRITE(53,*)D,DL,CQ
      WRITE(54,*)D,DL,CQ
WRITE(52,*)D,DL,CQ

 1    CONTINUE
C6    CONTINUE
      STOP
```

END

RESUME

Nagi E. Nassir ABDALLA was born in Riayena-Libya in 1966 and he graduated first and elementary education in (Abn-Khaldon school) Tripoli. He completed high school education in (Gargarsh High School) Tripoli 1983-1984, after that, he got BSc, Mechanical Engineering from (TRIPOLI UNIVERSITY-LIBYA) in 1990, and MSc, Mechanical Engineering from (BELGRADE UNIVERSITY-SERBIA) in 2006. He worked as an engineer in (TECHNOLOGY RESEARCH CENTER – TRIPOLI - LIBYA) 1992-2008, also he moved to work as a director and a lecturer in (Engineering Technician Faculty-Riayena-Libya) in 2009 until he moved to Karabuk University, Turkey to obtain a degree of PhD in Energy System Engineering.